I M P R O V E M E N T S T O T H E W E A K - P O S T W - B E A M G U A R D R A I L

A Thesis

Submitted to the Faculty

of the

Worcester Polytechnic Institute

in partial fulfillment of the requirements for the

Degree of Master of Science

in

Civil Engineering

by

_____

Klas Erik Engstrand
June 2000

APPROVED:

_____

Dr. Malcolm H. Ray, Major Advisor

_____

Dr. Frederick L. Hart, Department Head

ACKNOWLEDGEMENTS

The work presented in this report constitutes a Master of Science thesis in Civil Engineering and was carried out at Worcester Polytechnic Institute (WPI), Worcester, MA, USA. The work was performed for and sponsored by the Pennsylvania Department of Transportation.

I would like to thank my supervisor Professor Malcolm Ray for excellent support through out the project and for giving me the opportunity to perform my thesis at the Civil Engineering Department at WPI. I would also like to thank Mr. Chuck Plaxico, Ph.D. student at the Civil Engineering Department of WPI, for guidance and advice.

ABSTRACT

Recent full-scale crash tests of the weak-post W-beam guardrail system have resulted in unsatisfactory collision performance as evaluated by the National Cooperative Highway Research Program (NCHRP) Report 350. Since acceptable crash test performance is required in order to use a guardrail on a Federal-Aid Highway in the United States, the poor performance of the weak-post W-beam guardrail is a significant problem to those states that use it. The goal of this project was to improve the impact performance of the weak-post W-beam guardrail system so that it satisfies the requirements of NCHRP Report 350 at test level three.

TABLE OF CONTENTS

LIST OF FIGURES

LIST OF TABLES

1 INTRODUCTION

Full-scale crash tests have demonstrated that the performance of the weak-post W-beam guardrail system do not meet current safety standards that are required for use on Federally funded highways.(3) (11) The reason for the poor performance of the system has been attributed to the post-rail connections, splice failure, inadequate anchorage of the system and the mounting height of the W-beam on the posts.

The guardrail posts in the weak-post W-beam system are only intended to hold the W-beam in position until a vehicle impacts it. Guardrails should be mounted high enough to ensure that the first rail-vehicle contact happens at the bumper and fender of the vehicle. During impact the W-beam rail should release from the posts and remain in contact with the impacting vehicle until the vehicle has been redirected away from the system. In some cases, however, the W-beam does not separate from the posts and is pulled to the ground during impact, which allows the vehicle to override the guardrail and penetrate behind the system. In other cases the failure of the system has been the result of the W-beam rupturing at a splice location where the individual sections of W-beam are joined together.

As shown in figure 1, the current weak-post W-beam guardrail system (G2-system) is connected to the post with an 8-mm diameter bolt and a square washer under the bolt head. The bolt is tightened with a nut that clamps the post, rail and washer together. The rail is 2.67 mm thick and its center is mounted 610 mm above the ground. An additional

14-mm diameter bolt with nut is located below the rail to support the rail under snow loading. The posts are spaced 3810 mm apart. The splice connections between each rail section consist of eight 16-mm diameter bolts and the splices are located at every post. The 8-mm diameter post-rail connection bolt is supposed to fail at an early stage of an impact to prevent the rail from being pulled down with the post and effectively reducing the height of the guardrail.(2)

New guidelines for full-scale crash testing of highway longitudinal barriers were issued by the Federal Highway Administration (FHWA) in 1993.(11) These new crash test requirements, as specified in the National Cooperative Highway Research Program (NCHRP) Report 350, now include 2000-kg pickup trucks and 700-kg subcompact cars to accommodate a greater range of vehicles. Effective May 16, 1994, all newly developed barrier systems had to meet the requirements of NCHRP Report 350 before they could be installed on federally funded highways, whereas, existing barrier systems that had previously passed NCHRP Report 230 were temporarily exempt from this new testing requirement. Effective October 1, 1998, however, all new installations of barriers (including all existing and newly developed systems) that are to be used on federally funded highways must satisfy the requirements of NCHRP Report 350.

NCHRP Report 350 specifies two required tests for evaluation of longitudinal barriers to test level three:

- **NCHRP Report 350 test designation 3-10:** An 820-kg passenger car impacting the Length of Need (LON) of the longitudinal barrier at the Critical Impact Point (CIP) at a speed of 100 km/h and an angel of 20 degrees.(12)
- **NCHRP Report 350 test designation 3-11**: A 2000-kg pickup truck impacting the LON of the longitudinal barrier at the CIP at a speed of 100 km/h and an angle of 25 degrees.(12)

The safety evaluation of a barrier according to NCHRP Report 350 is performed on the basis of three factors. Structural Adequacy, Occupant Risk and Vehicle Trajectory.(12)

The weak-post W-beam guardrail system performed acceptably in previous full-scale crash tests at test level 2 but failed to meet test level 3 conditions.(3) (11) The barrier passed test designation 3-10 but failed test designation 3-11.(2) Sometimes the vehicle penetrated the barrier and sometimes the vehicle overrode the barrier. The G2-system mainly failed the test because it did not meet the Report 350 Structural Adequacy evaluation criterion which states that the “test article should contain and redirect the vehicle; the vehicle should not penetrate, underride, or override the installation although controlled lateral deflection of the test article is acceptable.”(12)

The major goal of this project was to improve the impact performance of the weak-post W-beam guardrail system so that it satisfies the requirements of NCHRP Report 350 at test level three. Since the weak-post W-beam system already meet test designation 3-10 the task of this project was to improve the current weak-post W-beam system so that it meets the requirements of test designation 3-11.

Specific issues related to the performance of the weak-post W-beam system were:

- Prevent guardrail ruptures at the splice connection,
- Developing a more reliable post-rail connection detail,
- Reducing the chance of rupturing the guardrail and
- Preventing the vehicle from vaulting over the guardrail.

This goal was pursued using a variety of techniques including structural design, laboratory experiments, finite element analyses and full-scale crash tests.

A secondary goal was to develop a finite element model of the splice connection. This model was used investigating the performance of the splice. The knowledge derived from modeling the splice can be used in a broader aspect when modeling bolted connections.

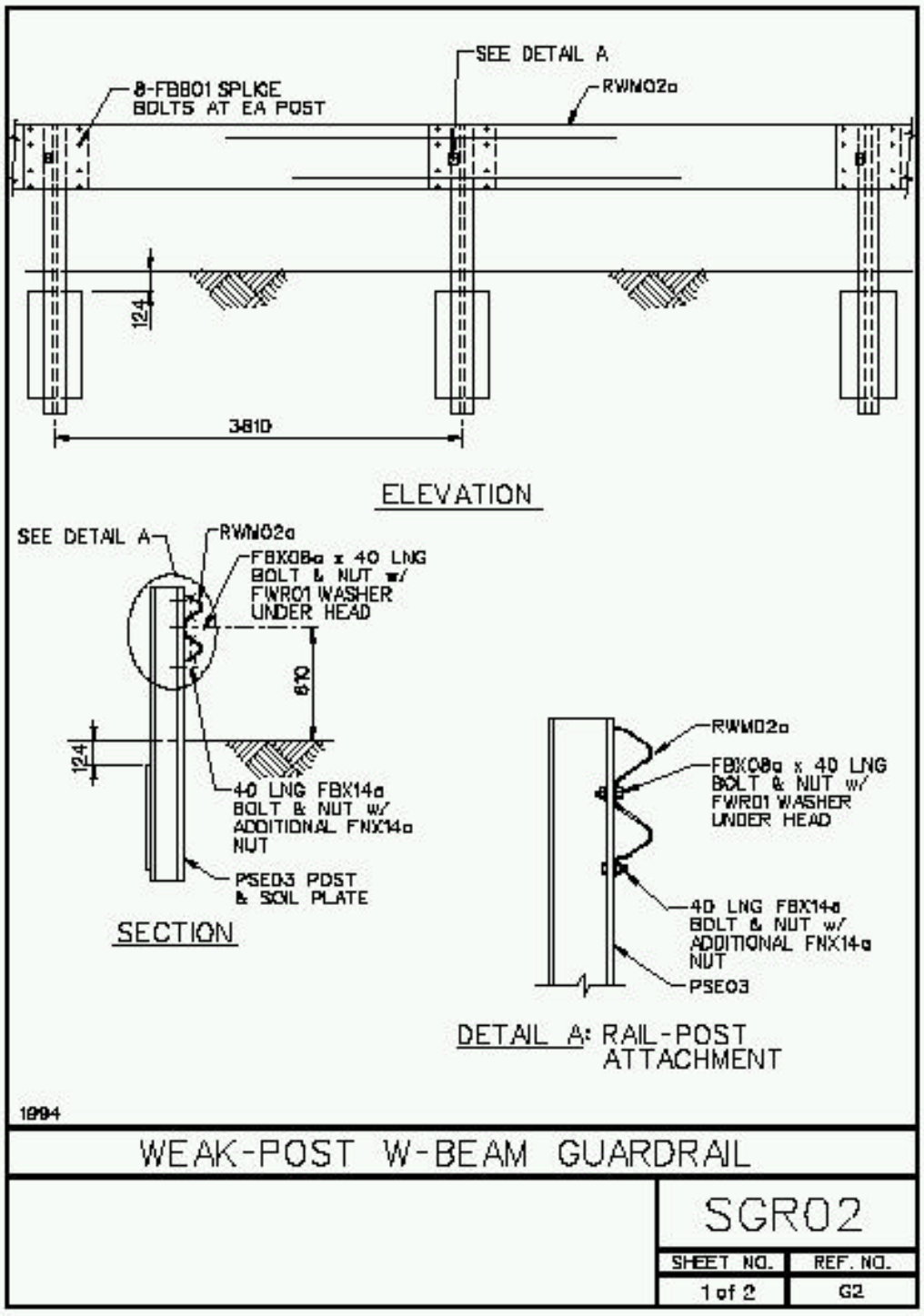

Figure 1: Weak-post W-beam guardrail system. (7)

2 LITERATURE REVIEW

2.1 Introduction

Ray and McGinnis describe the history, geographical distribution, geometry and performance of the G2-system.(2) The weak-post W-beam guardrail system shown in figure 1 is used in the eastern part of the United States in particular. New York, Pennsylvania and Connecticut use this system. Weak-wood post W-beam guardrails were once common in mid-western states like Ohio and Minnesota and they are still used in Ontario, Canada. Systems similar to the weak-post W-beam guardrail are used in the United Kingdom and other European countries.

The AASHTO-AGC-ARTBA Highway Barrier Hardware Guide includes drawings of the G2-system (designated SGR02a in the Hardware Guide as shown in figure 1), the 2-space W-beam guardrail and material specifications for guardrail steel.(7)

Ross, Sicking and Zimmer present recommended procedures for safety evaluation of highway features in the National Cooperative Highway Research Program (NCHRP) Report 350.(12) The authors specify impact conditions and evaluation criteria for full-scale crash tests of longitudinal barriers. Two different tests are required for a barrier to pass in order to meet test level 3 conditions. Test designation 3-10 conditions involves an 820-kg passenger car impacting the Length of Need (LON) at the Critical Impact Point (CIP) at a speed of 100 km/h and an angle of 20 degrees. Test designation 3-11

conditions involves a 2000-kg pickup truck impacting the LON at 100 km/h and an angle of 25 degrees.

2.2 Full-scale crash tests

Results from full-scale crash tests with the weak-post W-beam system and other systems essential for this research are presented in this section of the literature review. The tests are divided in two different groups dependent of the nature of the particular failure. The first group contains crash tests where the barrier failed to meet the test requirements cause the vehicle overrode the barrier and the second group contains crash tests where the barrier failed to meet the requirements cause the vehicle penetrated the barrier.

Vehicle override failures

Bronstad and Burket describe five full-scale crash tests performed in 1968 for the Ohio Department of Highways with a timber weak-post W-beam system.(1) This system used timber posts instead of steel and the purpose of these tests was to determine if the system met the then-current crash test requirements. Post size, notching of existing strong timber posts and post-to-rail attachment were the variables. The W-beam guardrail used in the timber weak-post system was the same as used in the steel weak-post system. The post-rail connection in test ODH-1 was composed of a 7.94-mm diameter bolt with front and rear washers and a nut behind the post. The vehicle, a full-size 2000-kg four-door sedan, impacted the system at a speed of 110 km/h and an impact angle of 25 degrees. The connection was supposed to fail due to shearing the bolt but the bolt and rear washer were

instead pulled through the post material. The authors conclude that: “Although the vehicle was redirected, loss of rail height and lack of sufficient post strength allowed it to straddle the rail. This contributed to multiple rollover… Rail separation from the posts, which occurred only at the posts in the immediate impact area, was due to forcing the bolt and rear washer through the post material.”(1)

One reason for the poor behavior of the system was that the guardrail was not released from the posts quickly enough but followed the posts to the ground allowing the vehicle to straddle the guardrail. Pulling the bolt and washer through the post material required more time and displacement than shearing the bolt. The problem with the post-rail connection was solved using a steel insert pipe in the wooden material and a thinner 6.35-mm diameter bolt instead of the former 7.94-mm diameter bolt. The steel insert pipe was inserted to “provide a shearing surface similar to that provided by the steel flange of the G2 standard post.”(1) This way the bolt was sheared off instead off pulled through. Despite these improvements, the timber weak-post guardrail post-rail connection was found unreliable in the field and quickly became obsolete.(2) This system has now almost totally disappeared from highways in the U.S.

Mak and Alberson present a full-scale crash test (TTI 7147-21) with a G2-system performed in 1993 by Texas Transportation Institute.(3) This test was performed at NCHRP Report 350 test level three conditions (i.e., a 2000-kg pickup truck impacting the guardrail system at the impact speed of 100 km/h and 25 degrees). The purpose of the test was to determine if the G2-system had the ability to contain and redirect a 2000-kg pickup truck at test level 3 conditions. The authors stated that: " The left front, left rear and right front tires of the vehicle overrode the guardrail and exited only when the end of the guardrail installation was reached. It is evident from reviewing the high-speed video that, had there been a longer run of guardrail, the vehicle would likely have vaulted over the guardrail completely… The impact performance of the G2 guardrail system was therefore considered unsatisfactory…."(3)

What is happening here is that the vehicle straddled the guardrail as can be seen in figure 2 to 5. The authors explain that "as the vehicle was being redirected, the W-beam rail element dropped and began to dig into the ground at 0.732 second. At 0.768 second, the left front tire began to mount the guardrail and was on top of the rail by 0.895 second."(3) The maximum deflection before failure was 2.4 m. The pictures of the collision show that the rail starts to drop just a little bit, which at this large deflection is enough to let the rail come in contact with the front right wheel and the vehicle starts to climb the rail.

Figure 2: Cash sequence at time » 0.3 sec (TTI 7147-21).

Figure 3: Cash sequence at time » 0.5 sec (TTI 7147-21).

Figure 4: Cash sequence at time » 0.6 sec (TTI 7147-21).

Figure 5: Cash sequence at time » 0.8 sec (TTI 7147-21).

Vehicle penetration failures

Kilareski, El-Gindy, St. John and Peacheux report the results of three full-scale crash tests with the G2-system performed in 1998 by Pennsylvania Transportation Institute.(11) These tests were at NCHRP Report 350 test level three conditions (i.e., a 2000-kg pickup truck, 100 km/h, 25 degrees) and the objective was to determine if the weak-post W-beam guardrail system meet the Report 350 level three requirements. The first two tests did not conform to test level three since the impact speed was much lower than the

required 100 km/h. The third test, however, did conform to test level three conditions. The test vehicle impacted the system between post 5 and 6. The rail ruptured at the splice at post 7 and the vehicle penetrated the barrier. The authors conclude that: ”The system performance, however, was poor with a rail splice rupture occurring at the splice on post #7. The rupture occurred approximately 0.228 s after impact and occurred when the right front corner of the test vehicle was between post 8 and 9.”(11) The maximum deflection was 1.5 m just before panel rupture.

Ross, Bligh and Menges report the results of a full-scale crash-test (TTI 472480-7) with a modified strong-steel post W-beam system (G4(1S)-system) performed by Texas Transportation Institute.(15) The system was modified with routed wood blockouts instead of the standard W150X12.6 steel blockouts. The test was performed with a 4X4 2300-kg Pickup Truck at the impact speed of 110 km/h and the impact angle was 20 degrees. This was not a standard NCHRP Report 350 test. The vehicle impacted the installation 0.7 m upstream of post 17. The rail ruptured at the splice at post 19. The authors describe the impact scenario as: “At 0.104 s, the left front tire snagged on post 18, and at 0.106 s, post 20 moved. The left front tire separated from the vehicle at 0.126 s, and at 0.154 s, the vehicle reached post 19. By 0.158 s, post 21 moved, and by 0.176 s, the rail tore from the top of the rail in a downward direction at post 19… At 0.213 s, the rail separated from post 19 and the vehicle was travelling at 86.6 km/h at an angle of 5.9 degrees. At 0.216, the rail ruptured.”(15) The maximum dynamic deflection before the

rail tore was 0.68 m. The vehicle climbed the rail but remained upright during and after the collision.

Buth, Zimmer and Menges present a full-scale crash test (TTI 405421-2) with a modified G4(1S)-system.(16) Stronger W150X17.9 steel block-outs were used instead of the standard W150X12.6. The test was performed at NCHRP Report 350 test designation 3-11 conditions. The vehicle impacted the installation 672 mm upstream of post 17. The authors describe the impact scenario as: “The vehicle began to redirect at 0.065s, the left front tire contacted post 18 at 0.087 s, and the tire began to turn toward the guardrail. By 0.192 s, the W-beam rail element ruptured near the splice at post 19 as the vehicle was at a 14.30 degree angle to the rail. The maximum deflection of the rail element before rupture occurred was 1.00 m.”(16) The vehicle penetrated the barrier and rolled over behind the guardrail. The failed guardrail element is shown in figure 6. A “strength analysis (ASTM A370) were performed on three specimens taken from the torn rail segment near the tear. Yield strength was 436 Mpa, tensile strength 514 MPa, and the percent elongation in 51-mm gauge length was 25 percent.”(16) The rail tension was obtained at three locations, between post 15 and 16, between post 18 and 19 and between post 22 and 23, from strain gauge bridges. The tension in the rail between post 18 and 19 was about 130 KN when the splice failure occurred. Worth mentioning is that the post-rail connection bolt tension was measured at post 17 and 18 and the splice displacement was measured at post 15, 19 and 23. The splice displacement was measured with splice

displacement transducers. The splice displacement at post 19 was about 50 mm at maximum and 35 mm when the splice failure occurred.

Figure 6: Ruptured rail element at splice in TTI Test 405421-2. (16)

Mak, Bligh and Menges report the results of four full-scale crash tests conducted with four different vehicles, a Ford Taurus, Chevrolet Lumina, Plymoth Neon and a Dodge Caravan.(17) A modified G4(1S)-system was used in these tests. The installation was modified with timber blockouts instead of the standard W150X12.6 steel blockouts. The crash test with the Chevrolet Lumina (TTI 472580-2) resulted in a splice failure at post 15. The 1500-kg vehicle impacted the rail 0.84 m upstream of post 14 with an impact speed of 98.4 km/h and an impact angle of 25.0 degrees and contacted post 14 at 0.041 sec. This was not a standard NCHRP test. The authors explain that “the vehicle began to redirect at 0.043 s and post 16 moved at 0.080 s. At 0.112 s, a tear appeared at the lower

edge of the W-beam rail at post 15 and, at 0.115 s, the vehicle contacted post 15…. The W-beam rail element ruptured at 0.122 s."(17) The vehicle penetrated the guardrail and ended up on its roof behind the guardrail installation.

Research was performed in order to determine the cause of the splice failure. Fifteen laboratory tests were conducted using coupons cut from the ruptured rail element to determine if the material met the AASHTO M180 specifications (i.e. 482 MPa in tensile strength). The results in Table 1 show that the tensile strength was just above the specifications in all cases but one. The zink coated rail coupons of the W-beam material tested in the independent laboratory was just below the specification. The authors concluded "there are significant differences in terms of tensile strength and percent elongation between the Trinity Laboratory testing results and the mill certificate. When compared to the testing results from the independent testing laboratory, the differences are even more striking. There are no apparent reason for such discrepancies and the differences are too large to be random variation."(17)

	Average Yield Strength (MPa)	Average Tensile Strength (MPa)	%Elongation
Independent Laboratory			
• Zinc coated rail	416	476	25
• Non zinc coated rail	415	486	23
Trinity Industries	453	572	23
Mill Certificate	445	529	31

Table 1: Laboratory test results for AASHTO M180 guardrail steel.(17)

The authors also stated that: "it is believed that the properties of the rail element did not materially contribute to the rail rupture."(17)

The investigators continued with the effort to determine what caused the splice failure by looking at the test data. They claimed that: “The rail element was not subjected to excessive deflection or general pocketing at the splice. The upstream anchor was barely disturbed, indicating that there was not excessive tensile load on the rail prior to rupture… However, it is clear from the two high-speed cameras located behind the rail that, shortly after impact, a hard point on the vehicle (apparently the frame horn) began to flatten the lower corrugation of the rail and continued with the flattening as the vehicle proceeded down the guardrail. A localized pocket was formed at the splice post, which led to a tear on the lower edge of the rail element and the eventual rupture of the rail.”(17) They also conclude that “it is unclear why or how that happened, or if this is unique or repeatable, or what can be done to alleviate this problem.”(17)

Mak, Bligh and Menges report the results of three crash tests conducted on the MELT-2 terminal.(18) In one of the crash tests (TTI 405541-4) performed at NCHRP Report 350 test designation 3-34, which involves an 820-kg passenger car impacting the CIP at a speed of 100 km/h and an angle of 15 degrees, the W-beam ruptured at a splice. The vehicle impacted the MELT-2 terminal at post 2. The vehicle began to redirect at 0.035 s. The right corner of the vehicle reached post 3 at 0.074 s. The authors explain that “at 0.091 s, the rail element began to tear at the lower bolt hole of the splice at post 3. The maximum dynamic deflection of the rail element just prior to the tear was 0.53 m. The rail element began to deform around post 4 at 0.116 s and then buckled at post 4 at 0.121

s. By 0.122 s, the rail element was completely ruptured at the post 3 splice."(18) The vehicle penetrated the rail.

Mak and Menges report the results of four full-scale crash tests performed with a Mini-MELT terminal for use with the G2-system.(19) The purpose of this crash test was to evaluate the adequacy and strength of the transition from the weak-post W-beam system to the strong-post Mini-Melt terminal. The second test (TTI 471470-23) was performed at NCHRP Report 230 Test Designation S31 conditions (2000-kg passenger car, impact speed 100 km/h and impact angle 25 degrees). The vehicle impacted the guardrail terminal 4.6 m upstream of the last wooden post of the terminal (post 5). The numbering in this test was different from the standard. The upstream end-post of the terminal was numbered 12 and the second post from the upstream end was numbered 11 and so forth. The vehicle contacted post 3 at 0.055 s, post 4 at 0.147 s and "at 0.148 s after impact, the W-beam rail element ruptured at the splice at post 5 (last wood post of the terminal section)."(19) The maximum dynamic deflection before rupture was 0.3 m. The ruptured W-beam element is shown in figure 7.

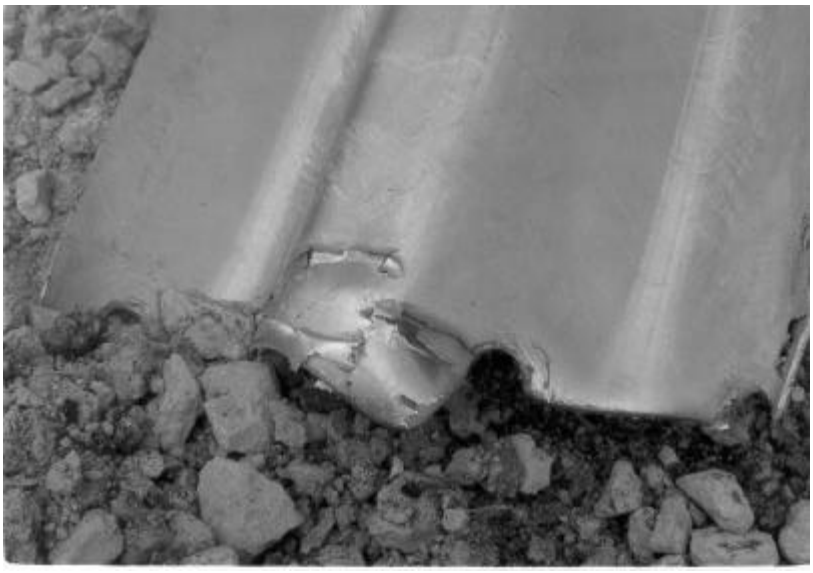

Figure 7: Ruptured rail element at splice in TTI Test 471470-23. (19)

The major conclusion from these full-scale crash tests is that the weak-post W-beam guardrail system does not meet the NCHRP Report 350 test level three criteria. The G2-system cannot contain and redirect an impacting 2000-kg pickup truck in a safe and stable way as required by NCHRP Report 350 test designation 3-11. Sometimes the guardrail ruptures and the vehicle penetrates the barrier and sometimes the guardrail drops and the vehicle overrides the barrier.(3) (11) A review of videos of prior full-scale crash tests showed that one cause of the guardrail dropping and allowing the vehicle to override the barrier was the inconsistent failure of the post-rail connection. An investigation of the post-rail connection is performed in this research.

Another conclusion is that barriers occasionally rupture at the splices in full-scale crash tests with other barrier systems than the G2-system. Splice failures have been observed in tests with the strong-post W-beam system, the MELT Terminal and the Mini-MELT

Terminal. (15) (16) (17) (18) (19) Essentially all W-beam barriers use the same type of eight-bolt splice connection to connect the W-beam sections and all such systems experience splice failures occasionally. An investigation was performed in this research to explore the performance of the splice in detail and to suggest modifications to guardrail systems that uses this connection that would prevent the rail from rupturing at the splice.

2.3 Finite element modeling

Finite element analysis is a good tool to simulate impacts. Laboratory tests and crash tests are often time consuming and expensive to carry out. It is therefore often useful to perform a simulated test before performing a physical test. This way weak spots in a structure can be identified at an early stage of the developing process, which saves money and time. The finite element program LS-DYNA is an “explicit three dimensional finite element code for analyzing the large deformation dynamic response of inelastic solids and structures” and was used for the simulations in this project.(8) LS-DYNA has been used with good results in crash-test simulations for years.

Plaxico, Patzner and Ray describe techniques they used in developing a finite element model of the guardrail post-soil interaction.(4) The interaction was modeled using springs between post and soil below grade. The model was compared with a pendulum test of a strong-post and the simulated results corresponded well to test data. These modeling techniques were used in the research described in this report.

Wright and Ray describe techniques for modeling steel materials in LS-DYNA for guardrail materials.(5) Quasi static laboratory tension tests were performed on AASHTO M-180 guardrail steel coupons and compared with finite element solutions of the same test. LS-DYNA material parameters were optimized to achieve the best correlation between laboratory tests and FE-tests. Two different LS-DYNA material models were used for modeling guardrail steel, the kinematic/isotropic elastic-plastic material model (Type 3) and the rate-dependent tabular isotropic elastic-plastic material model (Type 24).(5) There were two different sets of properties for material model Type 3, one bi-linear set covering elongations up to 11 percent and one elastic-perfectly plastic set covering elongations from 11 percent up to failure, which happens at about 25 percent elongation. Both sets of properties are accurate as long as they are used in the appropriate range of elongations. The authors came to the conclusion that "material Types 3 and 24 are not adequate for modeling strain rate effects for AASHTO M-180 guardrail" and they did therefore not include strain-rate effects in the models.(5)

3 PERFORMANCE OF GUARDRAIL SPLICES

3.1 Introduction

Weak-post W-beam guardrail sections are connected to each other with eight 16-mm diameters bolts and nuts. The splices are located at every post in the G2-system (figure 1). One problem that has been observed in the field and in full-scale crash tests with the G2-system is that the W-beam sometimes ruptures at the splice allowing the vehicle to penetrate the barrier.(11)

This problem is not unique to the weak-post W-beam system. Occasionally the guardrail ruptures at the splice in strong-post W-beam systems, guardrail terminals and guardrail-bridge rail transitions.(15) (16) (17) (18) (19) The design of the splice connection is the same in all these systems although the location of the connections in each system varies.

The objectives of this chapter are to determine why guardrails occasionally rupture at the splice and to suggest modifications that might prevent the rail from rupturing. A combination of laboratory tests and finite element simulations were used to explore the performance of splices in the weak-post W-beam system. A secondary goal of this chapter was to develop and evaluate a finite element model of the splice connection. This model was used for the finite element simulations described in this chapter and the knowledge from this task can also be used in a more general manner when modeling bolted connections.

First, a series of uniaxial tensile laboratory tests were performed to explore the response of the splice connection due to uniaxial loading and to collect data for evaluation of a finite element model of the connection. The model of the splice was used to explore the performance of the connection when subjected to a more realistic loading case in a simulation. The results from this simulation were used to derive a theory to explain why guardrails sometimes rupture at the splices. The theory was compared with the results from prior full-scale crash tests and an improved design that solves the problem was recommended.

3.2 Laboratory uniaxial tensile tests

A series of quasi-static laboratory uniaxial tensile tests of the guardrail splice connection were performed using a Tinius-Olsen 1780-kN (400,000-lbs) load test machine. The purpose of the uniaxial tensile test was to examine the uniaxial failure mechanism and ultimate strength of the splice and to collect data for validation of a finite element model of the splice connection.

Special grips to hold the ends of the guardrail when pulling the splice apart were designed and fabricated. These had to be able to withstand larger loads than the bolted splice connection and the rail cross-section. Each grip consisted of three steel hemispherical bars welded to a plate that was designed to fit in the grips of the load tester. Twenty-one 12.7-mm diameter A307 bolts were used to clamp the rail to each grip

fixture. Long plate washers were used between nuts and rail to increase the friction. Figures 8 and 9 show the test setup and the grips.

Three uniaxial tensile tests were performed with this setup. The first test was interrupted since the bolts used for the grips failed at around 390 kN. Weaker, 9.5-mm diameter bolts and small round washers were used to clamp the rail to the grips in the original design. The grips were improved by using stronger 12.7-mm diameter bolts and long plate washers between nuts and rail. The same test was continued and completed successfully. Two more tests were then performed successfully. The failure mechanism and maximum pulling force were considered consistent through out the tests.

Figure 8: Uniaxial tensile test setup.

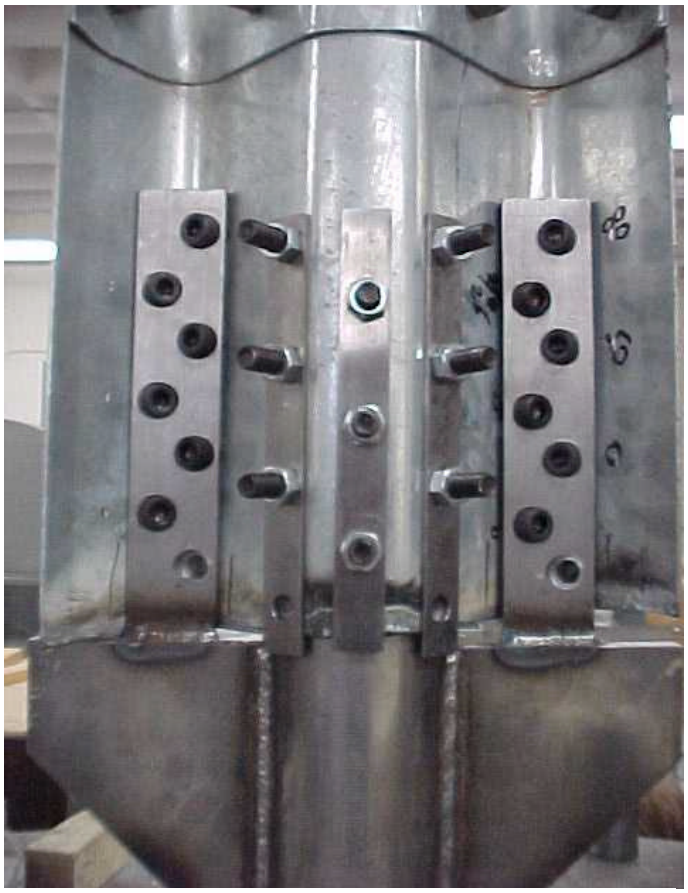

Figure 9: Test grips.

When the splice was loaded axially, the splice bolts rotated and bent the edges of the splice holes (figure 10). The sharp edge of the bolt head and nut tore the material around the holes on both layers of guardrail (figure 11). Finally, the bolts started to tear through the guardrail material around the holes and were pulled through the holes allowing the splice to be pulled apart completely. At the end of all three tests one of the outer splice bolts tore the guardrail material completely. The results from the physical uniaxial tension tests are summarized in Table 2. The splice failed at approximately the same displacement and force in all three tests. The curves up to failure differed somewhat, though (see figure 12), because the connection is sensitive to how the two layers of W-

beam are lined up relative to each other. The splice holes are actually slots and the force direction response will be affected by where in the slot the bolt is positioned.

The highest tension measured in the rail upstream of the impact point in a full-scale crash test of a weak-post guardrail system is usually below 300 kN.(9) What is happening at 400 kN in a uniaxial laboratory test is, therefore, probably not what happens in a real impact. The test is not very realistic but the force-displacement curves for the last two tests are valuable when evaluating the finite element model of the connection.

Figure 10: Failed splice connection.

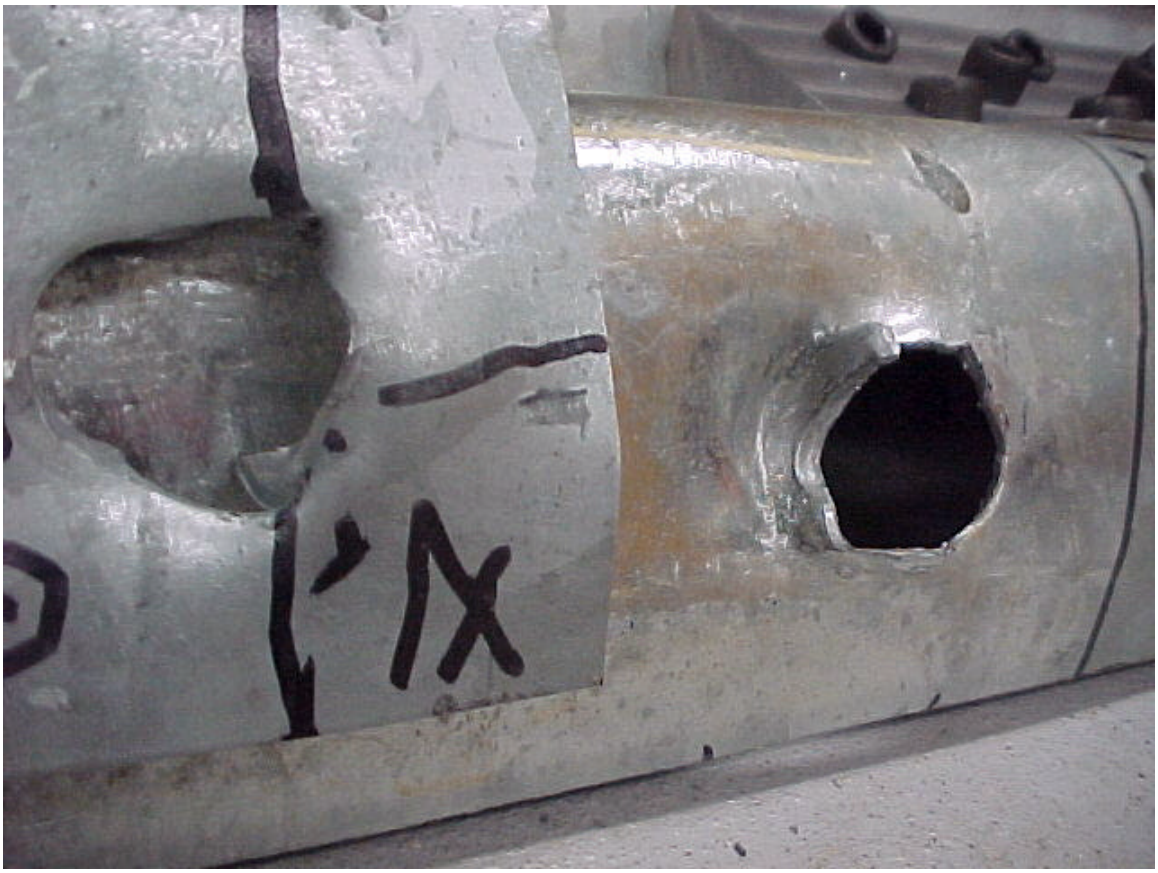

Figure 11: Guardrail damage caused by bolt-head and nut tearing material.

Test	Failure Mechanism	Max. Pulling Force (kN)	Displacement at max force (mm)
991222_01*	Splice bolts pulled through splice holes	438	NA
000117_01	Splice bolts pulled through splice holes	408	22.86
000322_01	Splice bolts pulled through splice holes	409	24.13

*Interrupted and continued after redesigning the test fixture. Displacement data lost when test interrupted.

Table 2: Uniaxial tension test results for a guardrail splice.

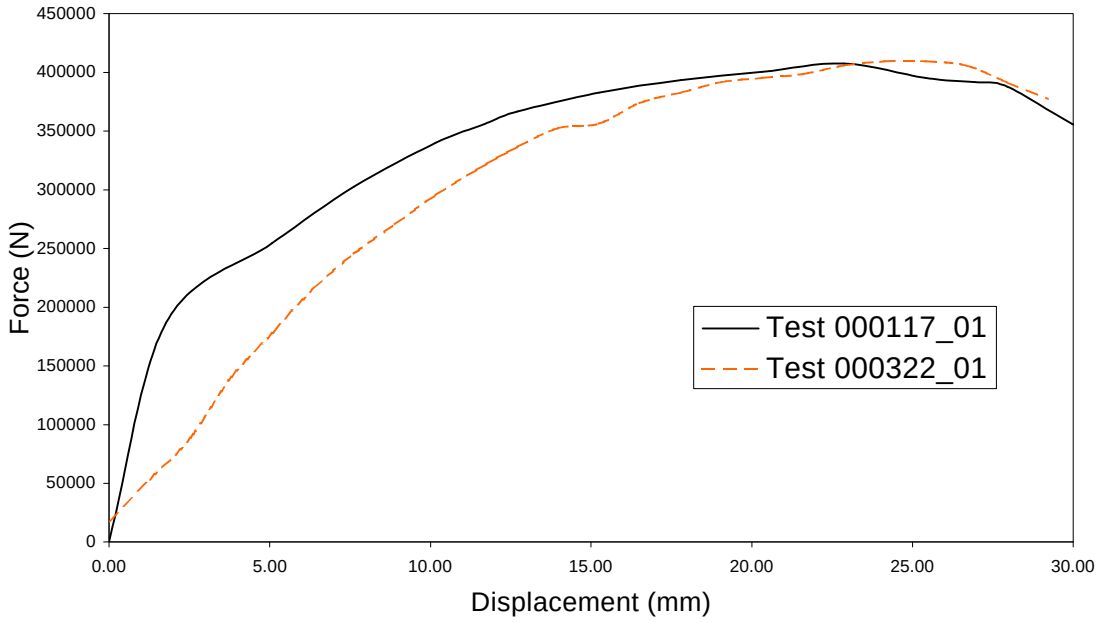

Figure 12: Uniaxial tension test force-displacement graphs.

It is difficult to perform a realistic laboratory test that replicates the loading on the splice connection in a full-scale crash test since the loading and deformations are very complex. Instead, a finite element model of the splice was developed and evaluated. The model was later implemented in a sub-model consisting of a weak-post and the rail section at the study post with the splice connection in the middle. Using the sub-model, the performance of the splice connection in a full-scale crash test could be simulated and studied in detail.

The next section in this report describes the modeling and evaluation of a finite element model of the splice connection.

3.3 Finite element model of the splice connection

Truegrid version 1.4.0 was used to generate the geometry and mesh of the finite element model of the splice and to apply boundary conditions.(20) Springs, dampers, material models and load curves were also implemented using this software.

An important feature of the mesh was that it should be easy to change. For example, making the mesh finer in particular areas of interests should be easy to do. This was accomplished using parameters for the number of nodes between indices in the mesh. This way, changing the value of a certain parameter changes the whole mesh in a predetermined and time effective manner. Another important feature of the model was the use of different material model definitions for each individual part. This feature made it possible to examine a particular part of the model, for instance a splice hole, using a post processor without being disturbed by other parts hiding the view. It also gives the opportunity to treat every part individually regarding material designation.

The shape of the W-beam was modeled with 51 nodes through the cross section to produce a smooth and accurate mesh. The coordinates for each node in the cross-section were collected from a drawing of the W-beam in the AASHTO-AGC-ARTBA Highway Barrier Hardware Guide.(7) The two W-beam guardrail sections, connected by the splice, were modeled as two different parts. Figure 13 shows the right-hand part. The geometry of the left-hand section is the same as the geometry of the right-hand section but mirrored. The rectangular holes in the rail shown in figure 13 make room for splice and

postholes, which were modeled as separate more finely modeled parts. It was essential to model the splice holes with a fine mesh since the distribution of stresses and strains around the holes were of interest in this investigation. A mesh that is too fine, though, is computationally expensive and makes the model impractical to use. A number of different meshes were generated and tested in simulated tests. The final and finest of the meshes is shown in figure 14. This is the mesh that was chosen for the splice model. The shape and positions of the splice holes were collected from the AASHTO-AGC-ARTBA Highway Barrier Hardware Guide.(7) The geometry of the splice bolts and splice nuts were collected from the same Hardware Guide. The accuracy of the splice bolt and nut geometry was important since it affects how hard the rail sections can be clamped together. Figures 15 and 16 show these components. Figures 17 and 18 show the complete assembled splice model, front-view and back-view.

The laboratory tensile test described earlier in this chapter was now simulated using the finite element model. The purpose of this simulation was to evaluate the performance of the model by comparing the simulation test results with physical test results.

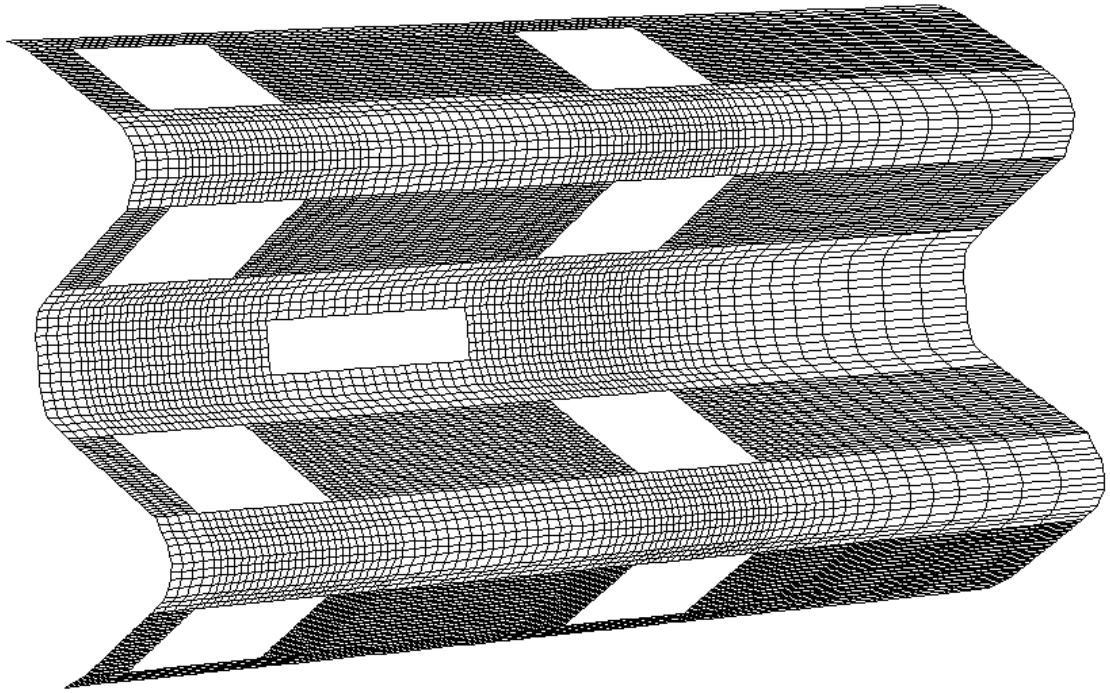

Figure 13: The right W-beam guardrail section.

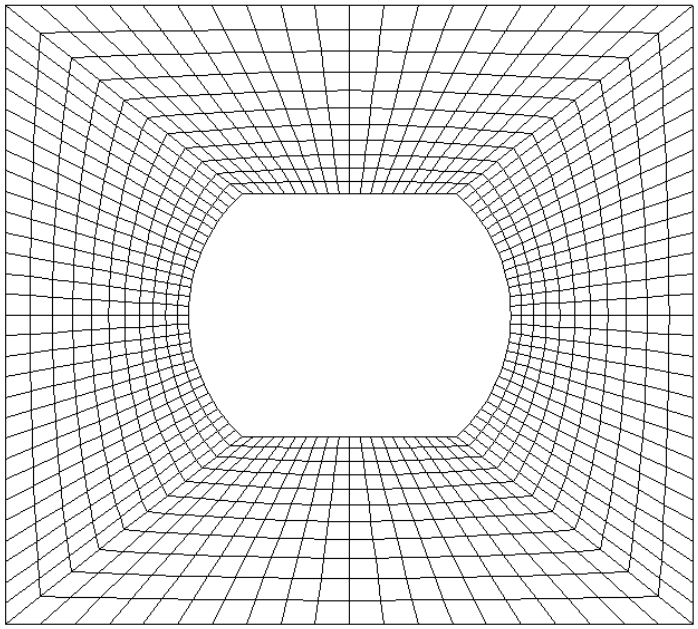

Figure 14: Model of the splice hole.

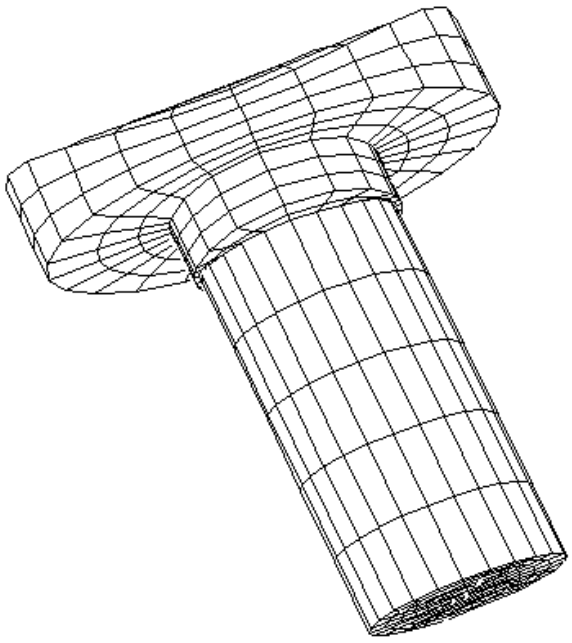

Figure 15: Model of the splice bolt.

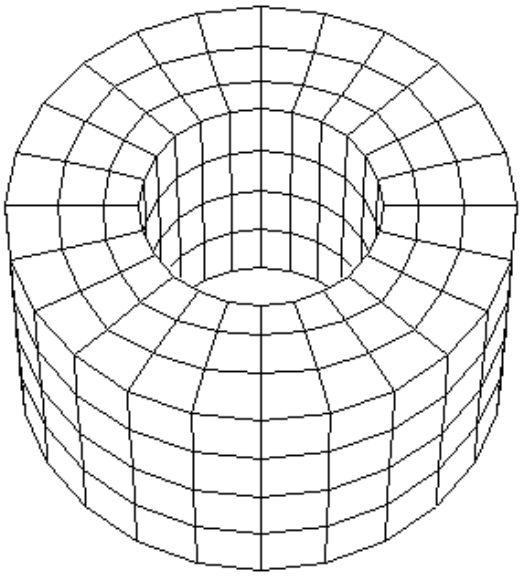

Figure 16: Model of the splice nut.

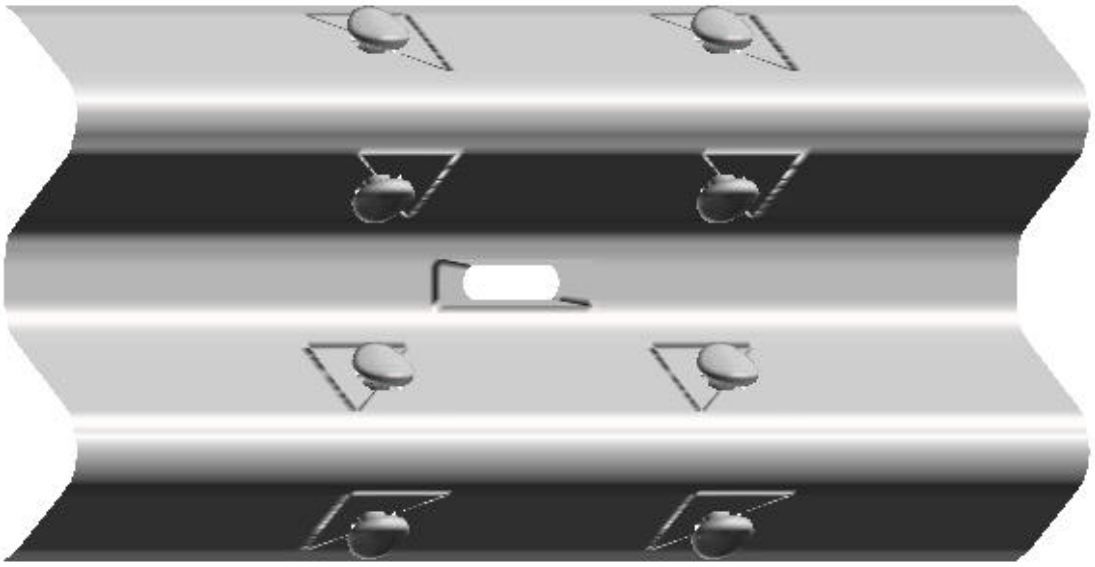

Figure 17: Front-view of assembled guardrail splice model.

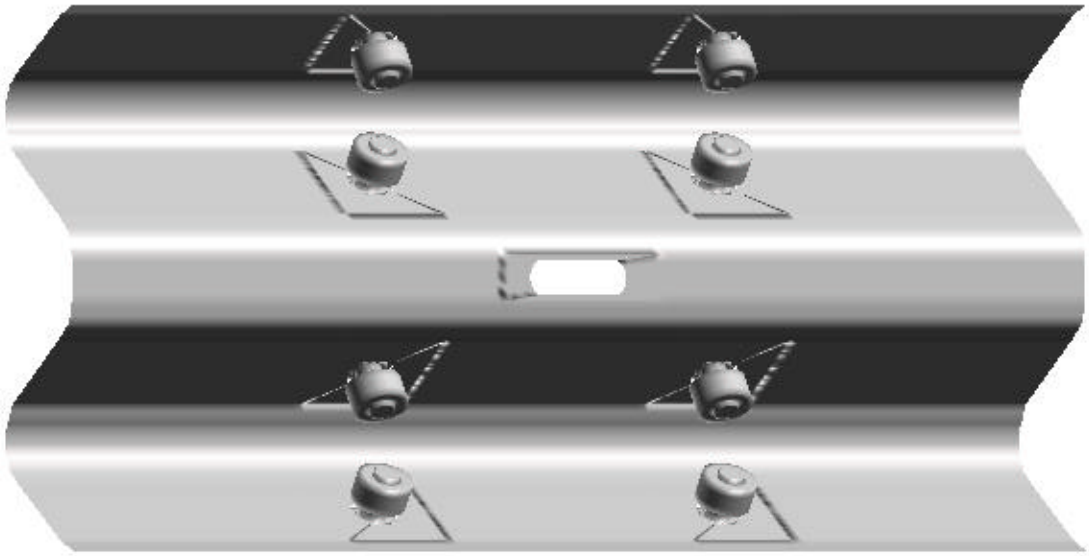

Figure 18: Back-view of assembled guardrail splice model.

3.4 Simulated uniaxial tensile test

LS-DYNA version 950c was used for the finite element simulations in this chapter.(8) The uniaxial tensile test was simulated using finite element analysis in order to evaluate the FE-model by comparing the physical test results with the simulation results.

Boundary and load conditions

Boundary and load conditions in the simulation should correspond to the physical test setup. The ends of the rail, where the grips were located in the physical test, were fixed in all directions but the axial direction. The axial load was applied at the ends of the rail with a nodal velocity boundary condition card.(8) To be able to compare the results from the simulation with the results from the laboratory tests, a cross-section definition for force output was implemented through the cross section of the rail quite near the rail end. The force output gives the total cross-section force as function of time and was easily re-plotted as force verses displacement (figure 20). Clamping the rail sections together really tight with the eight splice bolts and nuts was an important aspect of the model. The splice nuts should be clamped up against the shoulders of the bolts and then stay there throughout the tensile test. This was achieved by attaching springs and dampers between the nuts and the ends of the bolts. When the nuts had been fully pushed up against the shoulders of the bolts with the help of the springs they were merged together with the bolts preventing them from moving further (figure 19).

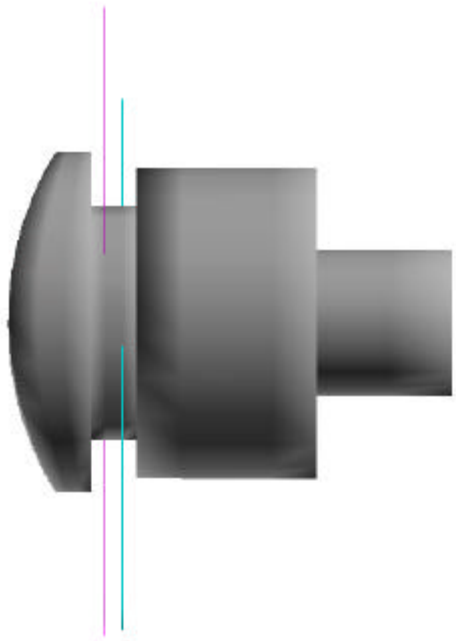

Figure 19: Nut pushed against the shoulder of the bolt.

Material and element properties

Wright and Ray developed two different LS-DYNA material models for guardrail steel, the kinematic/isotropic elastic-plastic material model (Type 3) and the rate-dependent tabular isotropic elastic-plastic material model (Type 24).(5) There were two different sets of parameter values for material Type 3, one bi-linear model valid for elongations up to 11 percent and one perfectly plastic model valid for elongations from 11 percent up to 25 percent. The advantage of the Type 24 model is that it is valid for all elongations. Both the Type 24 model and the Type 3 model were tested. The perfectly plastic material parameter values were used for the Type 3 model since the material was loaded until or near failure. LS-DYNA rigid material model Type 20 was used for the splice nuts and bolts.

No strain rate effects were considered. No failure condition was included in the model. The failure mechanism in LS-DYNA material model 24 uses the effective plastic strain as failure condition. When the effective plastic strain reaches a certain value the element stress is put to zero effectively removing the element from the model. This failure mechanism is mesh sensitive and a specific value of the maximum effective plastic strain has to be set for each mesh. Two different LS-DYNA 3D-shell elements were tested for the rail, the 4-node Hughes-Liu element and the simpler more computationally cost-effective 4-node Belytschko-Tsay element. Three and five integration points through the shell thickness were tested.

Simplicity worked better for this very hard-to-model loading case. There were a lot of edge-loaded shell elements in the simulation around the splice holes where the bolts were pressed up against the edges of the holes. Shell elements are not good in handling such load conditions. An alternative solution, from using shell elements, could be to use solid elements but that would make the computation time unreasonable high and the model would be unpractical to use. Instead all efforts were put on optimizing the performance of the model using shell elements. There were no apparent differences in the performance of the Hughes-Liu element and the Belytschko-Tsay element in this analysis. The Belytschko-Tsay element was chosen since it is less computationally demanding than the Hughes-Liu element. LS-DYNA material Type 24 is more computationally demanding than Type 3 and in general also more accurate for the entire elongation response. Simpler material models like Type 3 often causes less numerical and contact problems than more

sophisticated models and using them can be a good way to avoid these problems. For this simulation material Type 3 was more stable than Type 24. The axial loading of the splice causes a lot of edge loaded shell elements, which the simpler material model Type 3 handled better than Type 24. In other loading cases of the splice with not as high axial load but more bending the Type 24 model would probably perform better. Three integration points through the thickness of the shell element worked better than five points for this analysis. All material and element data is listed in Table 3.

	Material Type 3	Material Type 24
Density (Mg/mm^3)	7.86e-9	7.86e-9
Young's Modulus (MPa)	200e+3	200e+3
Poisson's Ratio	0.33	0.33
Yield Stress (MPa)	528.0	415.0
Tangent Modulus	300.0	-
Hardening parameter	Kinematic	Isotropic
Strain rate effects	None	None
Failure condition	None	None
Increments of strain	-	0. 0.02 0.08, 0.165 0.33 0.495 0.66 1.0
Increments of stress (MPa)	-	415 415 548 585 591 595 600 605.
Element type	Belytschko-Tsay	Belytschko-Tsay
No. of Integration points	3	3

Table 3: Material and element data for AASHTO M-180 Class A Type II guardrail steel.(5)

Contact definitions and friction

The LS-DYNA soft constraint formulation contact definition was used for all contacts in this model in order to avoid instability problems which may occur when using the penalty factor formulation. A lot of re-meshing had to be performed before the analysis was free from shooting nodes and other contact problems. The Young's modulus of the rigid bolts

was decreased by a factor of twenty in order to make the contact between the shell edges of the splice holes and the shanks of the splice bolts softer. This change did not affect the results of the simulation other than reducing numerical problems that resulted in shooting nodes and exploding meshes. The discrete nodes impacting surface (LS-DYNA contact definition Type 5a) was used between splice bolts and holes and between splice nuts and holes. Automatic single surface contact (Type 13) was used between splice holes and guardrail. The static and dynamic friction between all parts was set to 0.15 respectively 0.09 with a decay coefficient of $0.266*(10)^{-3}$.(14) The contact definitions were set to see shell thickness.

Figure 20 shows the resulting response of the simulated axial tensile test (labeled "Material 3") in comparison to the physical tests.

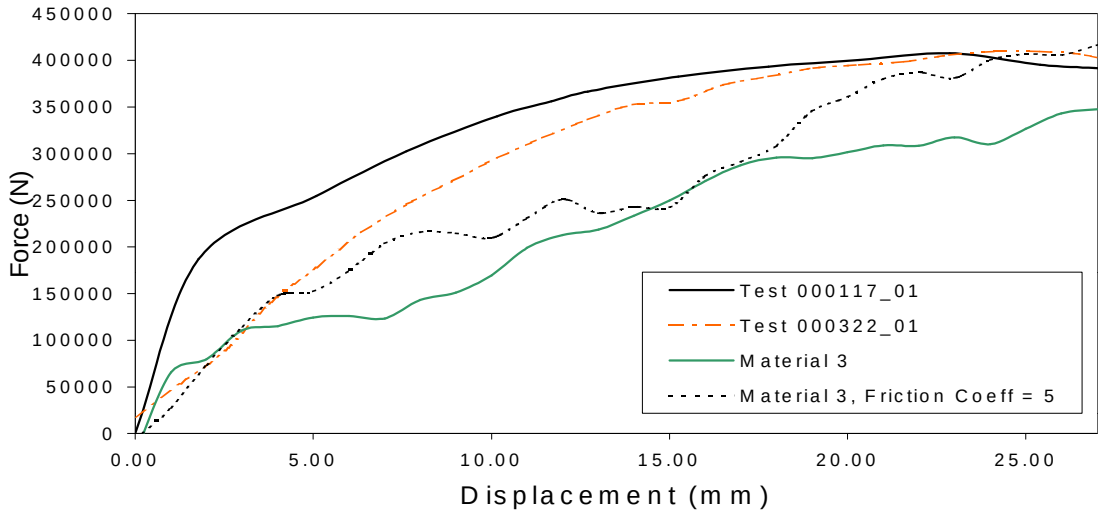

Figure 20: Force-displacement curves for uniaxial tension tests of splice (experimental and simulation).

3.5 Simulation characteristics

The cross-section force (mean nominal force) in the W-beam increases quickly as the splice is pulled apart and the splice holes are pushed against the bolt shanks (curve labeled “Material 3” in figure 20). Stress concentrations build up around the splice holes (figures 21 and 22). The heads of the bolts and nuts start to cut into the material around the splice holes as the bolts rotate resulting in high stress concentrations (figures 23 and 24). Figure 26 shows stress concentration factors for a few nodes located around a splice hole as function of time and figure 25 shows the locations. This factor decreases with the distance from the edge of the hole. The time and displacement when the maximum stress occurs in a particular element also increases with the distance from the hole. The response off the material surrounding the splice holes is a continous process through out the splice pulling. First the elements nearest the splice hole reaches its maximum axial stress and bend. Then the second row of elements and so on. Figure 27 shows how the

axial stress and bending moment changes through out the simulation for three different elements. The elements 34362, 34357 and 34353 correspond to the nodes 35864, 35690 respectively 35574 in figure 8. The first row of elements (element 34362 in this case) starts out with a high axial stress and bending moment forcing the element up against the bolt shank when yield stress is reached. Both the axial stress and the bending moment levels of and basically the element become in-plane loaded. The same procedure is repeated for the second row and so forth until no more material can be compressed up against the bolt shank. Then the material starts to fold around and under the bolt head which element number 34357 is an example of. Both the axial stress and the bending moments increases as the material around the hole is pushed against the bolt until the element finally reaches yield stress and the axial load drops. The bending moment continues to increase causing the folding behavior. The material surrounding the splice hole switches deformation modes from axial to a pure moment. Element number 34352 is located quite a distance from the hole and never reaches yield. Both bending moment and axial stress continue to increase through the run even though the moment changes sign after a while.

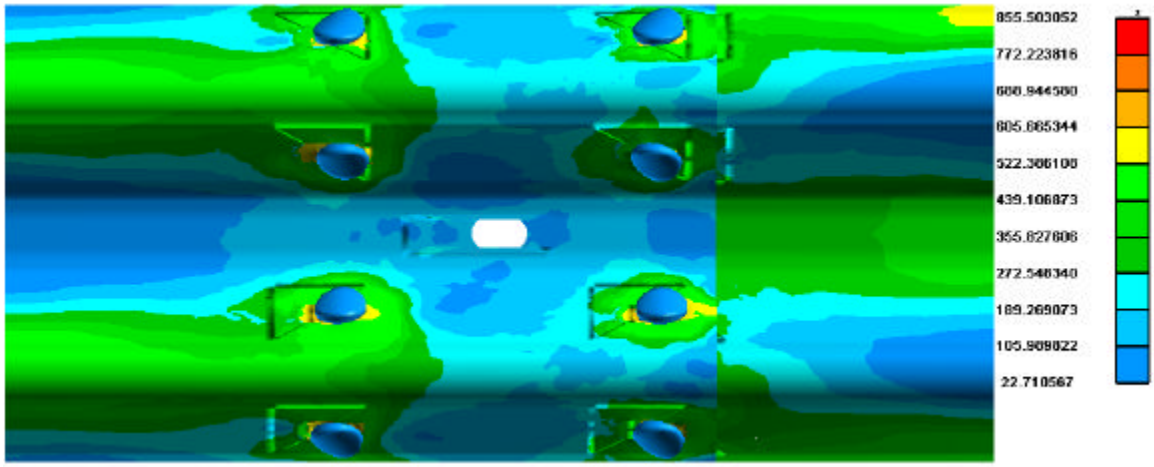

Figure 21: Von Mises stress (front-view) in the uniaxial splice pull simulation.

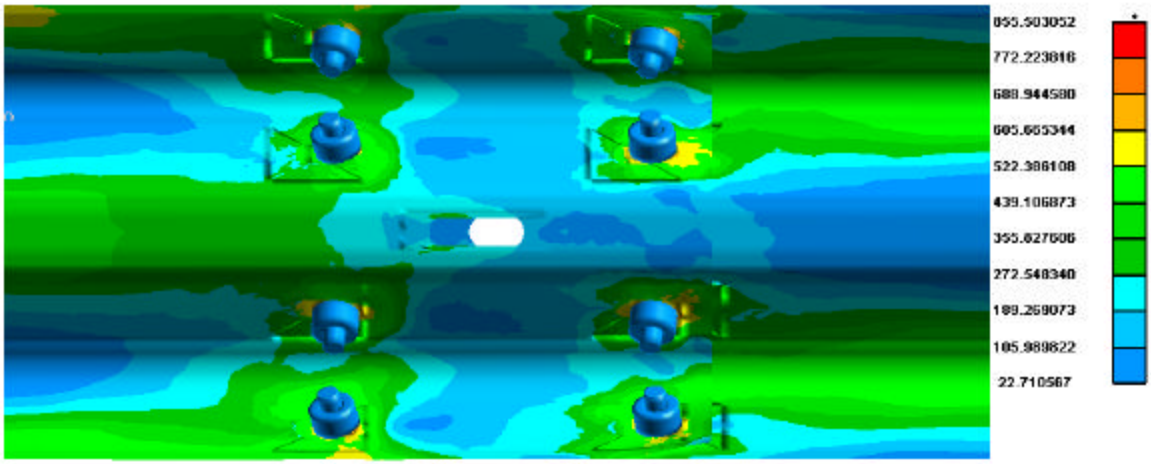

Figure 22: Von Mises stress (back-view) in the uniaxial splice pull simulation.

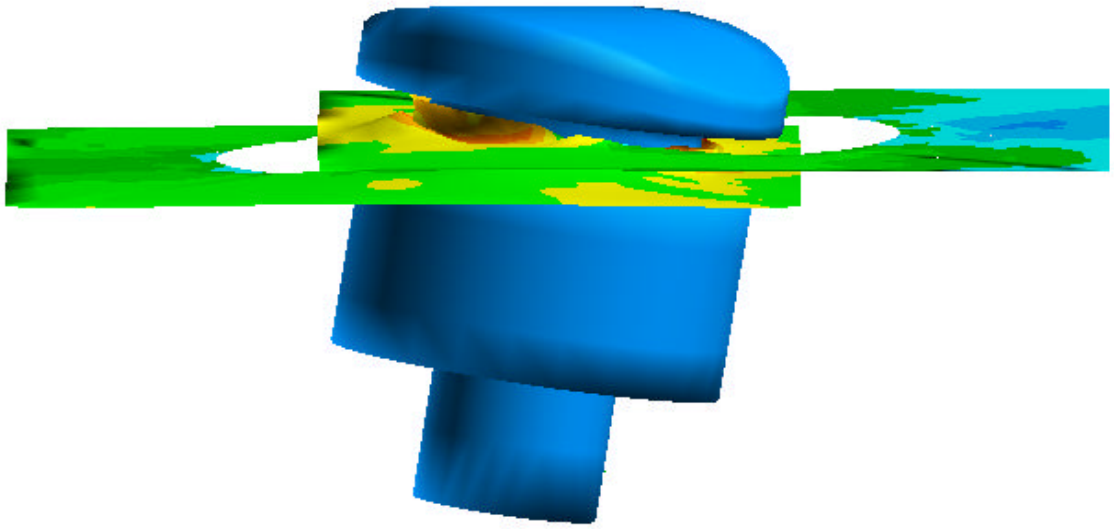

Figure 23: Rotating bolt in the uniaxial splice pull simulation.

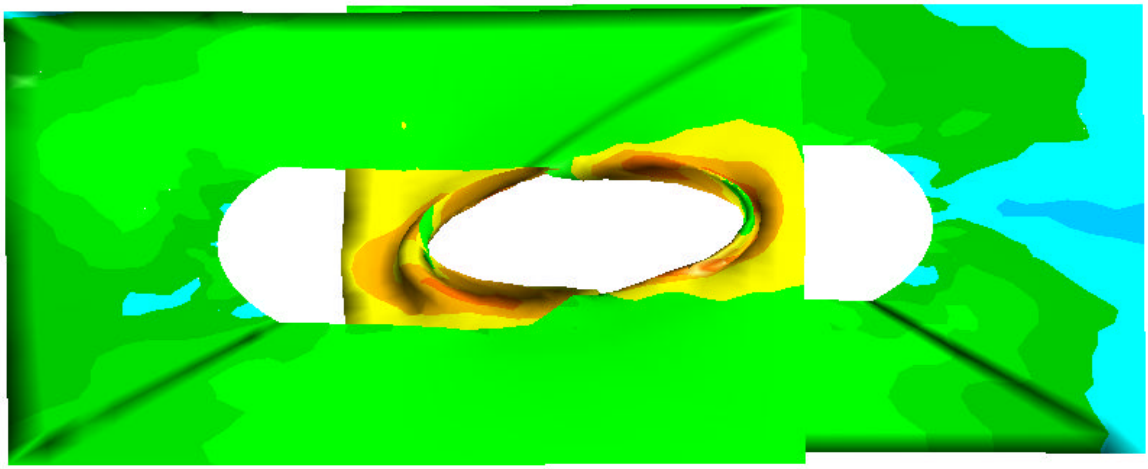

Figure 24: Guardrail material deformations in the uniaxial splice pull simulation.

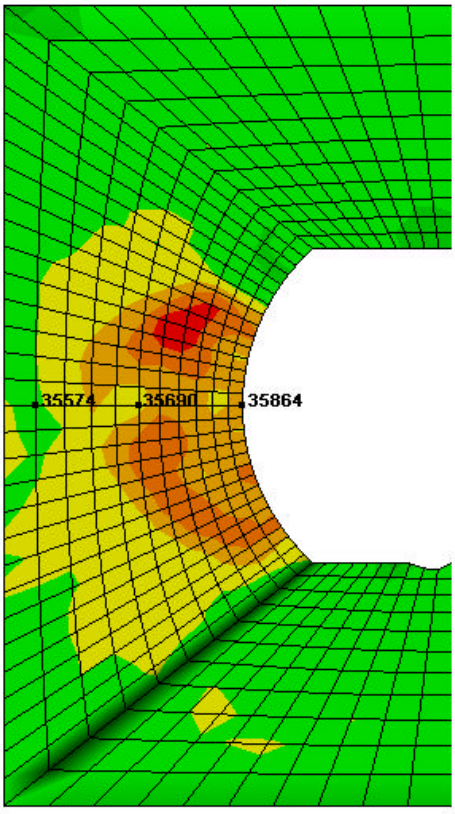

Figure 25: Stress concentration (undeformed view) in the uniaxial splice pull simulation.

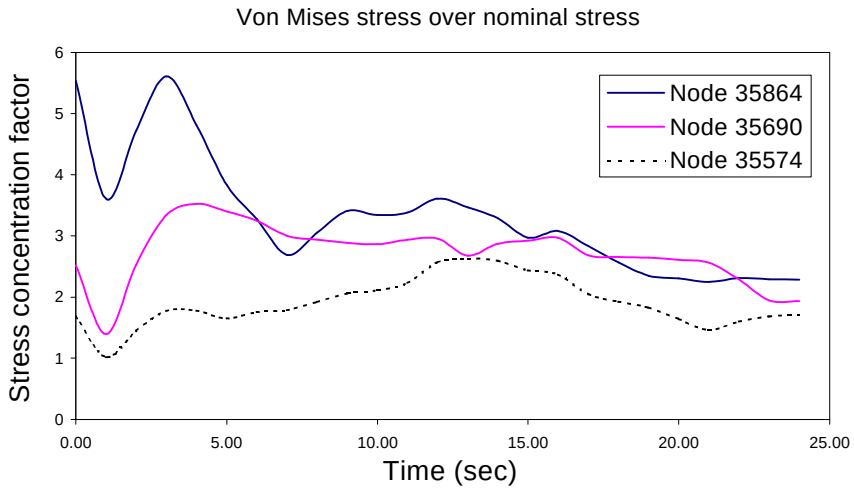

Figure 26: Stress concentration factors around splice holes.

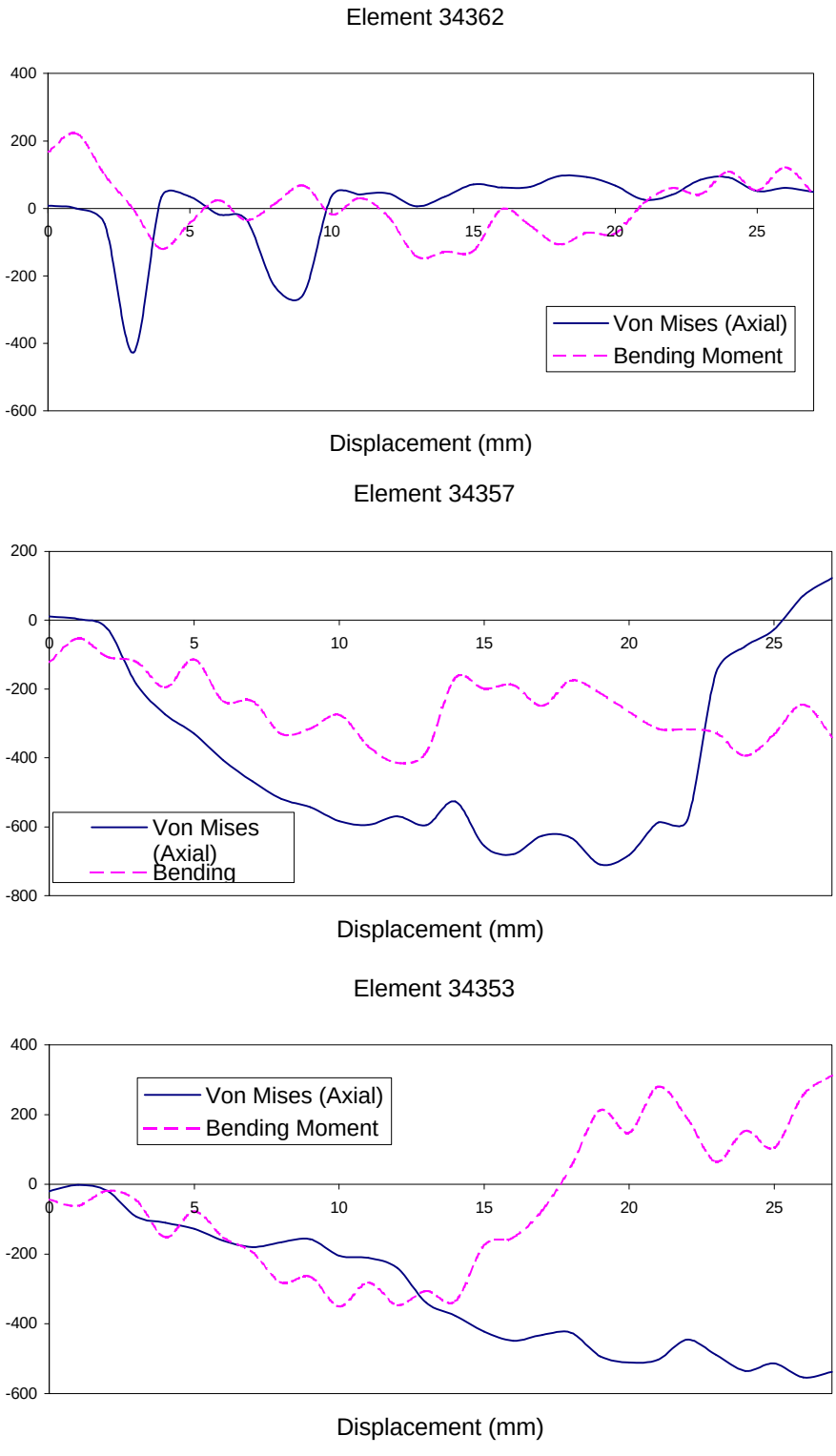

Figure 27: Axial Von Mises stresses and bending moments.

3.6 Evaluation of finite element model of the splice

Three uniaxial tensile laboratory tests of the splice connection were performed and a finite element model of the splice was developed. The uniaxial tensile test was then simulated in a finite element analysis using the splice model. The resulting force-displacement curves for two of the physical tests and also the simulated test (labeled Material 3) are shown in figure 20. Comparing physical and simulated test results is a good way to evaluate the performance of a model. This section describes such a comparison for the splice model.

The maximum load (failure load) in the physical test was approximately 400 kN and in the simulation 350 kN. The displacement at maximum load was 24 mm in the physical test and 26 mm in the simulation. No failure mechanism was implemented in the finite element model but the load leveled off at the same displacement in the simulation as it did in the physical test indicating the point of failure. There were differences between the slopes of the two physical load curves and also that the simulated load curve followed a more leveled path than the physical tests. The differences in slope of the two physical force-displacement responses indicate that the simulated force-displacement curve may fit within a broad envelope of load curves if a lot of physical tests had been performed. A reason for the differences between the two physical test responses could be that the splice connection is sensitive to how the two layers of W-beam are lined up relative to each other.

The simulated curve follows the laboratory curves reasonable well up to approximately 125 kN where the slope of the curve decreases considerably. The bolts in the simulation start to rotate at this point creating stress concentrations where the head of the bolt and edge of the nut cut into the material around the hole. This can be seen as local high stresses in the simulation and torn material in laboratory tests (compare figures 11 and 24).

The differences between the simulation test results and the physical test results were explained by poor performance of the shell elements when edge loaded. Shell elements are weak when loaded axially and bend too easy. When the element cannot take more axial load it bends down. The splice bolts start to rotate as the material around the splice hole bend against the bolt shank and the stress-displacement curve drops, which was what happened at 125 kN.

A new analysis was performed in order to verify this theory. An artificial way to increase the axial strength of the shell elements located closest to the bolt shank is to increase the friction between bolts and splice holes. This makes it harder for the edge of the hole to bend against and slip down the bolt shank. Both the static and the dynamic friction coefficient were set to 5.0 and the analysis was performed again. The higher friction coefficients were added very locally between bolts and splice holes. The load-displacement curve labeled “Material 3, Friction Coeff = 5” in figure 20 shows that the simulated force-displacement curve becomes more similar to the laboratory test curves by

adding friction essentially confirming the theory. The simulation curve corresponded well with physical test results up to 200 kN when higher friction coefficients were used.

Other solutions were tried in order to stiffen up the elements. It was, for instance, discovered that the material had thickened considerable around the holes in the physical tests, which complicate the rotations of the bolts. This could be one reason why the splice is stiffer in the laboratory than the simulated test is. It showed up to be very hard to implement shell thickening in the model. There was not enough time to examine this phenomenon in more detail in the scope of this research.

The model is considered to perform well enough to use for further research concerning the splice connection since the basic behavior of the model agrees with physical tests and maximum displacement and stress values correspond to physical test results. The axial tensile test is considered as “worst case” due to the incidence of high axial loaded shell elements. The model is assumed to work better for other cases with a more diverse loading. The stresses in the full-scale crash-tests usually stays between 100 to 150 kN and the simulation results agrees pretty well with laboratory test results in this area.

A finite element sub-model was developed to explore how the splice performs in a full-scale crash situation. This model consisted of a G2 weak-post and the W-beam with the splice connection at the post. The model was subjected to loads collected from the rail section at a particular post in full-scale crash simulation.

3.7 Sub-model of post and W-beam with splice

The sub-model shown in figure 28 consists of a G2 weak-post and the W-beam with the splice connection at the post. In order to investigate the performance of the splice in a full-scale crash situation, load conditions were collected from the system in the region of a particular post in a full-scale crash simulation and applied to the guardrail ends in this sub-model. This way, the full-scale crash test could be simulated just studying the particular post and the performance of the splice could be examined in detail. The vehicle in the full-scale crash simulation impacted the G2 installation mid-span between post 6 and 7. Post 8 was the study post (figure 58). It would be unreasonable to model the splice connection in detail in a full-scale model due to the computational time requirements. In order to decrease the analysis time further the loads were applied five times faster in the sub-model than they appeared in the full-scale simulation. The W-beam was attached to the post with a spot weld that was set to fail at a tensile load of 20 kN corresponding to the failure load of the 7.94 mm diameter A307 bolt used in a standard G2 post-rail connection.

The details of the full-scale simulation from which the loads were collected, and the details of how these loads were applied to this sub-model, as well as the material properties and post-ground connection are discussed in detail in chapter 5.2 and 5.3. The properties of this model will not be discussed further in this section.

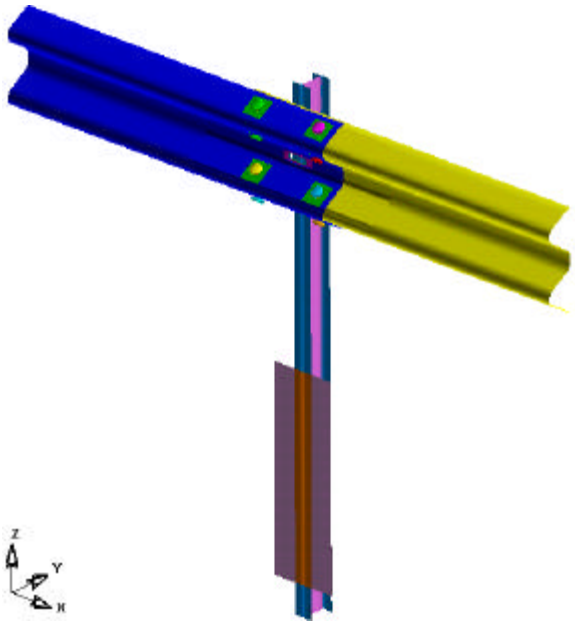

Figure 28: Sub-model of post and splice.

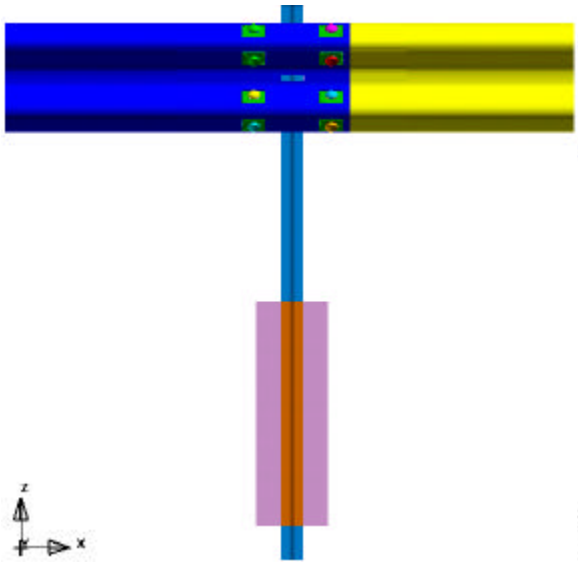

Figure 29: Front-view of sub-model.

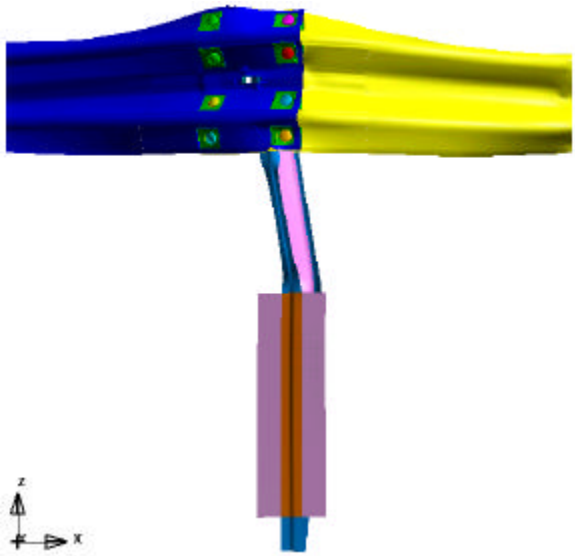

Figure 30: Front-view of deformed sub-model.

The rail displaced longitudinally upstream relative to the study post due to large lateral deflections in the impact event (figures 29 and 30). The post was twisted as it bent back

allowing the sharp edge of the twisted post to come in contact with the back layer of W-beam. When the post-rail connection failed the W-beam started to slide up against the post flange and, eventually, should have been pulled over the top of the post. Due to contact problems the analysis was terminated before this could happen. Though, the simulation was carried out far enough to draw conclusions about why guardrails occasionally fail at the splice. As shown in figures 31 and 32 there was a high stress concentration at time 34 msec. through the cross-section of the back layer of W-beam. This stress concentration passed through the right column of splice bolts. The stresses in the front layer of W-beam were much smaller than in the back layer and were of no significance regarding tearing. The high stresses were released by flattening out the W-beam at the stress concentration as is shown in figure 33. A plastic hinge was developed at the cross-section through the four right splice bolts and the W-beam was somewhat folded around the post at this location. The plastic hinge is clearly visible in figure 34 which shows the effective plastic strain in the back layer of the guardrail at time 42 msec. The sharp edge of the post flange contacted the back layer of W-beam at the lower edge of the rail were the effective plastic strain was really high as shown in figure 34. A tear would probably be initiated at this point in a crash test. A plastic hinge always follows a path through the highest stresses and strains as it propagates through material. Based on that fact, the most probable path for a tear to propagate through the cross-section of the back layer of W-beam was predicted and drawn in figure 34. The tear is most likely to follow a path close to, or through, the right four splice holes.

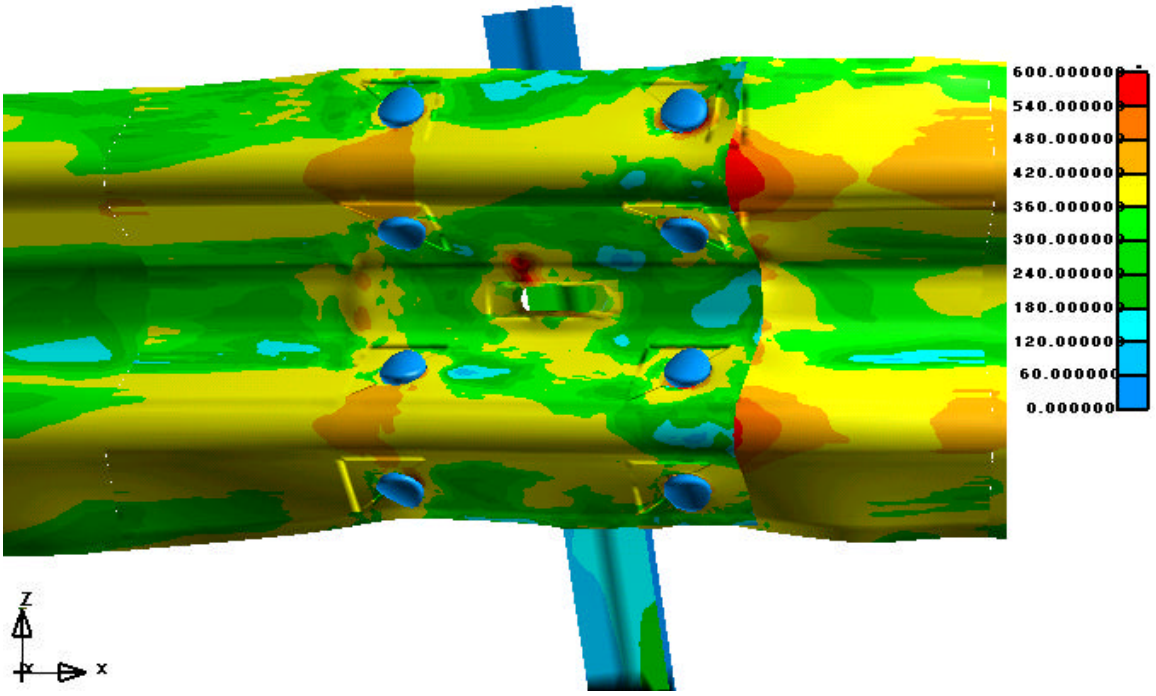

Figure 31: Von Mises stress contour plot at time 34 msec.

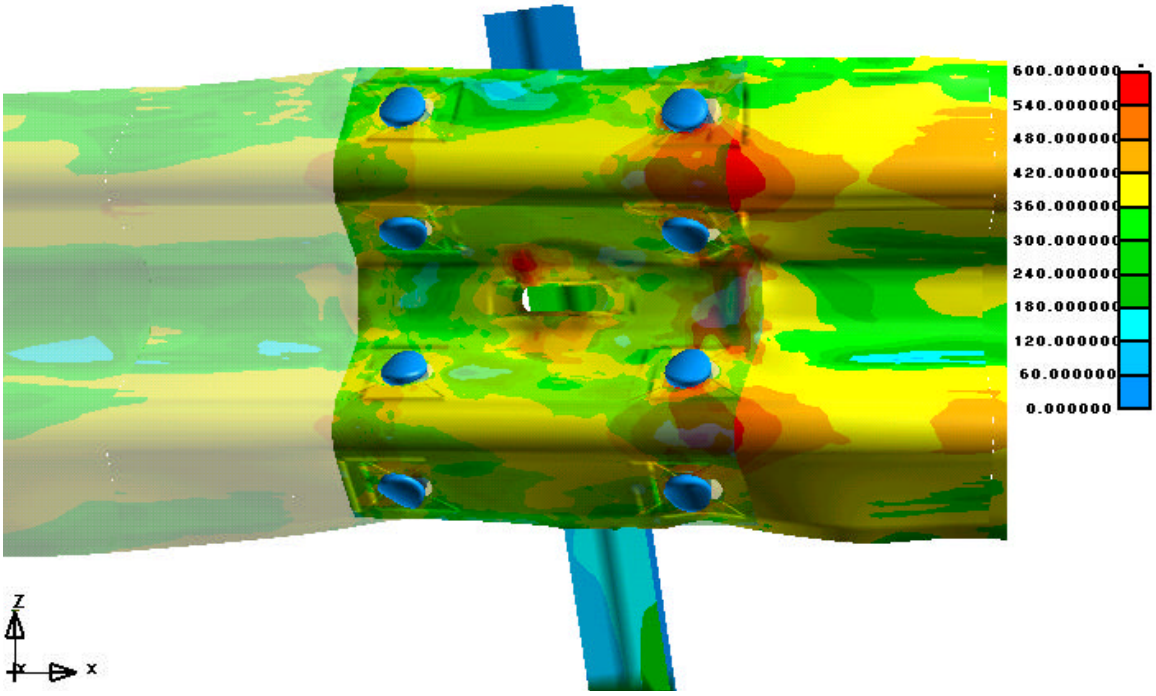

Figure 32: Von Mises stress contour plot at time 34 msec. showing back layer of guardrail.

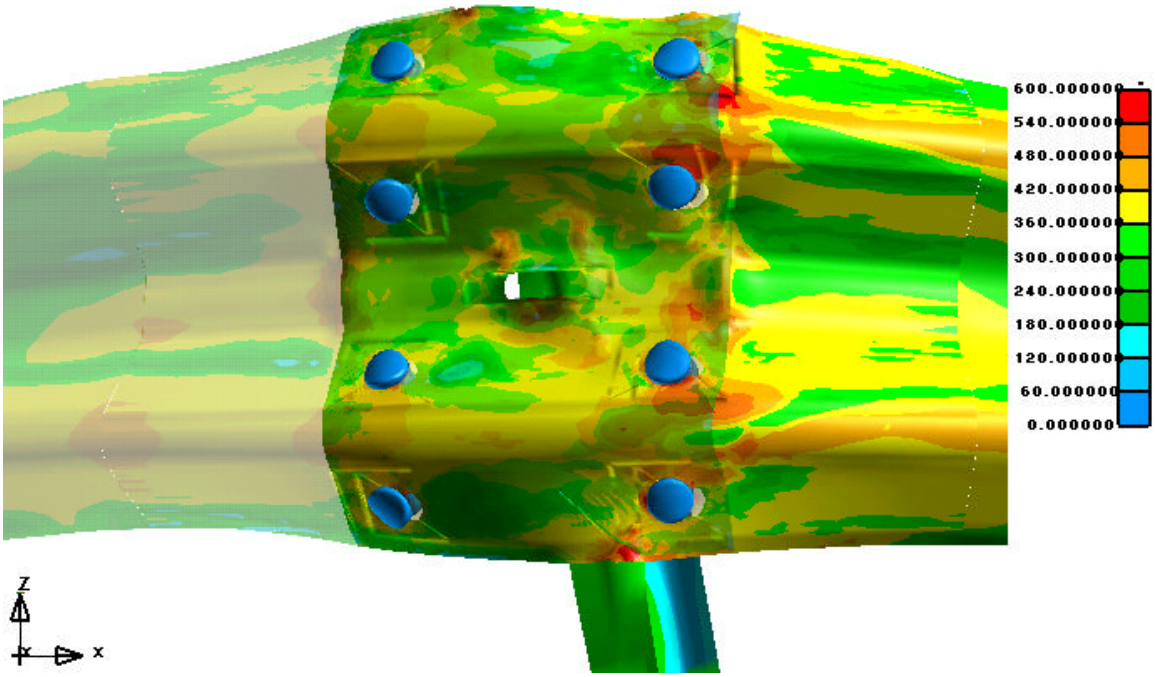

Figure 33: Von Mises stress contour plot at time 39 msec. showing back layer of guardrail.

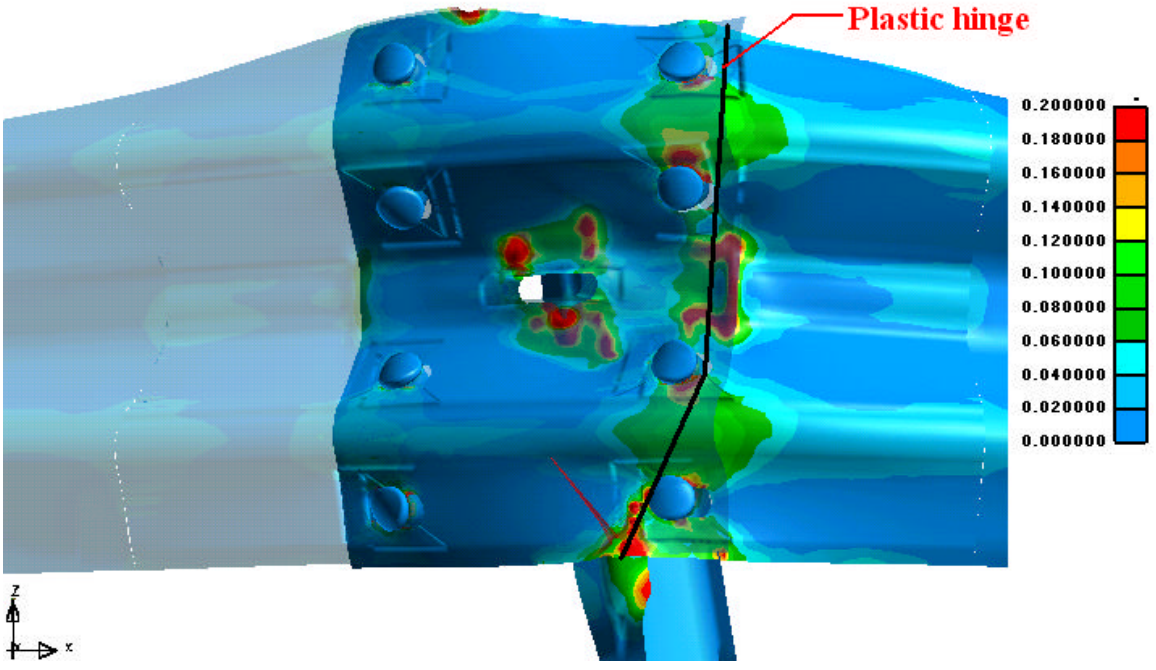

Figure 34: Effective Plastic Strain plot at time 42 msec. showing back layer of guardrail.

In order to confirm the splice failure theory derived from the finite element simulation the literature sources in the literature review concerning splice failures in full-scale crash tests were studied in detail. If the failures in the physical crash tests correspond to the suggested crack path in figure 34, then the theory will be confirmed.

3.8 Characteristics of splice failures

This section is a summation of the six full-scale crash tests in the literature review where the guardrail system failed to meet test requirements due to splice failure. The characteristics of these tests are summarized in Table 4. Most reports are sparse with data regarding splice failures, probably because it is unexpected when it happens. There is only one reference in this compilation of crash tests where the splice failed in a G2-system. Splice failures are, though, more general and occurs in all W-beam barrier systems that use the same splice connection as the G2-system. The design of the splice is the same in the G4-system and the MELT terminal and the characteristics of the splice failures observed in full-scale crash tests are similar for all systems with this connection.

The first conclusion from these splice failures was that the tear always passed through at least one splice hole and often through all four of the splice holes in the cross-section of the W-beam. Now remained to determine if the tear occurred at the same column of splice holes in the physical tests as predicted in the simulation and if the tear followed approximately the same path as predicted. In the simulation a tear would occur in the back layer of W-beam at the downstream column of splice holes and follow the path

drawn in figure 34. The tear would probably be initiated at the lower edge of the W-beam. The figures and impact descriptions of the crash tests in the test reports were studied and it was determined whether the splice failure in a particular test corresponded to the prediction derived from the FE-simulation or not. Four out of the six splice failures corresponded well to the prediction. It was not possible to tell from the information presented in the reports of the two remaining tests whether the failure happened as predicted or not although the tear passed through all four of the splice holes in the cross-section of the W-beam in both these tests indicating that the rail probably ruptured as predicted in these tests also.

Figures 35 and 36 shows a typical splice failure. These figures are from a test where a 1500-kg Chevrolet Lumina impacted a G4-system between post 13 and 14.(17) The authors describe the rail rupture as follows: “At 0.112 s, a tear appeared at the lower edge of the W-beam rail at post 15… The W-beam rail element ruptured at 0.122 s.”(17) Figure 36 shows the location of the study post where the rail tore and also the posts between which the vehicle impacted the system. Figure 35 shows a close-up view of the ruptured rail element. The back layer of W-beam at post 15 tore at the downstream column of splice holes. The tear was initiated at the lower edge of the W-beam and followed a path through all four splice holes. The failure corresponded to the prediction.

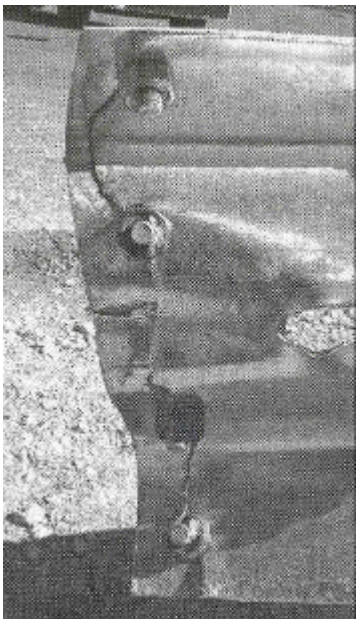

Figure 35: Close-up view on ruptured rail.(17)

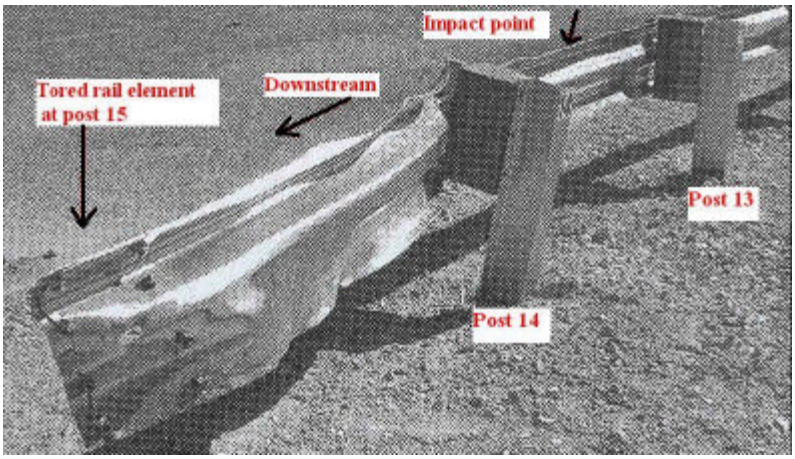

Figure 36: Location of splice failure and interesting posts.(17)

Figure 37 shows the ruptured rail element in TTI test 405541-4.(18) The back layer of W-beam tore at the downstream column of splice bolts as predicted from the FE-simulation. The tear was initiated at the lower post hole and followed a path very similar to figure 34.

Figure 37: Ruptured rail element in TTI test 405541-4.(18)

Figures of the torn rail elements from the crash tests described in reference 16 and 19 are shown in the literature review.

	Reference					
	11	15	16	17	18	19
Barrier Type	G2	G4	G4	G4	MELT	MELT
Test conditions	A	B	A	C	D	E
Max lateral deflection (m)	1.5	0.68	1.0	-	0.53	0.3
Rail tension at failure (kN)	-	-	130	-	-	-
Splice holes with cracks	4	4	1	4	1	4
Splice displacement at failure (m)	-	-	0.035	-	-	-
Failure similar to FE-simulation	Not known	Yes	Yes	Yes	Yes	Not known

Table 4: Characteristics of full-scale crash-test splice failures.

A. NCHRP Report 350 level 3-11: 2000-kg pickup, 100 km/h, 25 degrees.
B. Non Standard Test: 4X4 2300-kg pickup Truck, 110 km/h, 20 degrees.
C. Non Standard Test: 1500-kg passenger car, 100 km/h, 25 degrees.
D. NCHRP Report 350 level 3-34: 820-kg passenger car, 100 km/h, 15 degrees.
E. NCHRP Report 230 level S31: 2000-kg passenger car, 100 km/h, 25 degrees.

3.9 Conclusions

Since the splice failures observed in full-scale crash tests corresponded with the tearing theory derived from the finite element simulation, the theory was considered proven to be correct. The guardrail occasionally ruptures at the splice since a plastic hinge is developed at the downstream column of splice holes where the rail is bent around the post. The sharp edges of the splice bolts and splice nuts or the sharp edge of the post flange initiates a tear at the stress and effective plastic strain concentration. The tear propagates through the cross-section of the W-beam following the path marked in figure 34. The problem is the splice bending around the post. The most straightforward way to solve this problem is to move the splice to the mid-span between posts where it will be loaded more in tension than bending.

4 POST-RAIL CONNECTION

4.1 Introduction

Prior full-scale crash tests of the weak post W-beam guardrail have resulted in failures where the vehicle either overrode the guardrail or penetrated it.(3) (11) Reviewing of high-speed videos of prior tests revealed that one source of this poor performance was the post-rail connection detail. This section describes laboratory tests and full-scale crash tests done in the developing process of an improved post-rail connection.

The post-rail connection is supposed to fail in the early stages of the crash so that the guardrail is released from the post instead of being pulled down with the post. When the rail detaches early in the impact event it will remain in contact with the fender of the vehicle and be more effective in redirecting the vehicle. If the connection fails too late, the rail will be pulled to the ground along with the post and this may result in the vehicle vaulting over the barrier.

The weak-post W-beam guardrail system is a flexible traffic barrier. While redirecting an impacting vehicle, large lateral deflections are expected. The guardrail redirects the vehicle by transforming lateral forces into longitudinal tensile forces in the guardrail. The lateral deflection forces the posts to bend to the ground or break. The rail has to separate from the post at an early stage to prevent pulling the rail down with the post. If the rail height is decreased too much, the vehicle may override the barrier or the wheel may snag

the post. The desired performance of the post-rail connection is to fail at a low load level early in the impact event.

The separation mechanism for the current connection is for the bolt to fail and thereby release the guardrail from the post. Full-scale crash tests have shown, however, that current post-bolt connection behavior is inconsistent and unrepeatable. The objective of this section of the report was to design a connection with a more consistent and reliable failure mechanism.

Laboratory tests were performed on the existing post-rail connection to determine its characteristics and performance. From these results two new alternative connections were developed and tested. The most promising of the alternatives was then implemented in a complete G2-system and tested in a full-scale crash test.

4.2 Existing Connection

The current connection consists of:

- Two layers of guardrail (e.g., the post-rail connection is at a splice),
- One 7.94-mm (5/16-in) diameter A307A bolt,
- One 2.67 mm thick (12-gauge) square washer between the bolt head and the guardrail and
- One nut.

Several quasi-static load tests were performed on the existing connection. First, a series of tests was performed to determine the axial tensile capacity of the bolts themselves. According to the AISC Manual Of Steel Construction, the minimum tensile strength of a 7.94-mm diameter A307A bolt is 20 kN.(6) In Table 5, the bolts used for test one to three came from the PTI crash-tests and the bolts that were used for test four to six came from a PennDOT maintain garage. All the PTI bolts were above the minimum failure strength but that was not the case with the bolts obtained from the district maintain garage, which were sometimes weaker than the specification.

Test	Failure Strength (kN)
1	27.3
2	27.0
3	26.1
4	22.4
5	15.4
6	19.9

Table 5: Tensile strength of 7.94-mm diameter A307 galvanized bolts.

The loading experienced by the bolt during an impact is not necessarily a pure axial load. In order to explore the performance of the connection under a variety of more realistic loading cases, the connection was subjected to several quasi-static load tests. The tests were performed with a Tinius-Olsen 1780-kN (400,000-lbs) load test machine.

Two different support setups were used: (1) the guardrail mounted at a 30 degree slope about the rail axis (figure 38) and (2) the guardrail mounted at both 30 degrees from the guardrail axis and 15 degrees from the post axis (figure 39). These orientations were selected to represent the loading experienced by the connection as the post is bent back and twisted during an impact. The post bolt was positioned in two different positions of the guardrail slot, centered or at the edge. The ends of the rail section were anchored to the test machine base and the test machine grips were used to pull on the web of the post. This resulted in the loading being applied to the bolt in a manner similar to what would be experienced in a full-scale crash test but quasi-static instead of dynamic. The loading was applied at a rate of 89,000 N/minute.

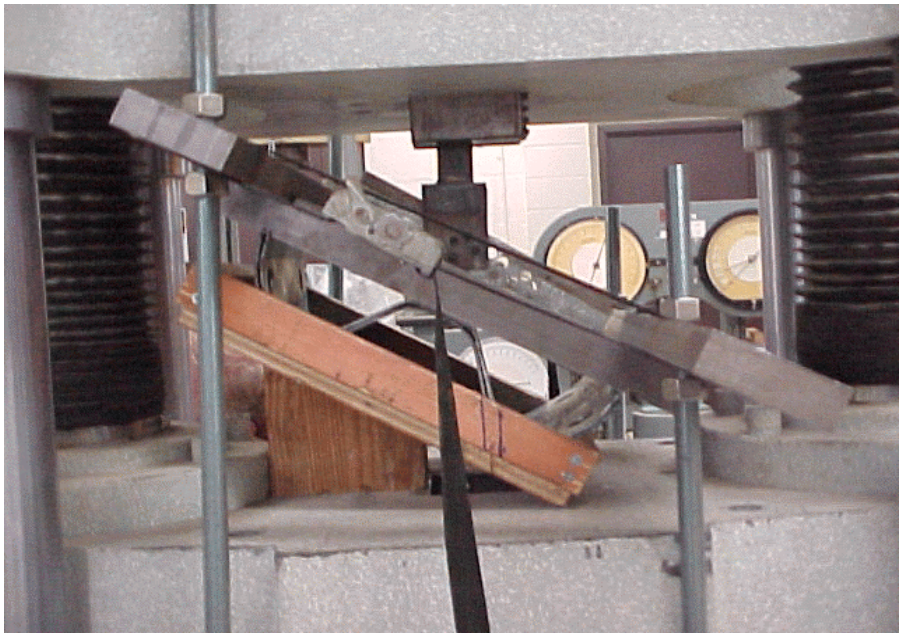

Figure 38: Test setup for the 30/0 degree load test.

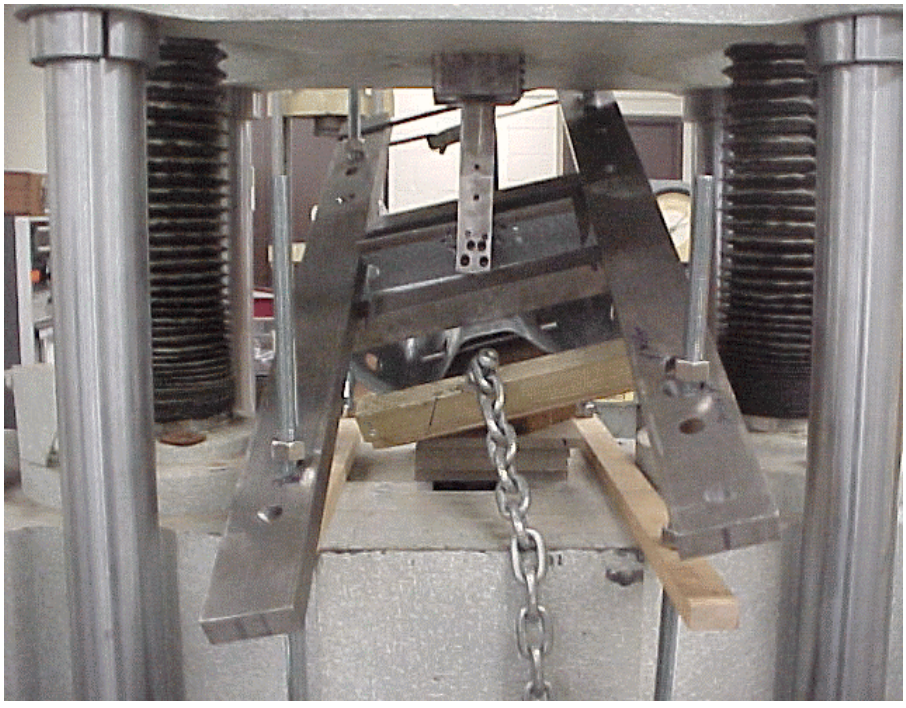

Figure 39: Test setup for 30/15 degrees load test.

Test	Orientation	Ultimate Force (kN)	Failure Type
99072001	30/0 edge	19.4	Washer pulled through slot
99072002	30/0 edge	19.9	Washer pulled through slot
99100601	30/0 centered	27.0	Washer pulled through slot
99072701	30/15 edge	22.5	Nut stripped threads
99073001	30/15 edge	17.7	Nut stripped threads
99080201	30/15 edge	18.5	Washer pulled through slot

Table 6: Summary of test results for existing connection.

The laboratory test results with the two different setups are presented in Table 6. The results showed that the connection behavior is inconsistent and has some undesirable features. In some cases the washer was pulled through the slot of the guardrail as shown in figure 40. In other cases the nut stripped the bolt threads as shown in figure 41. The load required to cause the connection to fail was sometimes as high as 27 kN. Although the load required to pull the washer through the guardrail slot, in most cases, was about the same as that required to fail the bolt, pulling the washer through the slot takes a lot of time and displacement. In a full-scale crash-test, this long duration failure may result in the rail being pulled with the post to the ground.

Similarly, the nut is stripped off the bolt in a series of jerks that require both time and displacement. This might result in a long duration failure where the rail is pulled down

with the post. Figure 44 shows the force-displacement curve for a series of jerks in a later performed test where the nut stripped the threads.

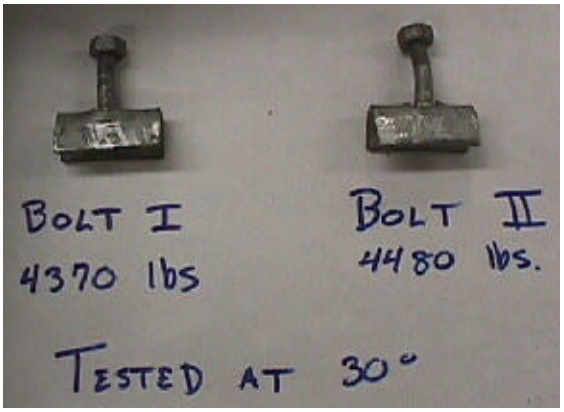

Figure 40: Result of test 99072001 and 99072002 showing the failed components.

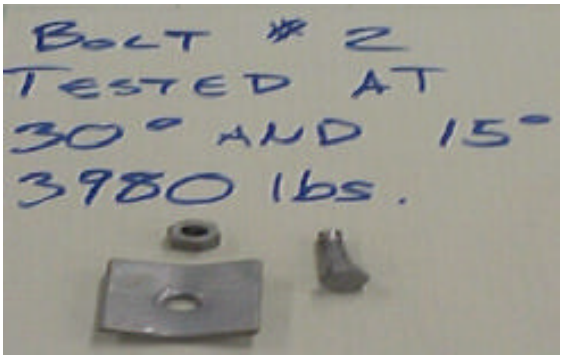

Figure 41: Result of test 99073001 showing the failed components.

The desired performance of this connection is for the bolt to fail at a low force level and for the failure to happen quickly. The failure mechanism also needs to be consistent and not sensitive to the direction of loading. The existing connection exhibits several different failure mechanisms (e.g., nut stripping threads, pulling the washer through the slot and bolt failure). The loads that cause failure are variable and the displacement that causes failure is relatively large. For these reasons, the existing connection is not considered to result in good impact performance.

4.3 Improved Connection

Some new alternatives were developed and tested in order to achieve a more consistent connection failure mechanism. Two new alternatives were tested.

The first design consisted of:

- One layer of guardrail (e.g., connection to post is not at a splice),
- One 7.94-mm diameter A307A bolt,
- Two 2.67 mm thick square washers between the bolt head and the guardrail and
- One nut tightened one full turn past snug.

In this design there is only one layer of guardrail because the splice connection has been shifted to the mid-span away from the posts. The reason for this is to prevent the splice from bending around the post. Excessive bending of the splice together with high tension in the rail could induce tearing and rupturing of the guardrail as described in chapter 3. Two washers are used instead of one in order to prevent the washers from being pulled through the guardrail slot.

A new series of quasi-static tests were performed to determine the performance of this new connection. As shown in Table 7, the nuts stripped off the bolt threads in the two tests. The force required to strip the nut off varied considerably between tests and was unacceptably high for the second test (test 99100701). In addition to the high force in the second test, the nut was stripped off the bolt in a series of jerks that required an additional

3 mm of displacement to fail the connection (figures 42 and 43). The force that was required to strip the nut off was considerably lower in the first test (test 99100602). Instead the jerking behavior was more prominent and an additional 14 mm of displacement was required to fail the connection because of the series of jerks (figure 44). The extensive amount of time, displacement and load required to strip the nut off the threads could result in the rail being pulled to the ground in a full-scale test so this alternative was not considered acceptable.

Test	Orientation	Ultimate Force (kN)	Failure Type
99100602	30/0 centered	18.7	Nut stripped threads
99100701	30/0 centered	32.9	Nut stripped threads

Table 7: Summary of test results for design alternative 1.

Figure 42: The result of test 99100701showing the failed components.

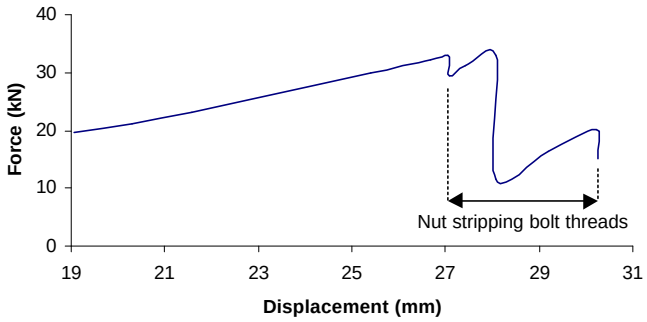

Figure 43: Force-displacement graph for test 99100701.

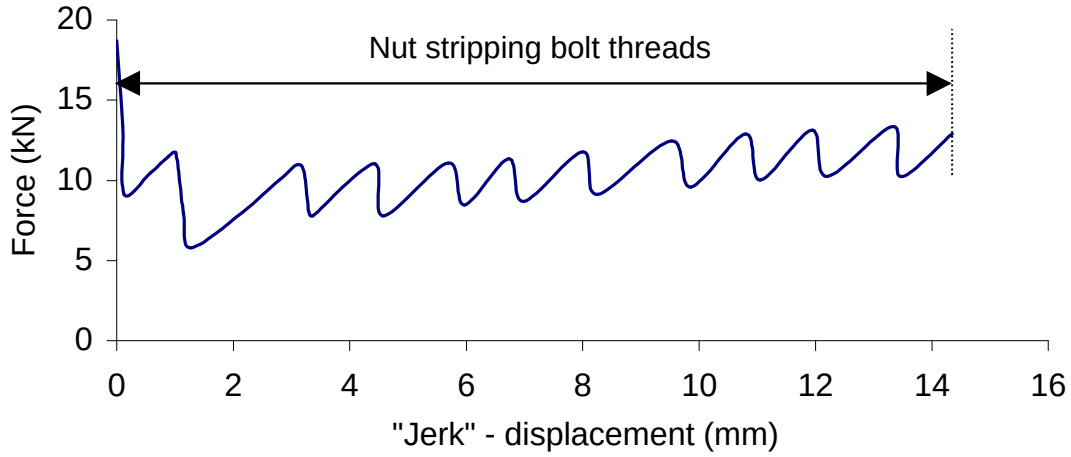

Figure 44: Force verses "jerk"-displacement graph for test 99100602.

Since the performance of the connection was not sufficiently improved, no further tests were performed on this design alternative. A second alternative connection was designed to prevent the nut from stripping threads and concentrate the failure in the bolt.

The second alternative consisted of:

- One layer of guardrail (e.g., the connection is not at a splice),
- One 6.35-mm (1/4-in) diameter A307A bolt,
- Two 2.67 mm thick square washers between the bolt head and the guardrail,
- Two nuts tightened one full turn past snug and
- One circular washer between the nuts and the post.

A weaker bolt than the former one is used in order to obtain an early failure of the bolt at a lower load level. Two nuts are used to prevent the nut from stripping the bolt threads

and to force the failure to occur in the threads of the bolt. The circular washer was used because the standard hole in the weak-post are sized for the 7.94-mm diameter bolts and are therefore a little large for the 6.35-mm diameter bolt. If the post were manufactured with smaller holes more appropriate for the 6.35-mm diameter bolt the circular washer could be eliminated.

The connection was tested at two orientations and with the connection positioned in two places in the slot. In the first several tests the connection was centered in the slot whereas in the third test the bolt was pushed to the edge of the slot to determine if the edge reinforced the connection resulting in a higher failure load. As shown in Table 8, the second design alternative resulted in a consistent failure of the bolt at a load of about 16 kN. The connection always failed by fracturing the bolt through the threads and the connection was not sensitive to the position of the bolt in the slot or the orientation of loading. In fact, the ultimate load decreased somewhat as the loading became more complicated. The double washers showed no sign of bending or pulling through the guardrail slot. The performance of design alternative two was considered acceptable and an improvement over the original design. Figures 45 and 46 show the failed components and the force-displacement curve for one of the tests.

Test	Orientation	Ultimate Force (kN)	Failure Type
99100702	30/0 centered	17.1	Bolt fractured
99100703	30/0 centered	17.8	Bolt fractured
99100704	30/0 edge	18.0	Bolt fractured
99101101	30/15 centered	13.4	Bolt fractured
99101102	30/15 centered	16.3	Bolt fractured
99101103	30/15 centered	13.0	Bolt fractured

Table 8: Summary of test results for improved connection 2.

Figure 45: Result of test 99101102 shows the failed components.

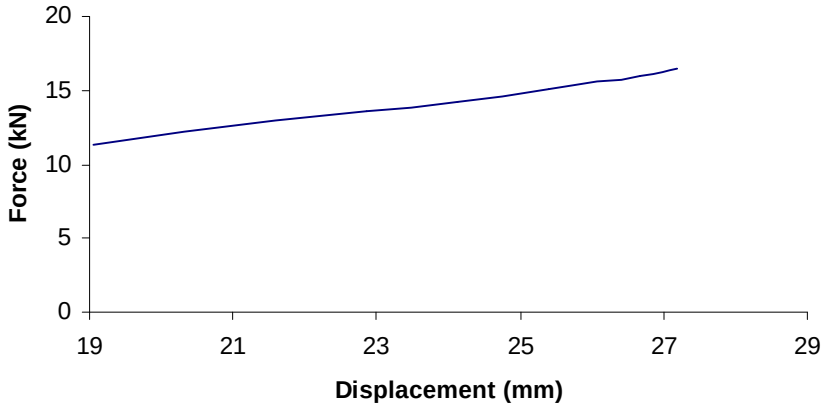

Figure 46: Force-displacement graph for test 99101102.

Conclusions from laboratory tests

An improved connection for the weak-post W-beam guardrail has been developed and tested. The connection uses two 2.67 mm thick (12-gauge) square washers under the head of a 6.35-mm (1/4-in) diameter A307A bolt. Two nuts tightened one turn past snug are used on the post side with one circular washer under the nuts. Splice connections are located between the posts. This connection consistently fails at a load of about 16 kN and the failure occurs quickly so that the guardrail in an impact should be able to separate easily from the post.

The connection was tested in a full-scale crash test implemented in a complete weak-post W-beam system.

4.4 Full-scale crash test (TTI 473750-1)

A full-scale crash test was performed on the 23rd of November 1999 at the Texas Transportation Institute with the improved connection implemented in a complete guardrail installation. The test installation was a standard G2-system modified with the new connection detail (e.g., one 6-mm diameter ASTM F568 Class 4.6 bolt with two square washers under the bolt head (figure 47) tightened with two nuts and a circular washer (figure 48)). Beginning in 1995 SI units were supposed to be used in all highway design. The bolts used in the full-scale crash test were, therefore, SI unit specifications rather than the U.S. Customary Units (USCU) specifications used in older specifications. The material properties of the USCU A307A bolt correspond to the properties of the metric ASTM F568 Class 4.6 bolt. The metric bolt that matches the 6.35-mm (1/4-in) diameter A307A bolt best in size is the 6-mm diameter bolt. The splice was positioned mid-span between posts (figure 49). The test was performed at NCHRP Report 350 test designation 3-11 (i.e., a 2000-kg pickup truck impacting the guardrail system at the impact speed of 100 km/h and with 25 degrees impact angle).

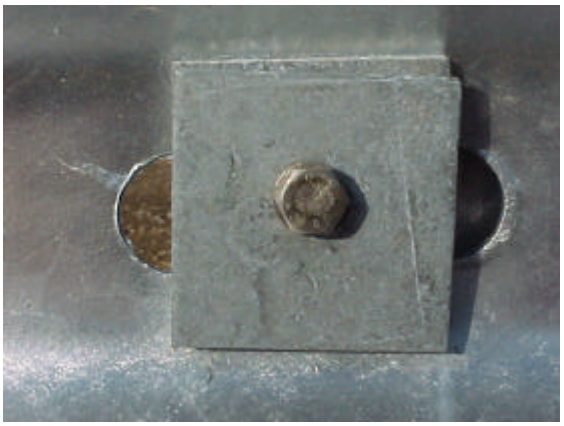

Figure 47: Post-rail connection detail showing one 6-mm diameter bolt and two square washers.(9)

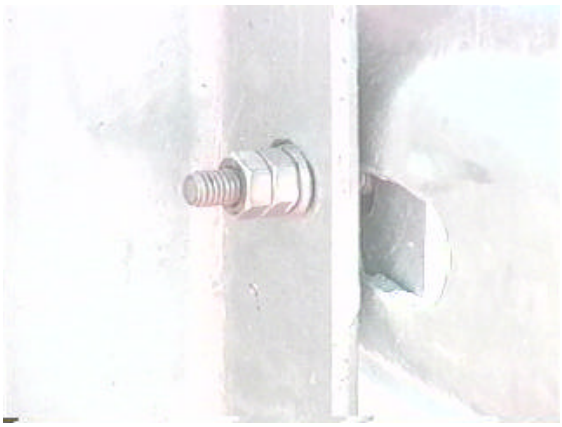

Figure 48: Post-rail connection detail showing two nuts and a circular washer.

As shown in figure 50 to 52, the rail unexpectedly tore and the vehicle penetrated the barrier. The failed guardrail end can be seen in figure 53.

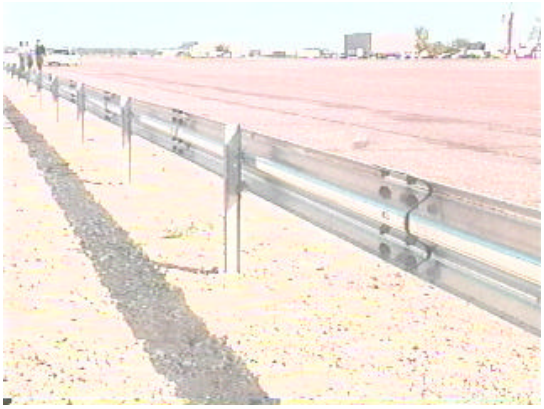

Figure 49: Guardrail installation of a modified G2-system with splice connection between posts.

A more positive result from this test was that the post-rail connection work properly. Figure 54 shows that the rail was released upstream from impact point, which indicates that the connection fails easily. Figure 55 shows that the bolt failed without stripping nuts or pulling the washers through the slots.

Figure 50: Crash sequence just before rail rupture (TTI 473750-1).

Figure 51: Crash sequence at rail rupture (TTI 473750-1).

Figure 52: Crash sequence after rail rupture (TTI 473750-1).

Figure 53: Torn guardrail.

Figure 54: Damage looking up-stream from the impact point.

Figure 55: Post-test view of connection components.(9)

It was difficult to observe the actual guardrail fracture in the full-scale crash test. The fractured guardrail segment shown in figure 53 was positioned at post 8. It appears, from viewing high-speed videotapes of the crash test, that the tear initiated when the rail was pulled over the top of post 8 creating a nick at the lower edge of the rail. This nick is shown in figure 50. The rail ruptured completely when the nick came to the tension side of the vehicle as shown in figures 51 and 52. The maximum tensile rail force upstream from impact point, as obtained from strain gauges, was 275 kN, and the maximum tensile strain downstream of the impact point was 151 kN.(9) The combination of a small cut and significant tension in the guardrail caused the crack to propagate through the cross-section of the rail and resulted in complete rupture of the rail. The rail was also fractured at other posts. Figures 56 and 57 show that tearing was initiated at the lower edge of the W-beam at other posts as well. These damages were similar to the nick that finally ruptured the rail. However, the tension in the rail at these other locations was never high enough to propagate the tear through the cross-section of the W-beam and rupture the guardrail completely. The conclusion is that the nicking and tearing of the rail is not a random phenomena but happens at every post as the rail is released from the post and pulled over it.

Figure 56: Guardrail tear initiated at a post.(9)

Figure 57: Rail deformation at a post.(9)

4.5 Summary

An improved post-rail connection for the weak-post W-beam guardrail was developed and tested in the materials laboratory. The connection used two 2.67 mm thick square washers under the head of a 6.35-mm diameter A307A bolt. Two nuts tightened one turn past snug were used on the post side with one circular washer under the nuts. The splice connections were positioned mid-span between the posts.

A full-scale crash test of a complete G2-guardrail system modified with the new post-rail connection was performed at NCHRP Report 350 test level 3 conditions. In the full-scale crash test a 6-mm diameter ASTM F568 Class 4.6 was used instead of the 6.35-mm diameter A307A bolt. The material properties of these two bolts correspond but their properties are specified in different units. The A307A bolt is specified in U.S. Customary Units and the ASTM bolt is specified in SI units. The new connection performed well.

The guardrail installation in TTI test TTI 473750-1 failed to meet the Report 350 Structural Adequacy criterion since the W-beam tore and the vehicle penetrated the barrier.

The following chapter of this report describes further investigations that were performed, using finite element modeling, to determine the cause of the guardrail rupture and to determine possible modifications to the system that would prevent it from happening in the future. It also describes a full-scale crash test performed with the new modifications implemented in a G2-system.

5 GUARDRAIL RUPTURE

5.1 Introduction

When developing structures like guardrail systems, it is very time consuming and expensive to perform full-scale physical tests to evaluate the impact performance. It is, therefore, important to use laboratory testing and computer simulations to evaluate the effects of any changes made to the system before full-scale crash tests are performed. It is also difficult to collect enough data to tell what happened if an unexpected failure occurs in a real test. Computer simulations give the opportunity to redo a crash test, collecting all data needed, and investigate the failed component in detail.

The guardrail rupture in the preceding crash test was unexpected and the data that was collected did not provide enough information to explore the failure completely. Full-scale and sub-model simulations, using LS-DYNA, were used to study the impact in more detail concentrating on the post-rail connection.

LS-DYNA, a nonlinear explicit three dimensional finite element code for analyzing the large deformation dynamic response of inelastic solids and structures, was used for the finite element analysis.(8) The pre-processor TrueGrid was used to generate the geometry and mesh of the involved objects and to include springs, dampers, loads etc.(20) The output file from TrueGrid is processed using the program LS-INGRID in order to produce a LS-DYNA input file. After the input file has been equipped with contact interface cards, time-history cards, etc. the analyses are performed using LS-DYNA. The

results were examined using two different post processors: PostGL and eta PostGL. PostGL was used to view overall deformations of the system and to generate contour plots of various stress and strain components. Eta PostGL was used to process specific time-history information such as internal energy, cross-section forces and nodal displacements.

This section describes finite element simulations performed to explore the interaction between post and rail. The objective of these simulations was to determine why the guardrail ruptured and what could be done to prevent it from happening in the future. Some modifications of the installation setup were developed and tested in a simulation. Finally, a new full-scale crash test was performed with the new modifications included in a weak-post W-beam guardrail installation.

5.2 Full-scale finite element model

The full-scale crash test (TTI 473750-1) failed to meet NCHRP Report 350 requirements since the guardrail ruptured and the vehicle penetrated the barrier. High-speed videotapes of the crash event showed that a tear was initiated at post 8 when the guardrail was pulled over the top of the post. The tear could be seen as a nick in the lower edge of guardrail. The guardrail ruptured completely when the nick came to the tension side of the vehicle. Post-test investigations of damaged guardrail segments showed fractures on the lower edge of the rail at other posts as well, similar to the nick that caused the rail to rupture. This scenario was explored using a full-scale finite element model of the installation.

The guardrail model (i.e., the W-beam with splice connections and the turn-down terminal) was developed based on the models of standard guardrail components developed by Ray and Patzner.(13) The post-soil interaction was modeled using non-linear springs attached directly to the face of each post below the ground surface as described by Plaxico, *et al*.(4) Figure 58 shows the installation with the splice connections positioned in the mid-span between the posts. The post-rail connections were modeled using the nodal rigid body spot weld option in LS-DYNA and the splice connections were modeled with non-linear springs. The post-rail connections were set to fail at a load of 17.8 kN. This failure load correspond to the failure load of the new connection detail (e.g., one 6-mm diameter ASTM F568 Class 4.6 bolt with two square washers under the bolt head tightened with two nuts and a circular washer). A turn-down terminal was modeled at the downstream end of the installation. The farthest upstream guardrail section was not modeled in order to reduce processing time. Instead, linear springs were attached to the upstream end of the guardrail to simulate a continuation of the guardrail. The stiffness of these end-springs corresponded to the stiffness of the upstream section of the installation that was not modeled.

The components in the model have been used with good results in finite element models of guardrail installations for several years.(13) (4) The overall performance of the simulation corresponded well to the real crash test up to the point where the guardrail ruptured. The simulation was therefore judged to perform well enough to be used for this research. Guardrail tearing could not be simulated in the full-scale model. Simulating

fracture using finite element analysis would require a mesh with very small elements, which would be very computationally demanding and impractical. The full-scale model that was used in the investigation, however, was able to locate the high stress regions on the guardrail that could lead to fracture.

The post of interest in this simulation was number 8 (figures 58 and 59) since the rail rupture occurred at this post. Figure 60 shows a nick at the lower edge of the rail that occurred after the rail had lost contact with post 8. This nick was created as the rail was dragged up and over the top of the post and was similar to the nick observed in the real test. As previously mentioned, the mesh was not fine enough to model the tearing of the rail but it was fine enough to show the overall performance of the rail and to capture the formation of the nick. The posts were bent and twisted as they were being pushed back and the sharp edge of the post caused high stresses on the rail as shown in figure 61.

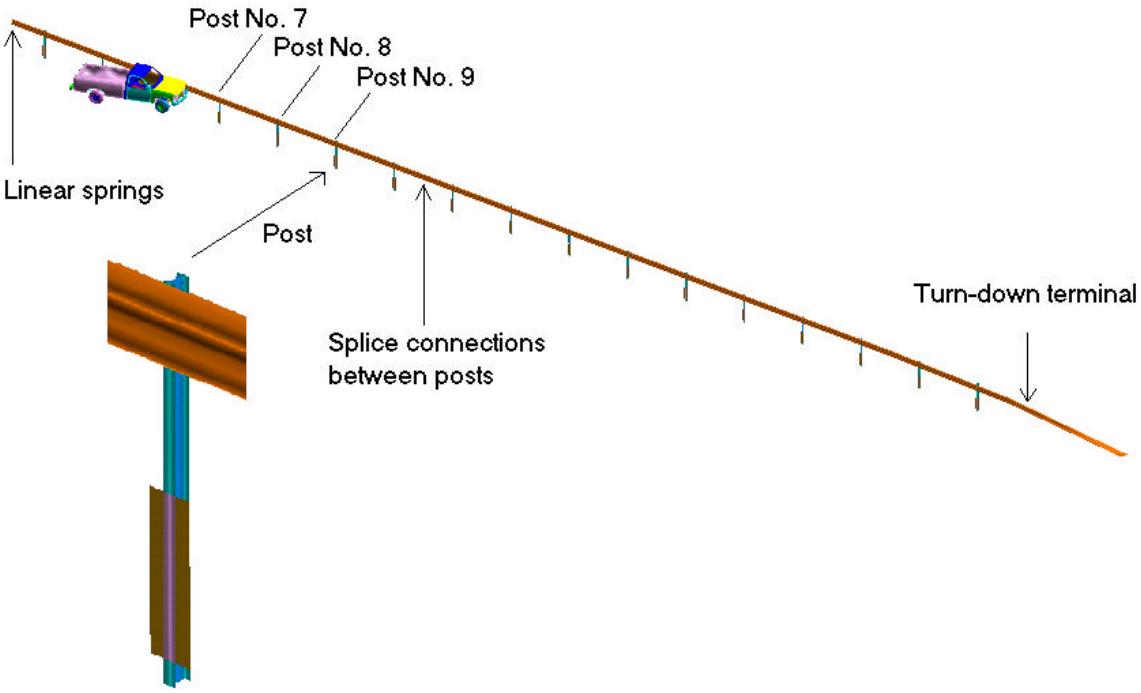

Figure 58: Simulated crash test with the interesting post marked.

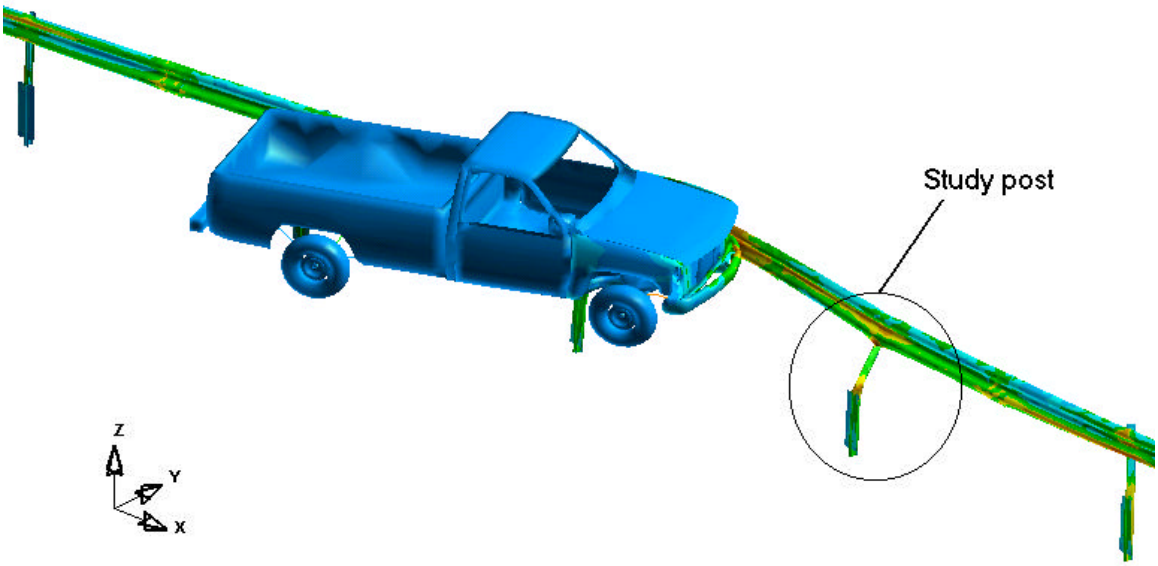

Figure 59: Full-scale finite element model of a standard G2-system modified with the new connection detail.

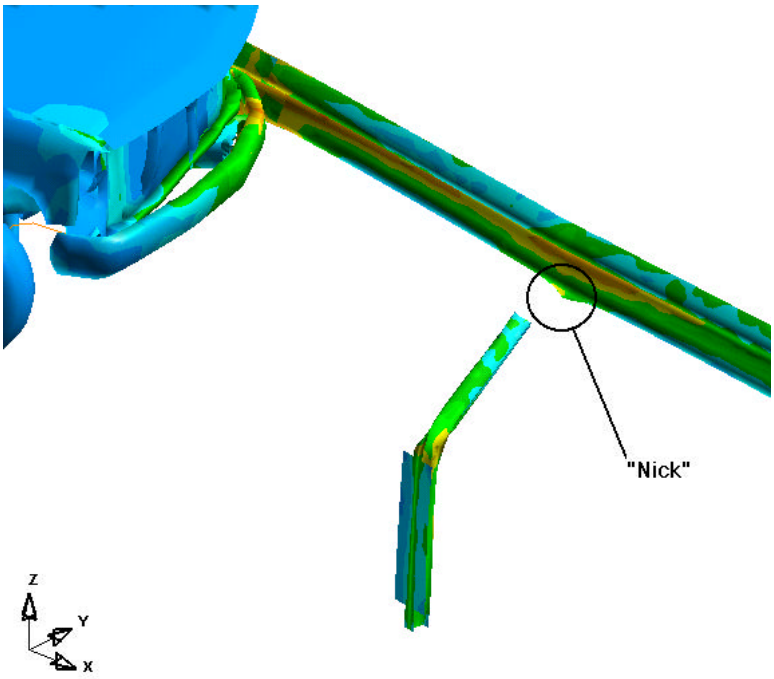

Figure 60: Close-up view of study post showing a nick at the lower edge of the rail.

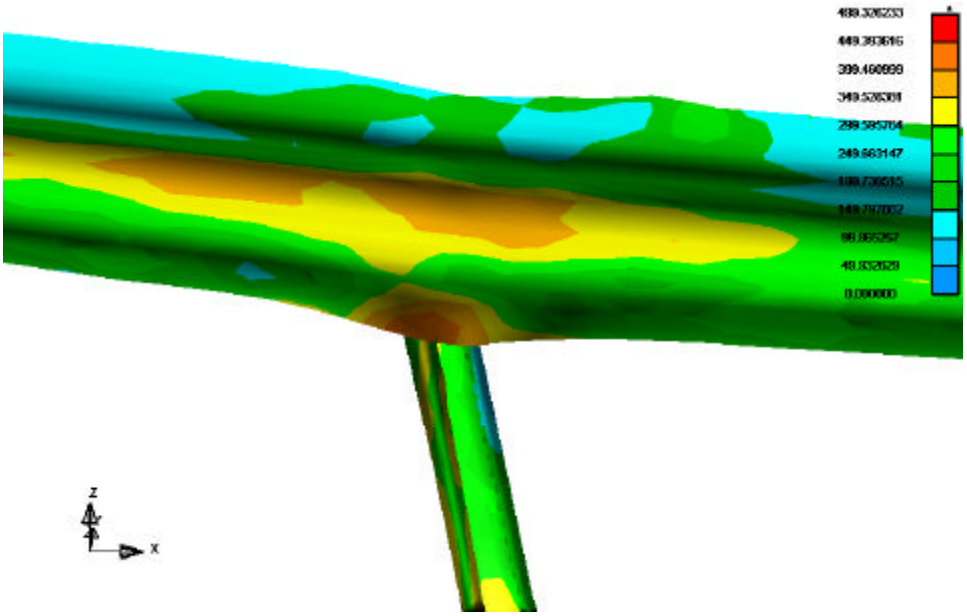

Figure 61: Close-up view of the study post showing Von Mises stresses.

Summary

The simulation and the high-speed videos of the full-scale crash test showed a nick at the lower edge of the rail. This nick occurred after the rail had been pulled over the top of post 8. The full-scale simulation revealed that the nick was created as the rail was dragged up against the post over the sharp flange of the top of the twisted post. When this nick came to the tension side of the vehicle, in the physical test, the rail tore apart and the vehicle penetrated the barrier. Basically, the simulation confirmed the theory formulated from viewing high-speed videos. The guardrail mesh in this full-scale finite element model was not fine enough to capture stress-concentrations in the post-rail interaction completely. It was, though, fine enough to give valuable data about the overall outcome of the test like displacements, velocities and accelerations and to capture the nick. The post-rail interaction needs to be further investigated in order to determine exactly why the tear occurs at the post. A sub-model of the guardrail section at post 8 was developed to examine the stress-concentrations in this region during impact.

5.3 Sub-model

A full-scale simulation of a crash-test is good for simulating the overall outcome of a test but may not give enough information about stress concentrations in the particular components. In this case, the post-rail interaction during the crash needed to be examined more closely where the crack was initiated and the rail tore. A section of the full-scale model, covering the study post, was therefore cut out to constitute a so-called sub-model (figure 62). A sub-model is a model that only involves specific components of a

particular system. The benefit of such a model compared to the full-scale model is that particular components of interest can be modeled with a much finer mesh so that high stress concentration regions can be studied in detail in a reasonable amount of computation time.

The sub-model consisted of two parts, the guardrail and the study post. Nodal time history data was selected from the cross-section of the rail in the simulated full-scale crash test, 952 mm upstream and downstream of the study post. These data contained the positions for all selected nodes and for every time-step throughout the crash. By normalizing each node position with the original position of the node, the time-displacement curve for each node was determined. These time-displacement histories were applied as loads at the guardrail ends in the sub-model. This way, the same full-scale simulation could be performed just looking at the post where the rail tore. No bolted connection was modeled between the post and the rail since the movement of the rail in the sub-model was pre-determined from the full-scale simulation and, also, the connection had already released the rail when the nick formed. The post-ground connection was the same as in the full-scale model.

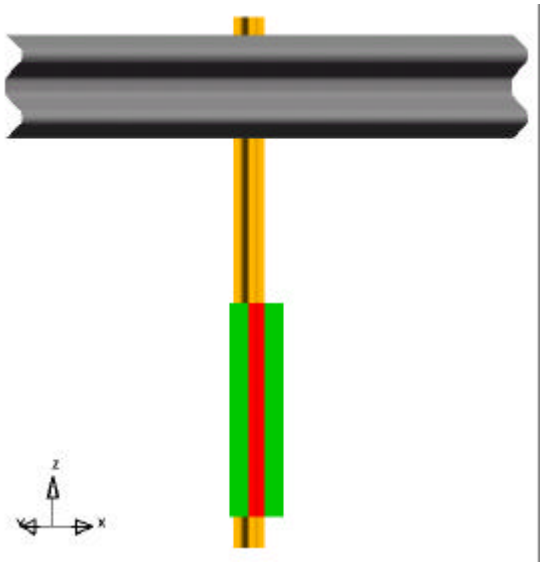

Figure 62: Sub-model of the study post.

In order to examine stress-concentrations, the rail and post in the sub-model was modeled with a fine mesh where they interact (where the rail is connected to the post) as can be seen in figure 63.

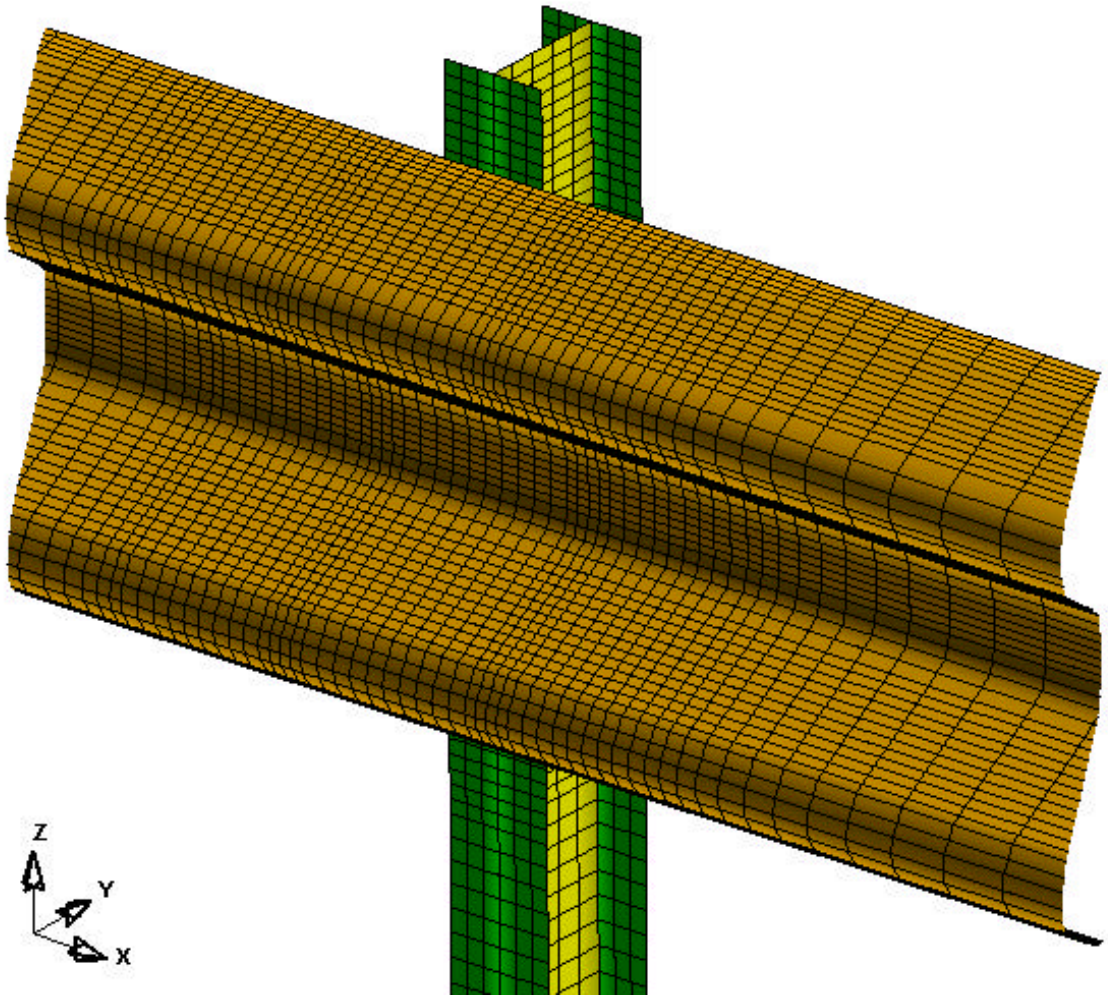

Figure 63: Sub-model mesh of the study post and rail.

Wright and Ray developed LS-DYNA material models for guardrail steel.(5) The material properties for these models were collected from laboratory experiments and literature sources. Basic material data like density, modulus of elasticity, and Poisson's ratio were obtained from material references and more complicated data like yield stress and the effective-stress verses effective plastic strain curve were determined from experiments.

Two different LS-DYNA material models were used for modeling guardrail steel, the kinematic/isotropic elastic-plastic material model (Type 3) and the rate-dependent tabular isotropic elastic-plastic material model (Type 24).(5) There were two different sets of properties for material model Type 3, one bi-linear set covering elongations up to 11 percent and one elastic-perfectly plastic set covering elongations from 11 percent up to failure, which happens at about 25 percent elongation. Both sets of properties are accurate as long as they are used in the appropriate range of elongations. The authors came to the conclusion that "material Types 3 and 24 are not adequate for modeling strain rate effects for AASHTO M-180 guardrail" and they did therefore not include strain-rate effects in the models.(5)

All these material models are good choices for modeling guardrail steel as long as they are used at appropriate levels of strains. Type 24 has the advantage of being accurate for all elongations. Type 3 is a simpler model than Type 24. Numerical and contact problems can sometimes be avoided using Type 3 instead of Type 24. The W-beam guardrail in the

sub-model experiences elongations over the entire elongation response. It was important, in this research, to have an accurate material model for the guardrail and Type 24 was the obvious choice. The perfectly-plastic material Type 3 model was chosen for the post since it will experience high elongations. Another reason was to avoid numerical problems.

The failure mechanism in LS-DYNA material Type 24 uses the effective plastic strain as failure criteria. When the effective plastic strain reaches a pre-specified value the element stress is put to zero, essentially removing the element from the model. This failure mechanism is very mesh sensitive and a specific value of the maximum effective plastic strain has to be set for each mesh. This value was not known for the sub-model and was therefore not implemented in the model.

Belytschko-Tsay 3D-shell elements with three integration points through the thickness were used for all materials in the model. Material and element data are summarized in Table 9.

	Material Type 3	Material Type 24
Density (Mg/mm^3)	7.86e-9	7.86e-9
Young's Modulus (MPa)	200.e+3	200e+3
Poisson's Ratio	0.33	0.33
Yield Stress (MPa)	528.0	415.0
Tangent Modulus	300.0	-
Hardening parameter	Isotropic	Isotropic
Strain rate effects	None	None
Failure condition	No	No
Increments of strain	-	0. 0.02 0.08, 0.165 0.33 0.495 0.66 1.0
Increments of stress (MPa)	-	415 415 548 585 591 595 600 605.
Element type	Belytschko-Tsay	Belytschko-Tsay
No. of Integration points	3	3

Table 9: Material and element data for AASHTO M-180 Class A Type II guardrail steel.(5)

The contact definitions in the LS-DYNA input file defines if and how different materials can interact with each other. Only one definition was necessary for the sub-model since the only contact was between the post flange and the rail. Automatic single surface (Type 13) was used for the contact. (8) The static coefficient of friction was set to 0.15, the

dynamic coefficient of friction to 0.09 and the exponential decay coefficient was set to 0.266e-3.(14)

The post was twisted as it was pushed back in the soil as is typical in weak-post guardrail collisions. The sharp edge of the post flange caused high stresses at the lower edge of the W-beam as the rail was dragged up against the post flange (figure 64). In order to investigate the affect of this stress-concentration on the potential for tearing the guardrail, a shell element in the high stress region at the lower edge of the rail was selected, as shown in figure 65. The Von Mises stress time history for the particular element (shell element 5449) is shown in figure 66. The first part of the post-rail interaction time the rail was pushed against the post flange and followed the post as it was bent back and twisted. The rail did not move much relative to the post flange during this period of time. Then, the rail started to move up the post at approximately 0.12 seconds and reached the top of the post just before 0.16 seconds. The curve shows that the intensity of the stress increases continuously during this period when the rail is dragged up the post flange and the rail is moving relative to the post flange. The post-rail contact ceased when the lower edge of the W-beam was pulled over the top of the post and correspondingly the element stress decreased rapidly after that time. The stress in the element reached a magnitude of 588 MPa just before the rail lost contact with the top of the post. This was the highest stress observed in the rail throughout the time of post-rail interaction. The stress increased from about 300 MPa to nearly 600 MPa during the period where the rail was moving up the post. After the rail had been pulled over the post, a kink in the high stress

region was evident as can be seen in figure 65. This deformation was similar to the nick that was observed in the physical test. The only difference between the simulation of the test was that the kink progressed into a tear in the physical test.

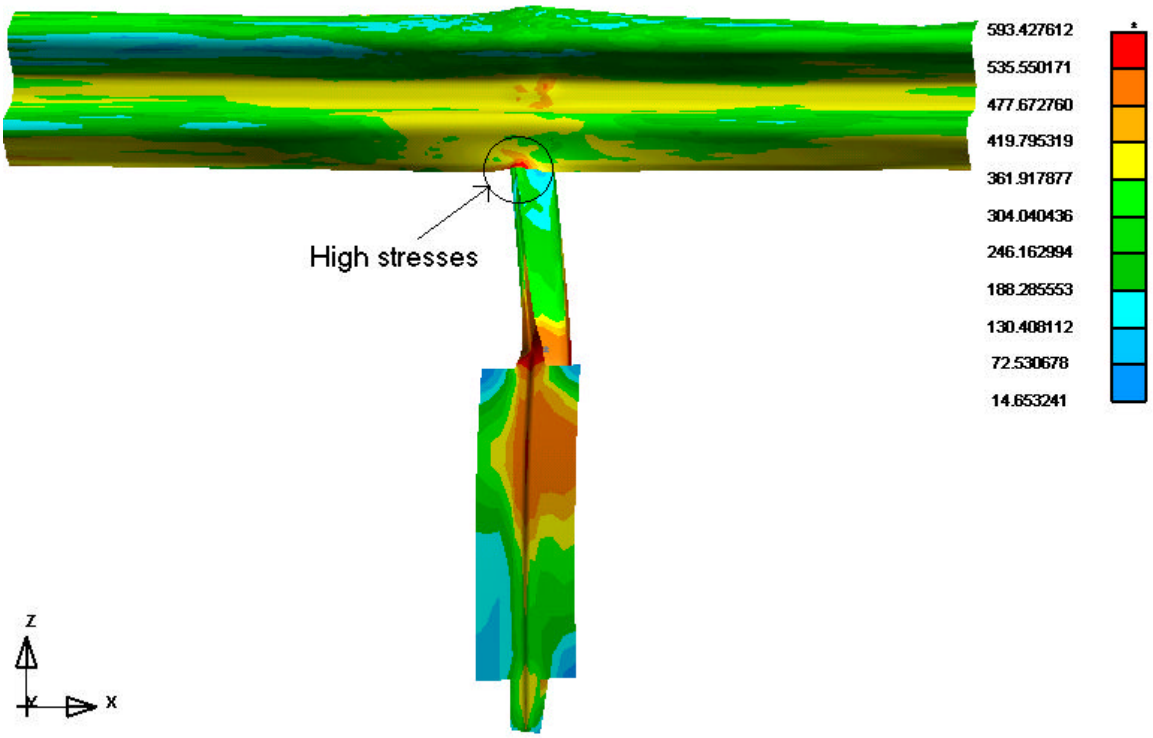

Figure 64: Mises stress contour plot.

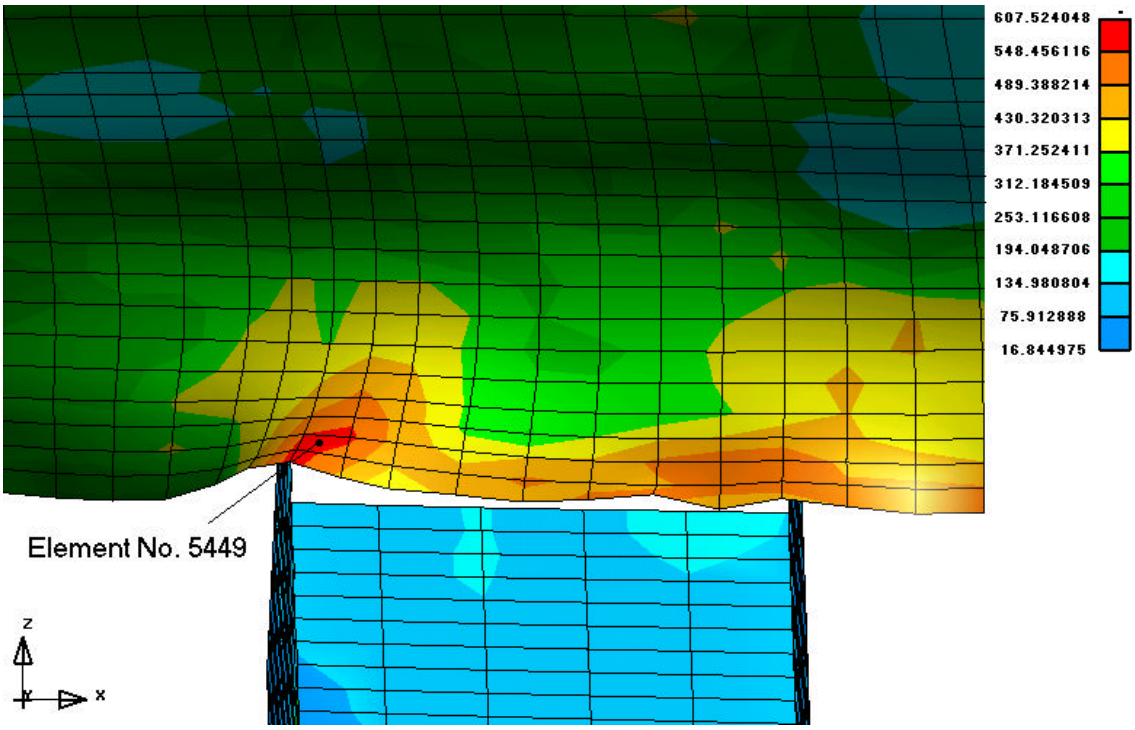

Figure 65: Location of shell element No. 5449 shown in a Von Mises stress contour plot.

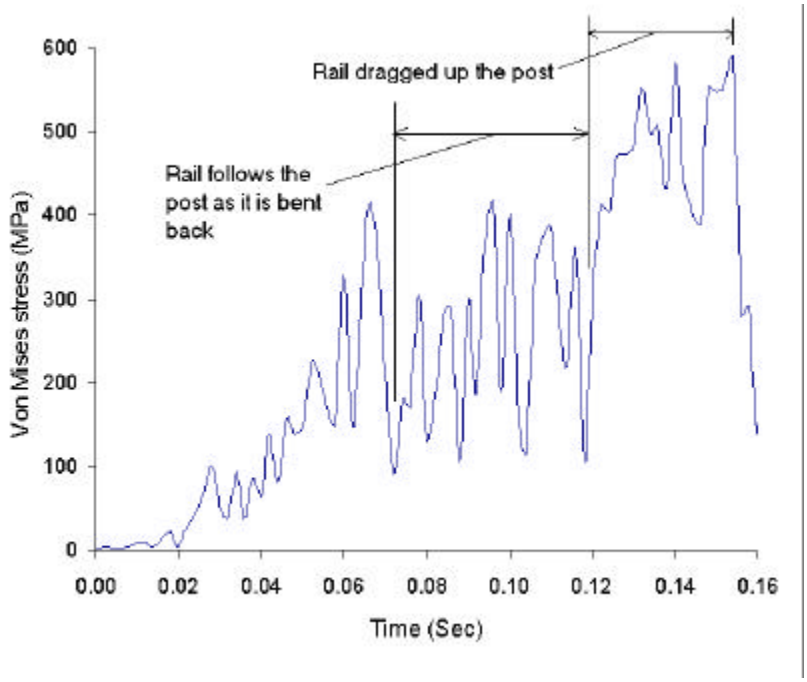

Figure 66: Von Mises stress verses time graph for shell element No. 5449.

The most probable location for a tear to be initiated was at the lower edge of the rail where the kink was formed in the simulation and where the nick was observed in the physical test. The highest stresses in the rail were found in this region of the W-beam and the beam experienced large plastic deformations in this region. These stresses were well above the yield point of 415 MPa so tearing is likely if the strains are large enough. Since no failure criterion was implemented in the guardrail material model, tearing was not observed in the simulated event.

The contour plot shown in figure 64 also show high stresses in the middle of the guardrail cross-section at the post. The maximum Von Mises stress in the middle guardrail cross-section was 515 MPa, which is beyond the yield point. Based on the stress contours a tear could be initiated here as well although not as likely as at the lower edge of the W-beam.

The effective plastic strain is a more direct measure of the potential for fracture than the stress since it is a measure of the cumulative permanent damage to the material. The effective plastic strain in the guardrail was examined to identify the location of a possible tear.

Figure 67 shows a concentration of effective plastic strain in the region at the lower edge of the rail where the kink was formed. The maximum effective plastic strain in the simulation was 0.37, which was observed in shell element 5453 (figure 68).

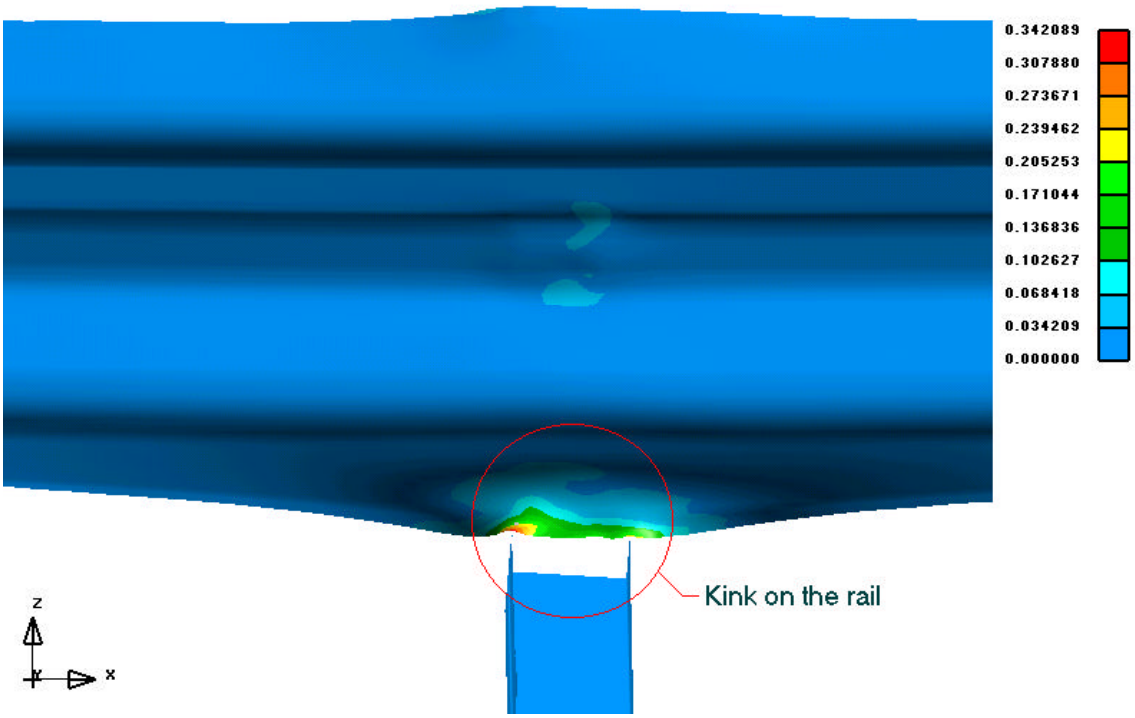

Figure 67: Effective plastic strain contour plot.

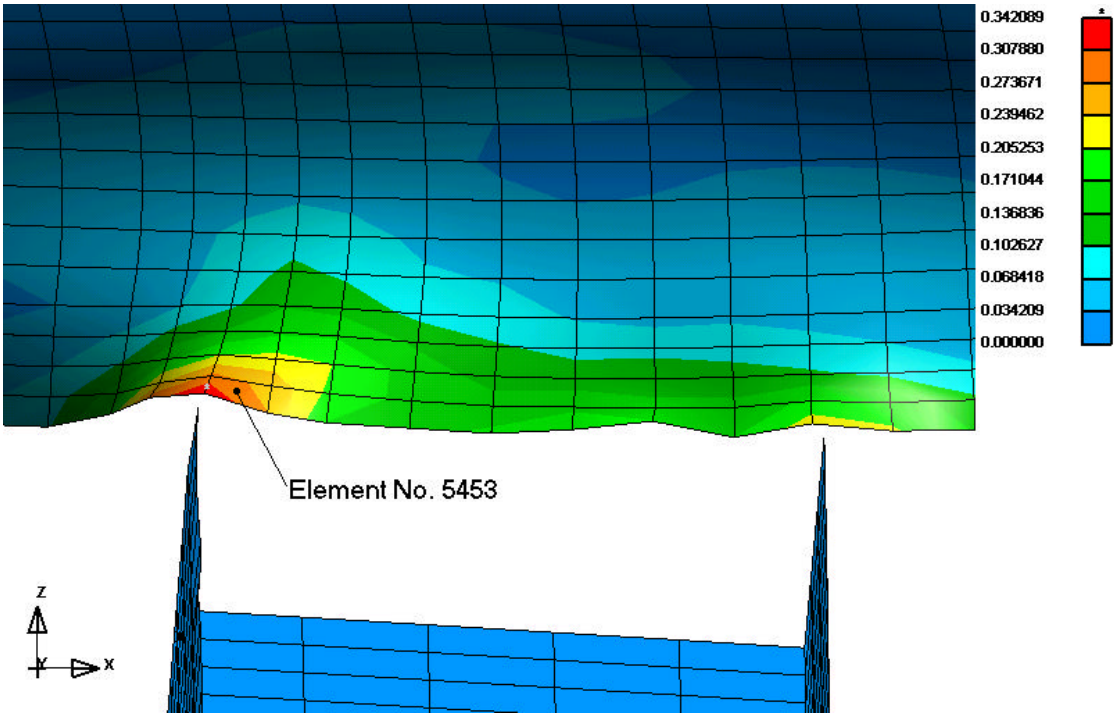

Figure 68: Location of shell element 5453 shown in an ef. plastic strain contour plot.

Figure 69 shows the effective plastic strain time history for element 5453. The effective plastic strain remains low during the time where the rail follows the post not moving relative to it. Then, the effective plastic strain increases rapidly as the rail is dragged up against the sharp edge of the post flange creating the kink.

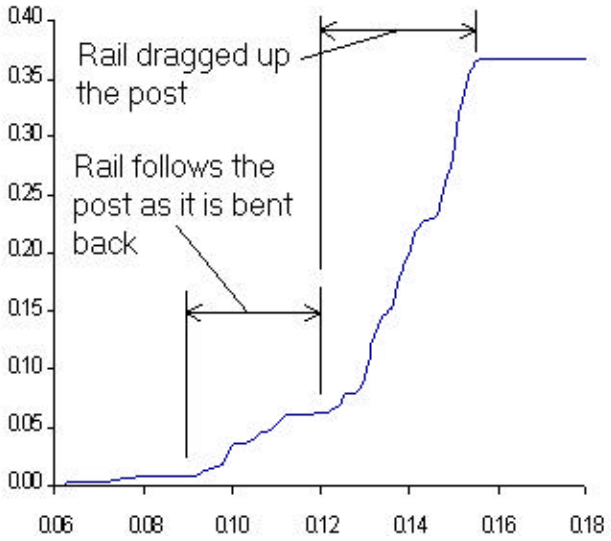

Figure 69: Effective plastic strain verses time graph for shell element No. 5453.

The full-scale and the sub-model simulation showed that the kink that was observed in the full-scale physical test at the lower edge of the rail was formed as the rail was dragged up against the sharp edge of the twisted post. Examinations of sub-model Von Mises contour plots showed that the highest Von Mises stresses in the rail were located where the nick was formed and contour plots of the effective plastic strain showed a clear concentration of plastic deformations in this region. The combination of high stresses and significant plastic deformation could initiate a tear, which then could propagate through the W-beam cross-section when the tension in the rail increases.

A failure criterion was now implemented in the model. A tear should, according to the theory previously discussed, be initiated at the lower edge of the rail where the nick was formed. Again, the effective plastic strain is very sensitive to the fineness of the mesh and

values collected from a simulation do not necessarily agree with values measured in physical tests. However, the failure strain for guardrail material was measured by Wright and Ray to about 25 percent and the highest effective plastic strain in the simulation was 0.37 so the mesh seems to be fine enough to capture the strains pretty good.(5) The effective plastic strain at failure was set to 0.15 and a new analysis was performed. The contour plot of the effective plastic strain of this simulation is shown in figure 70. A tear was initiated at the lower edge of the rail and propagated approximately 70-mm as the rail was moving up the post.

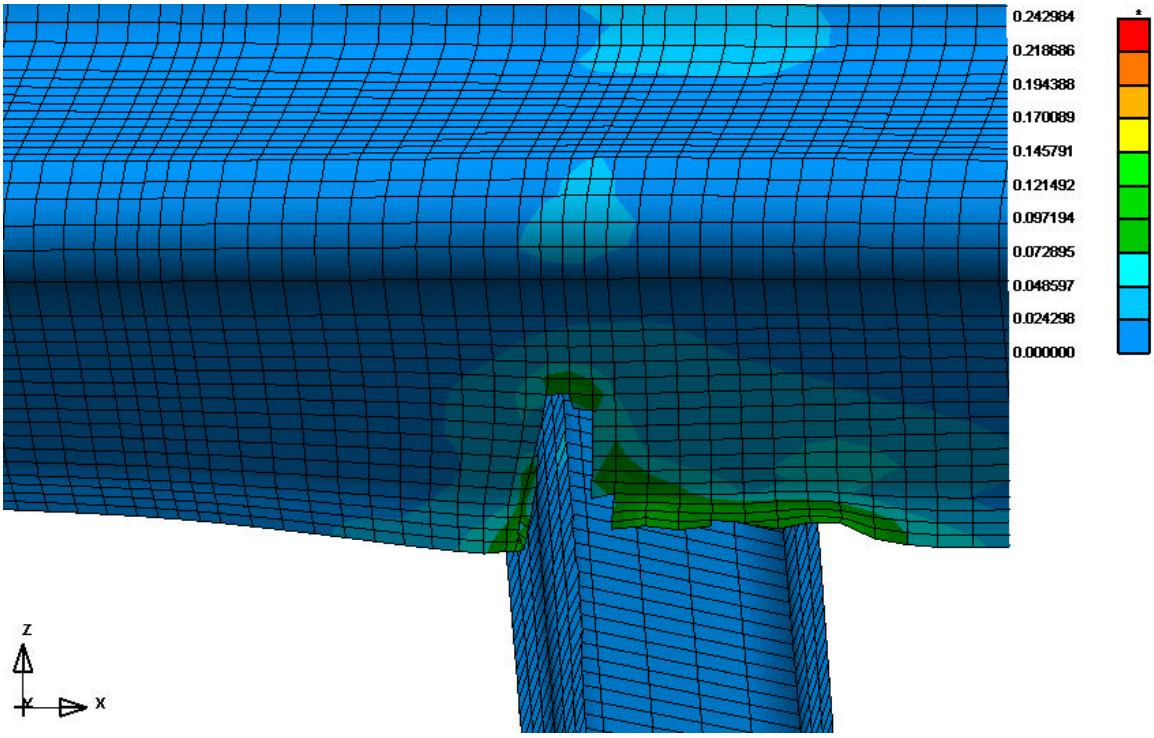

Figure 70: Effective plastic strain contour plot showing a tear initiated at the lower edge of the rail.

5.4 Conclusions from simulations

The nick that was observed in the physical full-scale crash test (TTI 473750-1) has been investigated using a full-scale finite element model and a sub-model. The results from these simulations show that the nick/tear was initiated as the post was dragged up the sharp edge of the twisted post. The problem is the sharp edge of the post and the rail moving relative to it.

There are two alternatives for solving this problem. Develop a new post without sharp edges (i.e., rounded geometry) or prevent the rail from coming in contact with the sharp edges of the posts. The most straightforward and least expensive solution is to use a standard W-beam backup plate behind the rail, as is used in the G4 W-beam strong-post system with steel block-outs. The backup plate prevents the sharp edge of the post from contacting and cutting the rail. The splice connections in a standard G2 system are located at every post and the double thickness of guardrail steel prevents the rail from tearing against the post the same way the backup plates do in a W-beam strong-post system. In this new setup with splices between the posts there is only one layer of rail at every post and it seems to be reasonable to use backup plates.

A back-up plate was added to the model and a new simulation was performed in order to test the ability of the backup-plate to prevent guardrail tearing.

5.5 Sub-model with backup plate

This model is the same as the former except a backup plate between the post and the rail was added (figure 71). The plate is made of the same W-beam guardrail material as the main guardrail.

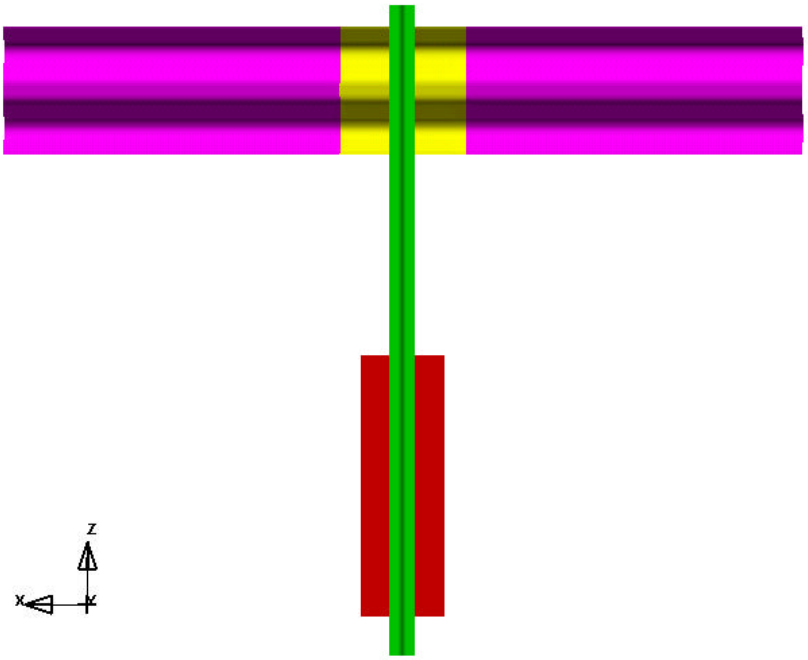

Figure 71: Sub-model with backup plate.

A finite element analysis was performed with this sub-model in order to find out how a backup plate might reduce the maximum Von Mises stress and the maximum effective plastic strain in the guardrail and thereby prevent rupture. Figure 72 shows the Von Mises contour plot for the guardrail. As observed in the simulation without backup plate, there was a stress-concentration at the lower edge of the rail where a dent was visible. A shell element was selected in this region (element 6015) and the Von Mises stress time history was plotted (figure 73). The element stress increases continuously during the time up to

approximately 0.12 seconds where the backup plate and rail follows the post as it is bent and twisted. The Von Mises stress reached 512 MPa just as the backup plate and rail starts to slide up against the sharp edge of the post flange. This was the highest stress observed in the rail. The stress does not change much during the period from 0.12 seconds to 0.16 seconds when the rail is moving up the flange and pulled over the top of the post.

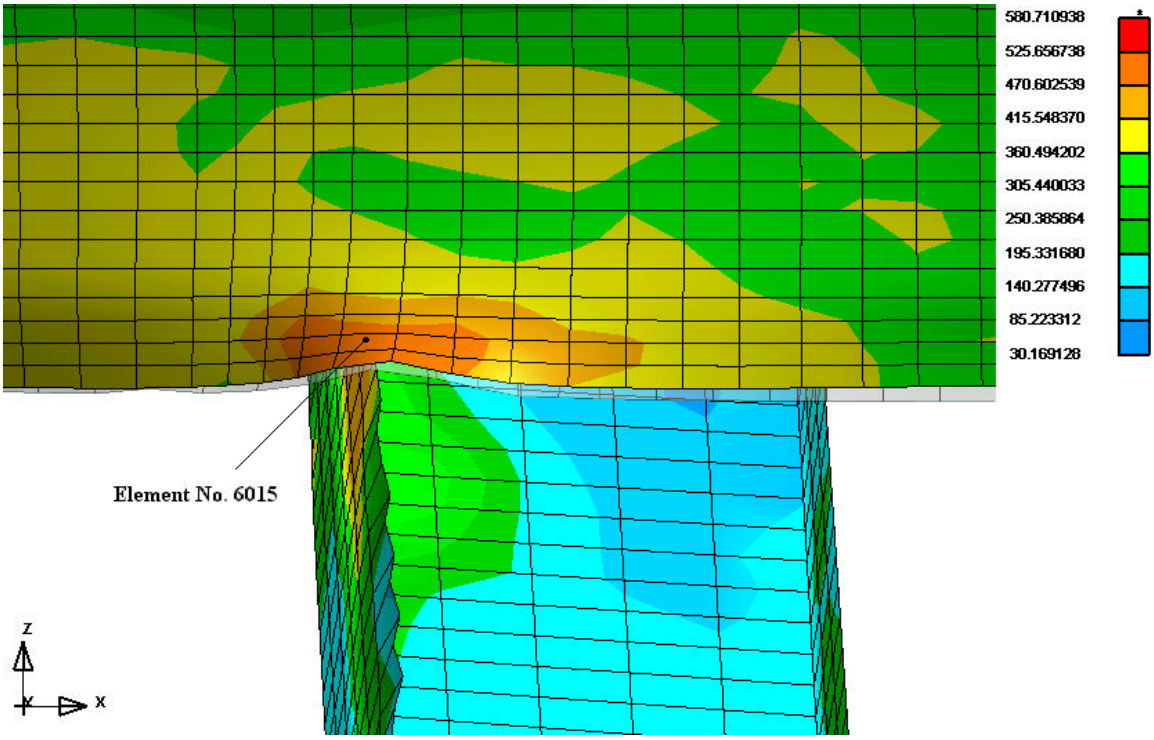

Figure 72: Von Mises stress contour plot.

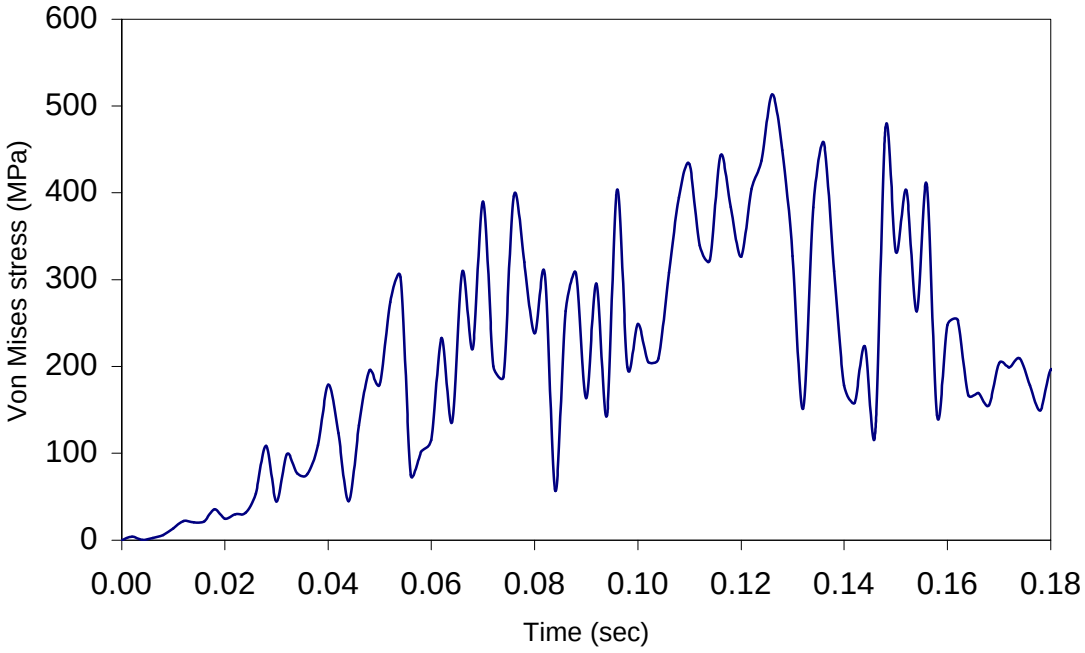

Figure 73: Von Mises stress verses time graph for shell element No. 6015.

A stress concentration was observed in the same region for both the simulation with and the simulation without backup plate, which is the region where the nick was observed in the physical full-scale crash test at the lower edge of the rail. However, the maximum Von Mises stress observed in the guardrail was 13 percent less with the backup plate behind the rail than without. The major difference was, though, that the stress in the guardrail did not increase during the period where the guardrail with backup plate was moving up the post as it did in the simulation without backup plate. The question was now if 13 percent less stress would prevent the guardrail from tearing. To answer this question a study of the effective plastic strain was performed.

The contour plot of the effective plastic strain in figure 74 shows a concentration where the dent was formed. An element was selected in this region (element 6022) and the effective plastic strain time history was plotted (figure 75). As observed in the simulation without the backup plate behind the rail the material at the lower edge of the W-beam formed a kink/dent as the rail moved up the post. This can be observed following the Von Mises time history curve from 0.12 to 0.16 seconds. The effective plastic strain reached 0.23 as the rail was pulled over the top of the flange. This was the maximum effective plastic strain in the model. Adding the backup plate to the model reduced the effective plastic strain by 38 percent.

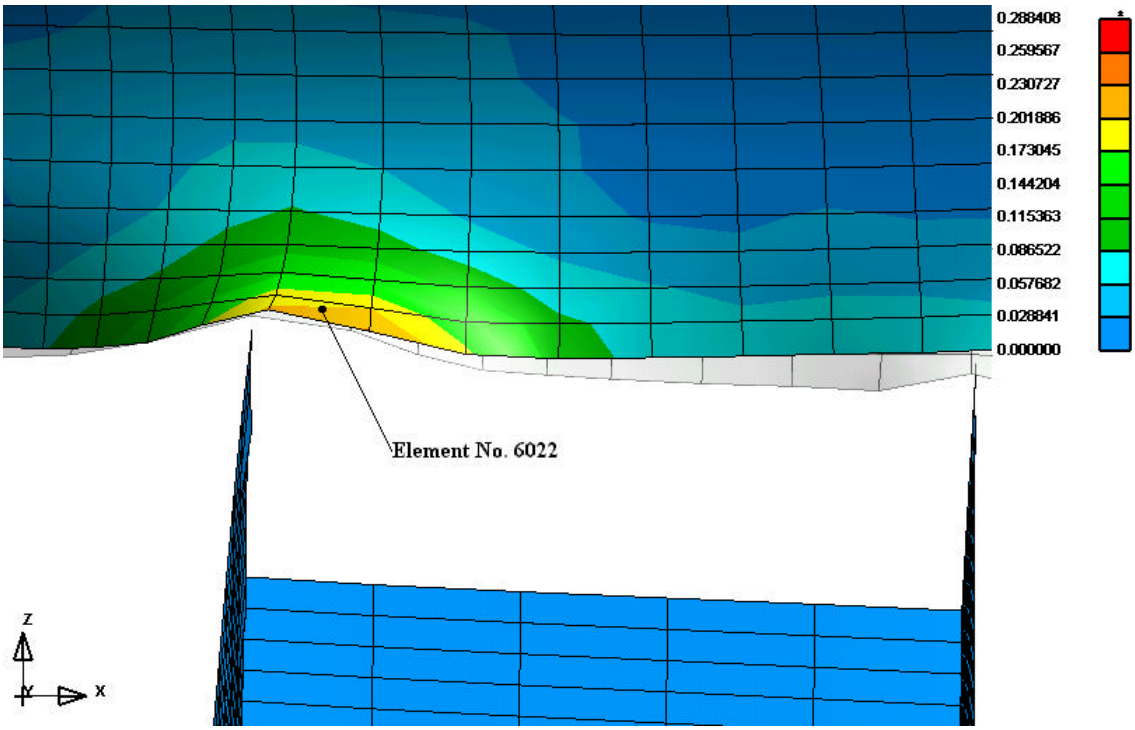

Figure 74: Effective plastic strain contour plot.

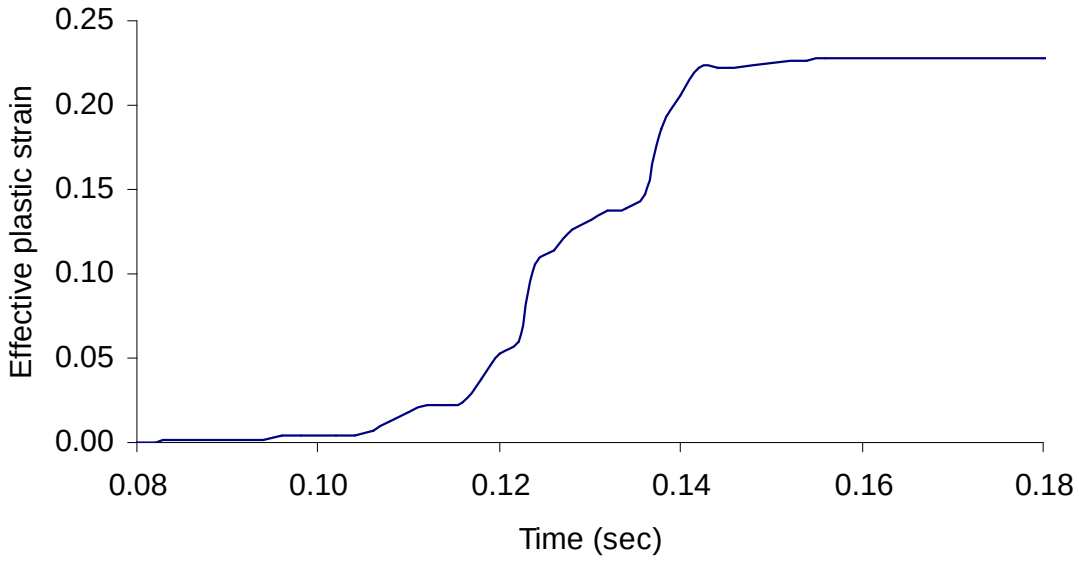

Figure 75: Effective plastic strain verses time graph for shell element No. 6022.

There was a stress-concentration at the lower edge of the backup plate as well (figure 76). The maximum element Von Mises stress in this region was 554 MPa and the maximum effective plastic strain was 0.28.

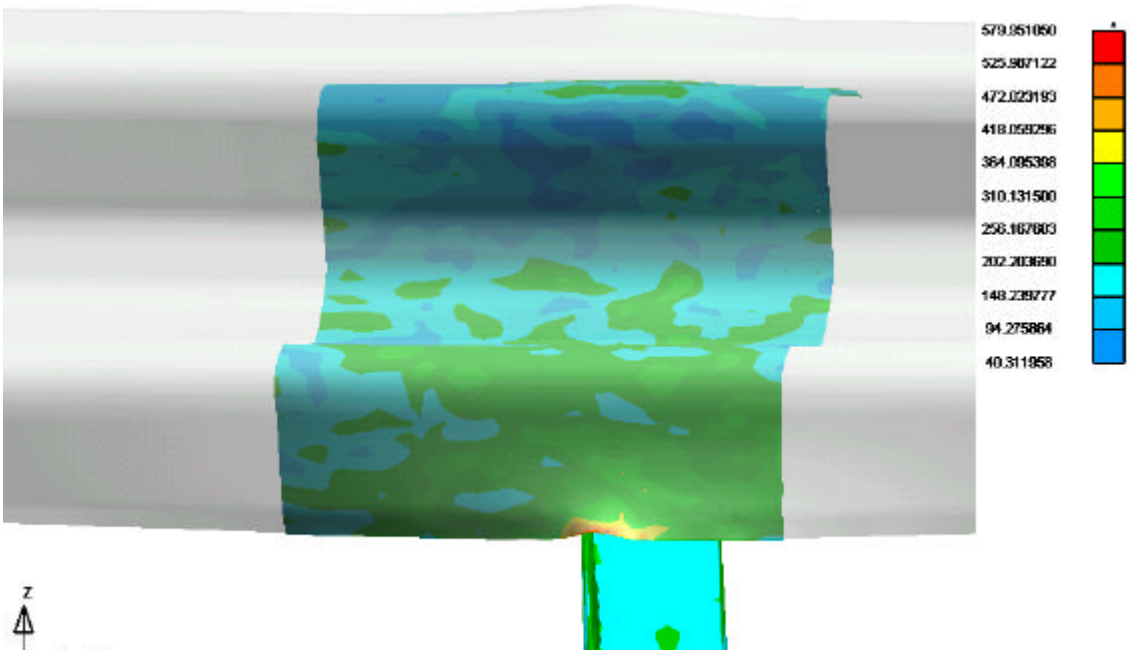

Figure 76: Von Mises stress contour plot of the study post.

	Guardrail (without backup)	Guardrail (with backup)	Reduction (%)	Backup plate
Maximum Von Mises stress (MPa)	588	512	13	554
Maximum effective plastic strain	0.37	0.23	38	0.28

Table 10: Summary

5.6 Conclusions

Table 10 summarizes all data from the simulations performed with and without the backup plate behind the rail. The Von Mises stress reduction was 13 percent in the

guardrail and the reduction in the effective plastic strain was 38 percent when adding the backup plate to the model. The backup plate prevented the guardrail from coming in contact with the sharp edge of the post and with the backup plate added to the model the guardrail did not move relative to any other material. The backup plate was judged to be a success based on these two facts and the 38 percent decrease in effective plastic strain. The backup plate should prevent the guardrail from rupturing. The higher stress and effective plastic strain in the backup plate is no problem since it is a sacrificed component.

5.7 Full-scale crash test (TTI 473750-2)

The full-scale crash-test (TTI 473750-1) was repeated the 6th of January 2000 except with backup plates behind the rail. The backup plates were mounted on 6-mm diameter post-rail ASTM F568 Class 4.6 bolts with increased length (figures 77 and 78). Another modification for this test was to eliminate the 14-mm diameter shelf bolt underneath the rail in order to eliminate the risk of initiating a tear through contact this bolt (figure 79).

Figure 77: Backup plate behind rail. (17)

Figure 78: Guardrail and backup plate mounted on a 6-mm diameter bolt with increased length.

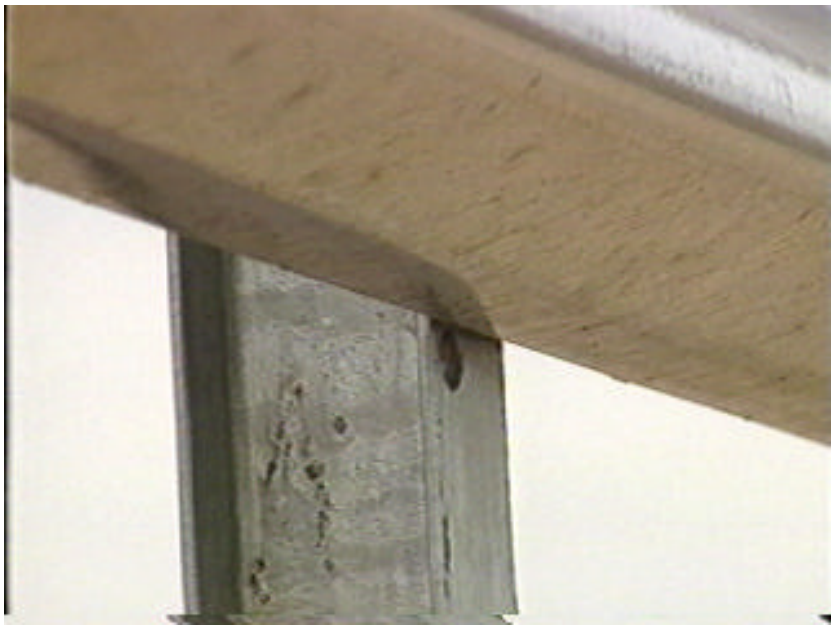

Figure 79: Eliminated shelf bolt.

The vehicle was redirected as it should in the beginning (figure 80, 81, 82) but toward the end of the impact event the rail dropped allowing the vehicle to override the barrier (figure 83,84,85). The guardrail did not tear and the post-rail connection failed like it should. Both modifications were successful although the test was a failure. Figure 86 shows a damaged backup plate. This damage could have grown and tore the rail without the plate as protection.

Figure 80: Crash sequence at time » 0.2 sec (TTI 473750-2).

Figure 81: Crash sequence at time » 0.3 sec (TTI 473750-2).

Figure 82: Crash sequence at time » 0.4 sec (TTI 473750-2).

Figure 83: Crash sequence at time » 0.6 sec (TTI 473750-2).

Figure 84: Crash sequence at time » 0.7 sec (TTI 473750-2).

Figure 85: Crash sequence at time » 0.9 sec (TTI 473750-2).

Figure 86: Typical backup plate damage.(17)

By viewing high-speed videos of the crash it is clear that the rail dropped slightly during impact. This loss of height was enough for the front right wheel of the vehicle to come in contact with the guardrail. The wheel pulled the guardrail down and the vehicle climbed over the guardrail and ended up on the wrong side of the barrier.

The guardrail installation in TTI test 473750-2 failed to meet the report 350 Structural Adequacy criterion since the vehicle overrode the installation.

The following chapter describes research performed, using finite element analysis, to determine the cause of the vehicle overriding the barrier and to determine possible modifications that would prevent it from happening in the future. It also describes a full-scale crash test with the modifications implemented in a G2-installation.

6 GUARDRAIL MOUNTING HEIGHT

The mounting height of the guardrail, 610 mm from the ground to the center slot of the guardrail, is well suited for passenger cars but may not be for pickup trucks. The full-scale crash test (TTI 473750-2) performed well until the front right wheel came in contact with the guardrail late in the event. When this happened, the wheel pulled the rail to the ground allowing the vehicle to climb over the rail. The rail did not need to drop much for this to happen. One solution to this problem would be to mount the guardrail higher. If it is too high, though, passenger cars may underride the guardrail and if it is too low the pickup truck will override the rail. The best compromise height suitable for the pickup truck and small car had to be identified.

6.1 Full-scale finite element simulations

The top of the rail in the standard G2-system is located 770 mm above ground. Full-scale finite element simulations were performed at NCHRP Report 350 test designation 3-10 and 3-11 conditions with the height of the guardrail increased 50 mm to 820 mm above ground to test the performance of the installation in impacts with both small cars and pickup trucks.

Figures 87 through 90 show the results of a simulated test at NCHRP Report 350 test designation 3-10 conditions. The vehicle, an 820-kg Honda Civic, was contained and redirected as required. The major concern for this simulation was to make sure that the

passenger car did not underride the guardrail at the higher mounting height. As shown in the figures, the first rail-vehicle contact happened at the fender of the vehicle and the rail remained in contact with the fender through out the impact. The increased mounting height of the guardrail was considered not to have affected the performance of the G2-system at test designation 3-10 conditions.

The results of the simulation at NCHRP Report 350 3-11 conditions are shown in figures 91 through 93. The first rail-vehicle contact happened at the bumper of the vehicle and the rail was in contact with the fender through out the impact. The vehicle did not override the barrier and the increased rail height was considered a good solution based on the simulation.

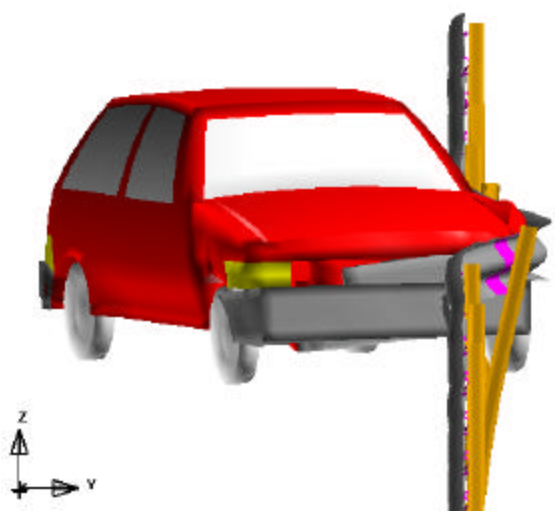

Figure 87: Crash sequence at time » 0.06 sec (test designation 3-10).

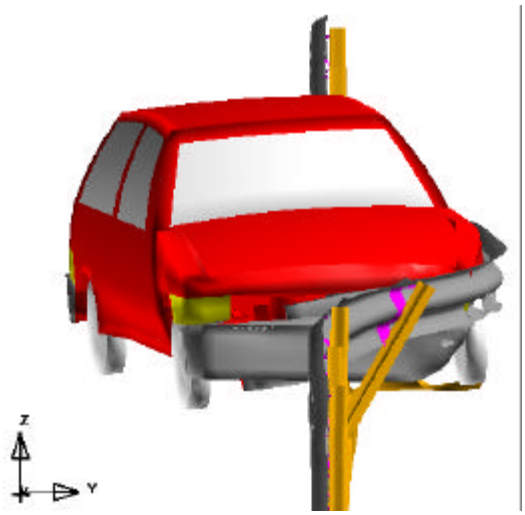

Figure 88: Crash sequence at time » 0.16 sec (test designation 3-10).

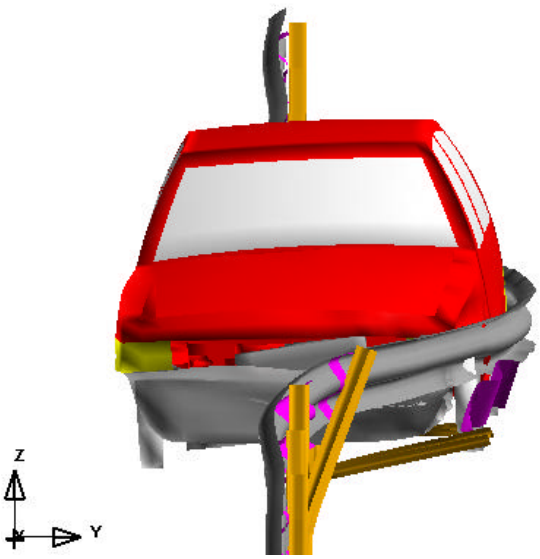

Figure 89: Crash sequence at time » 0.25 sec (test designation 3-10).

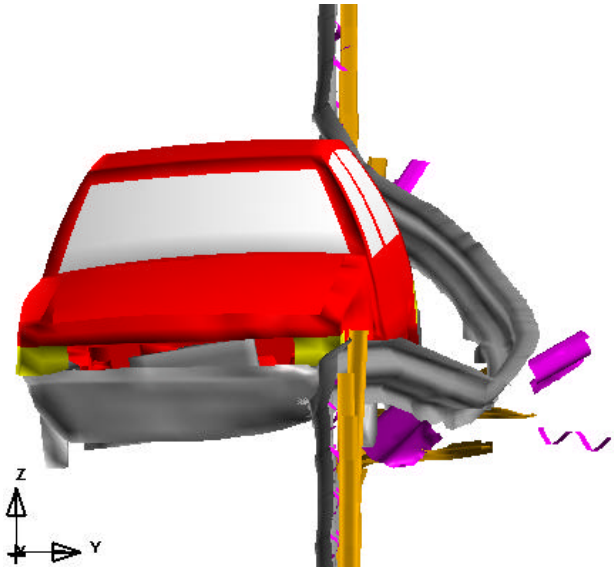

Figure 90: Crash sequence at time » 0.58 sec (test designation 3-10).

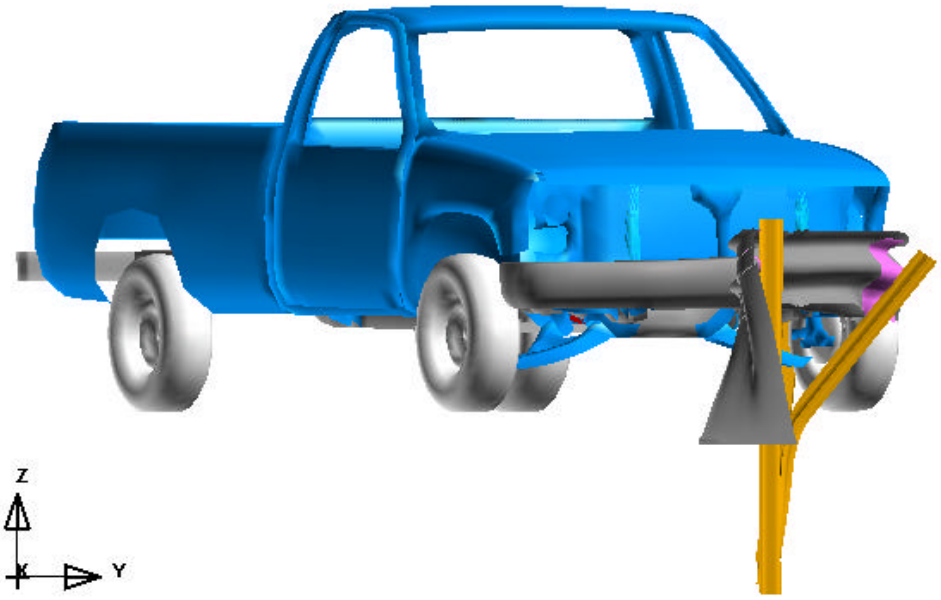

Figure 91: Crash sequence at time » 0.07 sec (test designation 3-11).

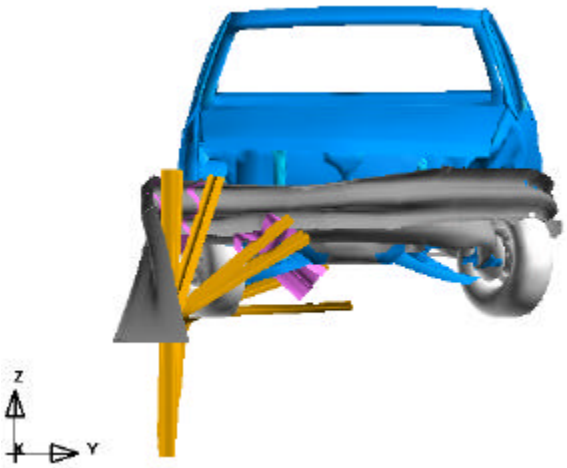

Figure 92: Crash sequence at time » 0.55 sec (test designation 3-11).

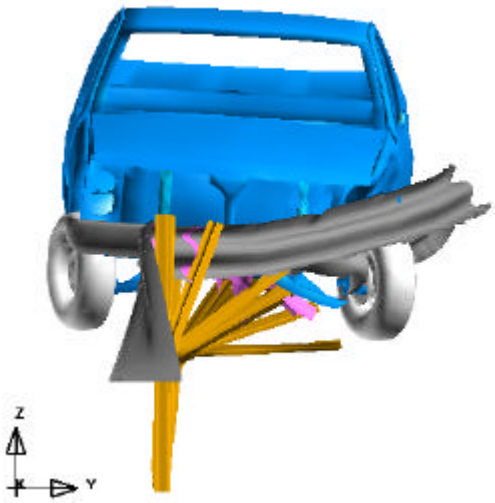

Figure 93: Crash sequence at time » 0.95 sec (test designation 3-11).

The finite element simulations indicated that the modified G2-system with a rail height of 820 mm should satisfy the Report 350 test 3-10 and 3-11 test requirements. A full-scale crash test was, therefore, scheduled to verify the finite element simulation results.

6.2 Full-cale crash test (TTI 473750-3)

All three full-scale crash tests that were conducted for this project were performed at NCHRP Report 350 test designation 3-11 conditions (i.e., a 2000-kg pickup truck impacting the guardrail system at the impact speed of 100 km/h and with a 25 degrees impact angle). The objective of the project was to develop a weak-post W-beam system that satisfies the requirements of this test.

A review of the videotapes of the previously performed full-scale crash test (TTI 473750-2) raised the question that the post-rail connection possibly failed too easy. Therefore, an 8-mm diameter ASTM F568 Class 4.6 bolt with increased length was used instead of the 6-mm diameter bolt that was used before. The purpose of the bigger bolt was to increase the failure load without changing the failure mechanism. The desirable failure mechanism for the connection should still be to fracture the bolt without stripping threads or pulling washers through the central slot. The two square washers under the bolt head were therefore kept and likewise the bolt was still tightened with two nuts behind a circular washer. Figures 95 and 96 shows the post-rail connection detail. Also, the 14-mm diameter shelf bolt underneath the rail was put in place again to gain some extra support for the rail (figure 97).

The full-scale crash test was performed on the 9th of May 2000 with some modifications. The purpose of these modifications was to prevent the guardrail from dropping and the

vehicle from overriding the barrier. The major modification of the system was to raise the rail 50 mm so that the top of the rail now was located 820 mm above ground (figure 94).

Table 11 shows a comparison between the standard weak post W-beam guardrail installation and the modified G2-system that was tested in this full-scale crash test (TTI 473750-3).

Feature	Standard G2-system	Modified G2-system (TTI 473750-3)
Rail height (mm)	770	820
Splice	At every post.	Between posts (figure 62)
Bolt	8-mm diameter	8-mm diameter
	ASTM F568 Class 4.6	ASTM F568 Class 4.6
Washer	1	2
Nut	1	2
Backup plate	None	Yes

Table 11: Comparison between the standard G2-system and the modified G2-system tested in the full-scale crash test (TTI 473750-3).

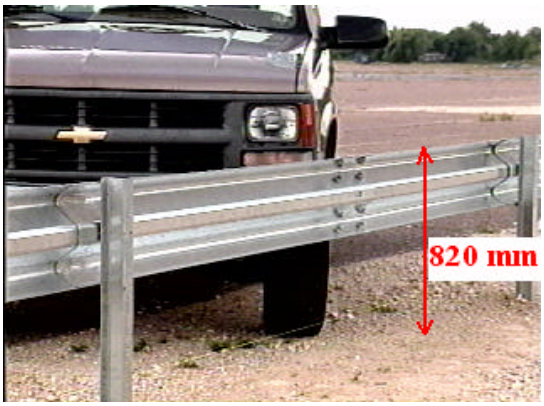

Figure 94: Splice connections located between posts. Backup plates behind the rail at posts.

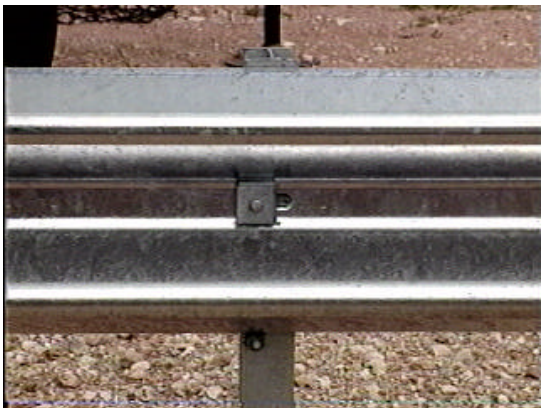

Figure 95: Post-rail connection detail showing one 8-mm diameter bolt and two square washers.

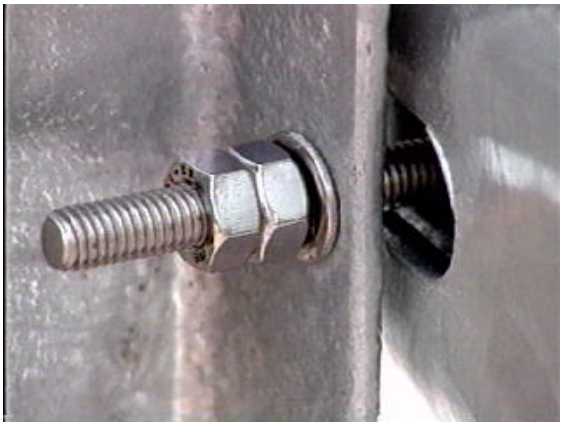

Figure 96: Guardrail and backup plate mounted on an 8-mm diameter bolt with increased length tightened with two nuts behind a circular washer.

Figure 97: Shelf bolt.

When this report was written the TTI test report had not yet been completed. While evaluations were performed to determine if the test was a success, all the data was not yet available. The high-speed videotapes were, though, available and the following was observed from viewing these.

The vehicle was contained and redirected and the vehicle did not penetrate, underride or override the installation as can be seen in figures 98 to 103. This means that the barrier should pass the NCHRP Report 350 Structural Adequacy criterion.(12) The vehicle was redirected parallel to the guardrail and did not intrude into adjacent traffic. The test should, therefore, fulfill at least two of three of the factors in the NCHRP Report 350 Vehicle Trajectory criterion. The third factor includes occupant velocities and accelerations and these data were obtained directly from TTI. The longitudinal occupant impact velocity was 3.9 m/s, which is well below the upper limit of 12 m/s. The occupant ridedown acceleration in the longitudinal direction was –5.9 g's, which is well below the upper limit of 20 g's. The test should, therefore, pass the Vehicle Trajectory criterion. The vehicle remained upright during and after collision and should fulfill the first of two factors in the NCHRP Report 350 Occupant Risk criterion. The second factor says that no elements of the installation should present a hazard to other traffic, pedestrians or personnel in a work zone. The post-test videotapes showed that two posts had been pulled out of the ground and thrown out on the lane (figure 104). These posts appear to have been dragged into the road by the vehicle and did not pose a threat to other vehicles on the roadway.

Figure 98: Crash sequence at time » 0.18 sec (TTI 473750-3).

Figure 99: Crash sequence at time » 0.30 sec (TTI 473750-3).

Figure 100: Crash sequence at time » 0.50 sec (TTI 473750-3).

Figure 101: Crash sequence at time » 0.77 sec (TTI 473750-3).

Figure 102: Crash sequence at time » 1.20 sec (TTI 473750-3).

Figure 103: Crash sequence at time » 2.73 sec (TTI 473750-3).

The weak-posts are supposed to bend back and release the guardrail and not to break or be pulled out of the ground. Figure 105 shows a post that was not bent and the post-rail connection was still intact. The post rotated in the ground and allowed the rail to deflect without bending the post or fail the post-rail connection. Reviewing the videotapes of the test raised questions about the firmness of the soil. The soil appeared to be saturated after several days of rain at the test site. A good firm soil should support and hold the post enough to keep the post base in position allowing the post to bend and the post-rail connection to fail. It appeared that the poor condition of the soil made the post-ground connection weak allowing the posts to rotate in the ground and be pulled out. Also, the post embedment was 50 mm less than typical in this test due to the increased rail height, which further weakened the post-soil connection. The latter could easily be avoided by mounting the soil-plates 50 mm lower on the posts so that it remains at the proper location (124 mm below ground).

Despite the assumed poor soil conditions and/or post embedment that resulted in the posts being pulled out of the ground, the overall outcome of the test was a success. The fact that the soil condition was poor and the post embedment was less than standard should have increased the likelihood of pulling the rail to the ground, however, the system performed well even under these adverse circumstances. This indicates that the increased mounting height was an appropriate design change.

Figure 104: Posts pulled out from the ground.

Figure 105: Post-test close-up on post.

7 RESULTS

The major goal of this project was to improve the impact performance of the weak-post W-beam guardrail system so that it satisfies the requirements of NCHRP Report 350 at test level three. Since the G2-system already had passed test designation 3-10 (i.e., the small car test) the objective was to pass test designation 3-11.

Specific issues related to the performance of the weak-post W-beam system were:

- Prevent guardrail ruptures at the splice connection,
- Developing a more reliable post-rail connection detail,
- Reducing the chance of rupturing the guardrail and
- Preventing the vehicle from vaulting over the guardrail.

The modified weak-post installation that was developed in this project was crash tested under NCHRP Report 350 test designation 3-11 conditions by Texas Transportation Institute in test TTI 473750-3. The new system contained and redirected the vehicle, a 2000-kg pickup truck, without rupturing or vaulting over the guardrail. All the specific issues mentioned above are fulfilled by the modified weak-post guardrail system. It was not known at this time whether the installation passed or failed the final full-scale crash test at NCHRP Report 350 test designation 3-11, but the improvement in the performance of the system was apparent. The final modifications of the weak-post W-beam system are listed in table 11.

A finite element model of the splice connection was developed within the scope of this report, which was a secondary goal of this research.

8 CONCLUSIONS

First, a new post-rail connection was developed and tested both in the materials laboratory and in a full-scale crash test (TTI 473750-1) implemented in a complete weak-post W-beam guardrail installation. The connection consisted of one 6-mm diameter ASTM F568 Class 4.6 bolt with two square washers under the bolt head tightened with two nuts and a circular washer. The splice connections were positioned mid-span between posts. The connection itself worked satisfactory but the guardrail ruptured in the full-scale crash test. A tear was initiated at the lower edge of the rail as it was dragged up against the sharp post-flange edge of a twisted post in the crash test. This tear grew as the tension increased in the rail and finally tore the rail completely. Using F.E. modeling it was determined that a possible solution to this problem was to use backup plates between the W-beam and the posts.

A second full-scale crash test (TTI 473750-2) was performed with backup plates added behind the rail. The 14-mm diameter shelf bolt underneath the rail was removed to eliminate the risk of initiating a tear through contact with this bolt. The backup plates prevented the guardrail from tearing but the test failed again since the car overrode the rail due to decreased rail height. Since the rail did not tear and since the post-rail connection failed easily and quickly as it should a more fundamental problem had to be solved in order to achieve a G2-system that fulfills NCHRP Report 350 test designation 3-11 conditions. The vehicle overrode the guardrail when the W-beam dropped allowing

the front left wheel to come in contact with guardrail and pull the rail to the ground. Finite element simulations were performed with the guardrail mounted 50 mm higher than the standard 610-mm from the ground to the center slot. Both passenger cars and pickup trucks performed well in the simulated full-scale crash-test. The G2-system was originally developed to sustain and redirect typical passenger cars, not pickup trucks. Increasing the height of the rail might prevent the pick-up truck from overriding the rail but one has to be careful so that a small car does not underride the rail either.

A third full-scale crash-test (TTI 473750-3) was performed with the guardrail mounted 50-mm higher than in the standard G2-system. A review of the videotapes of the full-scale crash test (TTI 473750-2) raised the question that the post-rail connection may have failed too easily. Therefore, an 8-mm diameter ASTM F568 Class 4.6 bolt was used instead of the 6-mm diameter bolt that was used in the two previous tests. Also, the 14-mm diameter shelf bolt underneath the rail was put in place again to gain some extra support for the rail. The overall performance of the installation in the crash test was satisfactory. The vehicle was contained and redirected according to the NCHRP Report 350 evaluation criteria, although some posts had been pulled out of the ground and thrown back into the traffic lane possibly violating NCHRP Report 350. From viewing high-speed videos of the impact it appeared that wet soil conditions were the likely cause of the posts pulling out of the ground. The final test report from TTI was not completed prior to the submission of this thesis so it was not known whether the installation passed or failed the test although the test appeared to be a success.

Future work with this installation includes a full-scale crash test at NCHRP Report 350 test designation 3-10 conditions that is scheduled in June 2000 to test the performance of the modified weak-post W-beam system when impacted by a small car. If these tests, the test at test designation 3-10 and the test at 3-11, are successful the system will meet NCHRP Report 350 at test level three and will be acceptable to use on Federal-Aid Highways in the United States.

9 REFERENCES

1. Bronstad, Maurice. E., and Burket, Robert. B. *Evaluation of timber weak-post guardrail systems*. Highway research record 343, Transportation Research Board, Washington D.C, 1971.

2. Ray, Malcolm. H., and McGinnis, Richard. G. *Guardrail and Median Barrier Crashworthiness, A synthesis of Highway practice*. In NCHRP Synthesis 244, Transportation Research Board, National Academy Press, 1997.

3. Mak, King. K., and Alberson, Dean. C. *Test Report NO. 7147-21 (Draft report).* Texas Transportation Institute, Texas A&M University System, 1993.

4. Plaxico, Chuck. A., Patzner, Gregory. S., and Ray, Malcolm. H., *Finite-Element Modeling of Guardrail Timber Posts and the Post-Soil Interaction*. In Transportation Research Record 1647, Transportation Research Board, Washington D.C, 1998.

5. Wright, Amy. E., and Ray, Malcolm. H. *Characterizing Guardrail Steel for LS-Dyna3D Simulations*. In Transportation Research Record 1528, Transportation Research Board, Washington D.C, 1996.

6. AISC, Manual of Steel Construction: Load and Resistance Factor Design, Vol. II.2nd Edition, American Institute of Steel Construction, Chicago, IL, 1995.

7. AASHTO-AGC-ARTBA Joint Committee, *A Standardized Guide to Highway Barrier Hardware,* American Association of State Highway and Transportation Officials, the American Road and Transportation Builder's Association and the Association of General Contractors, 1979.

8. LS-Dyna User's Manual, *Nonlinear Dynamic Analysis Of Structures In Three Dimensions (version 940)*, Livermore Software Technology Corporation.

9. Buth, Eugene. C., Menges, Wanda. L., and Schoeneman, Sandra. K., *NCHRP Report 350 Test 3-11 On The Modified PennDOT Type 2 Guide Rail*, Texas Transportation Institute, Texas A&M University System, College Station, Texas, January 2000.

10. Buth, Eugene. C., Menges, Wanda. L., and Schoeneman, Sandra. K., *NCHRP Report 350 Test 3-11 On The Modified PennDOT Type 2 Guide Rail-Test 2*, Texas Transportation Institute, Texas A&M University System, College Station, Texas, February 2000.

11. Kilareski, W. P., El-Gindy, M., St. John, B. D., and Peacheux, B. Final report : *Type 2 Weak post guardrail testing*. In Agreement No.359704, Work Order 20, Pennsylvania Transportation Institute, Pennsylvania State University, 1999.

12. H.E.Ross, Jr.,D.L.Sicking,R.A.Zimmer and J.D.Michie, *Recommended Procedures for the Safety Performance Evaluation of Highway Features*, National Cooperative Highway Research Program Report 350, Transportation Record Board, National Research Council, Washington, D.D.,1993.

13. M.H.Ray and G.S. Patzner, *Finite-Element Model of Modified Eccentric Loader Terminal (MELT)*, In Transportation Research Board 1599, National Academy Press, Washington, D.C., 1997.

14. C.A. Plaxico, R.M. Hackett and W. Uddin, *Simulation of a Vehicle Impacting a Modified Thrie-Beam Guardrail*, In Transportation Research Board 1599, National Academy Press, Washington, D.C., 1997.

15. Ross, Hayes. E. Jr., Bligh, Roger. P., and Menges, Wanda. L. *Evaluation of Roadside Features to Accommodate Vans, Minivans, Pickup Trucks, and 4-Wheel Drive Vehicles (Preliminary draft).* Texas Transportation Institute, Texas A&M University System, College Station, Texas, November 1999.

16. Buth, Eugene. C., Zimmer, Richard. A., and Menges, Wanda. L. *Testing and evaluation of a modifies G4(1S) guardrail with W150*17.9 Steel Blockouts*. TTI Report No. 405421-2. Texas Transportation Institute, Texas A&M University System, College Station, Texas, January 1999.

17. Mak, King. K., Bligh, Roger. P., and Menges, Wanda. L. *Crash testing of Ford Taurus, Chevrolet Lumina, Plymouth Neon, and Dodge Caravan - In Support of Finite Element Computer Modeling (Draft report).* Project No. 472580. Texas Transportation Institute, Texas A&M University System, College Station, Texas, May 1999.

18. Mak, King. K., Bligh, Roger. P., and Menges, Wanda. L. *Testing and evaluation of the MELT-2 Terminal (Draft final report).* Texas Transportation Institute, Texas A&M University System, College Station, Texas, August 1996.

19. Mak, King. K., and Menges, Wanda. L., *Testing Of State Roadside Safety Systems Volume X: Appendix I - Crash Testing And Evaluation Of A Mini-Melt Terminal For A W-beam, Weak-Post (G2) Guardrail System (Draft Report).* Texas Transportation Institute, Texas A&M University System, College Station, Texas, June 1996.

20. TrueGrid Manual version 1.4.0, XYZ Scientific Applications, Inc., June 1998.